HEAT TRANSFER ENHANCEMENT IN NANO-FLUIDS SUSPENSIONS: THERMAL WAVE EFFECTS AND HYPERBOLIC HEAT CONDUCTION

by

Johnathan J. Vadasz

Supervisor: **Professor Saneshan Govender**

In fulfillment of the requirements for the degree of Master of Science in Mechanical Engineering at University of KwaZulu-Natal

December 2005

Acknowledgements

I would like to thank *Professor Saneshan Govender* as my supervisor for assistance in my Masters thesis research. Specifically for supplying me with some Journal paper publications and other relevant literature to my research. I also thank *Professor Peter Vadasz* for many more Journal paper publications and help in the literature survey, and for assistance in learning *FORTRAN* programming.

ABSTRACT

The spectacular heat transfer enhancement revealed experimentally in nanofluids suspensions is being investigated theoretically at the macro-scale level aiming at explaining the possible mechanisms that lead to such impressive experimental results. In particular, the possibility that thermal wave effects via hyperbolic heat conduction could have been the source of the excessively improved effective thermal conductivity of the suspension is shown to provide a viable explanation although the investigation of alternative possibilities is needed prior to reaching an ultimate conclusion.

KEYWORDS: *Nanofluids, Nanoparticles Suspension, Heat Transfer Enhancement, Effective Thermal Conductivity.*

TABLE OF CONTENTS

NOMENCLATURE

Latin Symbols

r_{w*} = radius of the platinum wire.

c_* = wave speed, equals $\sqrt{\alpha_*/\tau_*}$.

d_{w*} = diameter of the platinum wire.

Fo = Fourier number, equals $\alpha_*\tau_*/L_*^2$.

i = electrical current.

k_* = effective thermal conductivity of the suspension.

l_* = length of the platinum wire/strip.

L_* = gap distance between the walls of a slab.

q_* = heat flux.

q_{L*} = horizontal heat flux on the boundary of the platinum strip, at $x_* = L_*$.

$\dot{q}_{*l}$ = rate of heat generated by Joule heating in the platinum wire per unit length of wire.

R = electrical resistance, dimensional.

r_* = radial variable coordinate.

t_* = time.

T = dimensionless temperature.

T_{C*} = coldest wall temperature, dimensional.

T_{1*} = temperature measured at time t_{*1} .

T_{2*} = temperature measured at time t_{*2} .

V = voltage across the platinum wire/strip, dimensional.

x_* = horizontal variable co-ordinate.

O = order of

Greek Symbols

α_* = effective thermal diffusivity of the suspension.

τ_* = relaxation time in hyperbolic heat conduction.

ρ = fluid density.

θ = angle between vector **V** and ∇T

γ = Euler's constant.

λ = Eigenvalues

δ = Kronecker delta function

Subscripts

$*$ = dimensional values.

cr = critical values.

CHAPTER 1
INTRODUCTION

1.1 Motivation

Heat conduction in fluids at the macro-level is very poor because most affordable fluids have very low thermal conductivity values compared with solids. Crystalline solids have thermal conductivity values of 1 to 3 orders of magnitude larger than those of fluids (Eastman *et al.* , 2001).

Traditional enhancement of heat transfer in fluids is possible mainly by adding a mechanism of convection to the thermal conduction process. Unfortunately, in addition to the relatively low thermal conductivity of fluids, the convection effect requires substantial amount of pumping power. The reason for the latter is that the heat transfer by convection is governed by the energy equation that can be presented in the following form

$$\frac{\partial T}{\partial t} + \boldsymbol{V} \bullet \nabla T = \alpha \nabla^2 T \qquad (1\text{-}1)$$

where T stands for temperature, $\boldsymbol{V}$ is the velocity field, $\alpha = k/\rho c_p$ is the thermal diffusivity, k is the thermal conductivity, ρ is fluid's density, and c_p is the specific heat at constant pressure. From equation (1-1) it is obvious that when the fluid flow is perpendicular to the temperature gradient the convection term vanishes identically, i.e. $\boldsymbol{V} \bullet \nabla T = 0$ when $\boldsymbol{V}$ is perpendicular to ∇T. The latter occurs because $|\boldsymbol{V} \bullet \nabla T| = |\boldsymbol{V}||\nabla T|\cos(\theta)$, where θ is the angle between the velocity vector direction and the temperature gradient direction. When they are perpendicular, $\theta = \pi/2$, and the scalar product vanishes. However, according to Fourier law the temperature gradient is proportional to the heat flux, i.e . $\boldsymbol{q} = -k\nabla T$, where $\boldsymbol{q}$ is the heat flux. Therefore, the obvious conclusion is that whenever the heat flux is perpendicular to the velocity, the convection mechanism vanishes and the heat is transferred by conduction only. It is because of this reason that most convection driven devices use one of the two following methods to enhance the convection mechanism:

(a) Classical/traditional method: "brute force" – apply very high flow rates and additional means to guarantee that the flow is in the turbulent regime (high Reynolds

number) and as a result of the temporal and spatial velocity fluctuations within the turbulent regime preventing the velocity to be perpendicular to the heat flux. The price of applying this method is the substantial pumping power required to keep the flow within the turbulent regime.

(b) Modern methods: elegant design of compact heat exchangers attempt to control boundary layers by focusing on shape changes of the solid-fluid interface (that acts as the heat transfer area). While the latter method is indeed more efficient it is limited in the amount of heat that can be removed and it also requires substantial pumping power (although less than the former) to overcome the friction due to enhanced heat transfer area.

Pumping power is a substantially more expensive commodity than the corresponding energy in the form of heat rate. Thermodynamically, the value of mechanical energy transfer (pumping power) is between 2 to 3 times more expensive (in terms of thermodynamic cost) than the same energy amount in the form of heat transfer. For example 1 kW of heat transferred is equivalent to between 0.35 - 0.5 kW of mechanical (pumping) power. The latter is a consequence of the second law of thermodynamics linked with practical state of the art efficiencies related to available technologies. This makes savings in pumping power while providing the same amount of heat transfer rates an important engineering objective that holds potential for great returns.

The reported breakthrough in substantially increasing the thermal conductivity of fluids by adding very small amounts of suspended metallic or metallic oxide nanoparticles (Cu, CuO, Al_2O_3) to the fluid (Eastman *et al.* 2001, Lee *et al.* 1999), or alternatively using nanotube suspensions (Choi *et al.* 2001), as well as Xuan and Li (2000) is intriguing. The latter is important not only because of the face value of its possibility to direct implementation in technological applications but also because both results clearly conflict with theoretical anticipations based on existing theories and models (see discussion on the conflict between theory and experiments in Choi *et al.* 2001). These results, if independently confirmed, open two distinct avenues of opportunities: (a) Their direct application to different technologies in improving substantially the operating efficiencies and reducing both operating as well as capital production costs. Better efficiency allows for lower pumping power and less heat transfer area, hence saving in both operating as well as fixed costs. Better efficiency

also minimizes the adverse impact that energy-producing technologies have on the environment, i.e. less pollutants per kW generated. (b) By discovering the correct mechanism and theory that underlies this phenomenon may extend design options in developing processes and devices that apply these mechanisms, hence opening the door to yet unknown and limitless possibilities of new processes and devices that use heat transfer.

1.2 Potential applications

There is a vast field for applications of nano-fluid suspensions. One such application is in the motor and trucking industry. Recent experiments yielded an increase in thermal conductivity when suspending nano-copper particles in oil and ethylene glycol (anti-freeze). This would allow for great savings in the trucking industry by increasing the efficiency of the engine cooling system. By increasing the thermal conductivity the heat from the engine would be drawn away more efficiently. This would allow for reduced fuel consumption, which equals large economical savings for truck companies. As far as passenger vehicles are concerned, sales would increase if new cars were to come with a substantially lower fuel consumption index. Other possible applications include aeronautics, power generation, cooling of microelectronics etc. The limits are virtually endless when it comes to where nano-fluid suspensions can be used.

CHAPTER 2
LITERATURE SURVEY

2.1 Heat transfer enhancement in Nano-fluids suspensions

The results reported by Eastman *et al.* 2001 for a "suspended nano-particles" system were redrawn and are presented in Figure 2-1 where two major deductions can be made: (a) The impact of the copper nano-particles (that the authors, Eastman *et. al.* 2001 succeeded to keep stable in the suspension due to the particular technique they used to manufacture them) on the effective thermal conductivity of the suspension is unexpectedly high. A very small amount (less than 1% in terms of volume fraction) of copper nano-particles can improve the thermal conductivity of the suspension by 40%. (b) Even metal-oxides at small quantities (4% in terms of volume fraction) can produce a substantial increase of about 20% in the effective thermal conductivity of the suspension.

The experimental results reported by Choi *et. al.* (2001) of multiwalled carbon nano-tubes suspended in oil were redrawn and are presented in Figure 2-2. An even more impressive improvement of the effective thermal conductivity is detected. Over 150% improvement of the effective thermal conductivity (a factor of 2.5 higher thermal conductivity) at a volume fraction of 1% is indeed spectacular.

Moreover, Choi *et al.* (2001) compared their results with exiting theories, some of them going back to the start of the last century, e.g. Maxwell (1904), Hamilton & Crosser (1962), Jeffrey (1973), Davis (1986), Lu & Lin (1996) and Bonnecaze & Brady (1990, 1991). The reported experimental results are by one order of magnitude greater than the predictions based on existing theories and models. More recent approaches (Wang, Zhou and Peng 2003) also cannot explain this discrepancy.

On the other hand a reduction in the effective thermal conductivity of the nanoparticle-host medium is anticipated by existing theories for length scales smaller than the phonon mean free path in the host material (Chen, 1996, 2000). There is a clear and appealing need to settle the conflict between the recent experimental results and the theories or models. It is very difficult and expensive to experiment for all possible combinations of circumstances. It is because of this latter reason that reliable theories and models can be used to bridge the gap between different experiments. Possible explanations for the divergence between theory and

experiments were suggested and explored very basically by Keblinski *et al.* (2002). Brownian motion of the particles, molecular-level layering of the liquid at the liquid/particle interface, the nature of heat transport within the nanoparticles and effects of nanoparticle clustering were investigated. While these investigations were not done in detail but mainly at the very basic level, Keblinski *et al.* (2002) show that the "*key factors in understanding thermal properties of nanofluids are the ballistic, rather than diffusive, nature of heat transport in the nanoparticles*, combined with direct or fluid mediated clustering effects that provide paths for rapid heat transport". If this conclusion is correct then the experimental results obtained at the macro-system level reflect the wave effects impact on the macro-system behavior rather than the diffusion mechanism. It implies that Fourier Law (representing the diffusion mechanism) is not valid even at the macro-system level when nanoelements are suspended in the fluid. The immediate conclusion from the latter deduction is that the Transient Hot Wire method (THW) that was used by Eastman *et al.* (2001), Lee *et al.* (1999) and by Choi *et al.* (2001) to measure the nano-fluid suspension's effective thermal conductivity is not appropriate because it uses the Fourier Law of heat conduction as its fundamental principle for estimating the thermal conductivity (Kestin and Wakeham 1978, Perkins *et al.* 2000). Eastman *et al.* (2001) indicate the way the thermal conductivity is being evaluated by using Fourier Law in the Transient Hot Wire method (THW). Therefore, based on this simple logic the excessive values of effective thermal conductivity calculated based on the experimental data might need a correction to account for deviations from Fourier Law. Still the question of why this apparent substantial heat flux enhancement occurred was not yet addressed. The mechanisms suggested by Keblinski *et al.* (2002) are all possible. However, the way these nano or molecular level mechanisms are being lumped into such an impressive effect at the macro-system level is not yet known, nor proposed by Keblinski *et al.* (2002). Recent research results presented by Xue *et al.* (2004) eliminate the molecular-level layering of the liquid at the liquid/particle interface as a possible heat transfer enhancement mechanism. The authors Xue *et al.* (2004) conclude that "the experimentally observed large enhancement of thermal conductivity in suspensions of solid nanosized particles (nanofluids) can not be explained by altered thermal transport properties of the layered liquid". While the reported results are a direct consequence of the presence

of nano-elements in the suspension, the measurements were not performed at the nanoscale, but rather at the macro/meso-scale. As a result the interest should be focused not only on what occurs at the nanoscale but rather on how the heat transfer at the macro/meso-scale is substantially affected by a very small presence (less than 1% in volume) of extremely small suspended elements (nano-elements).

There are about six possible reasons for the anomalously increased effective thermal conductivity, which can be classified as follows:

(i) Hyperbolic (Cattaneo, 1958 and Vernotte 1958, 1961) or Dual-Phase-Lagging (Tzou 1997, 2001 and Vadasz 2005 a,b) thermal wave effects not accounted for in using the THW data processing & extremely high values of the time lag due to the heterogeneous mixture (see Vadasz 2005 a,b),

(ii) Thermal resonance due to hyperbolic thermal waves combined with an amplified periodic signal possibly from short-radio-waves or cellular phones (1.9 Ghz, 800Mhz frequencies),

(iii) Particle driven, or thermally driven, natural convection,

(iv) Convection induced by electro-phoresis,

(v) Hyperbolic thermal natural convection,

(vi) Any combination of the above.

The first particular possibility that needs exploration is that the nano/molecular level wave effects at the nanoelements' interface make the hyperbolic (wave) heat transfer effects at the macro-level significant. Then, a corresponding correction of converting the experimental data into the effective thermal conductivity results needs to be introduced. The latter forms the objective of the present investigation in terms of introducing the hyperbolic thermal wave corrections based on Cattaneo (1958) and Vernotte (1958, 1961) constitutive relationship for heat conduction and checking whether such effects may have been the reason behind the excessive effective thermal conductivity results in nanofluid suspensions.

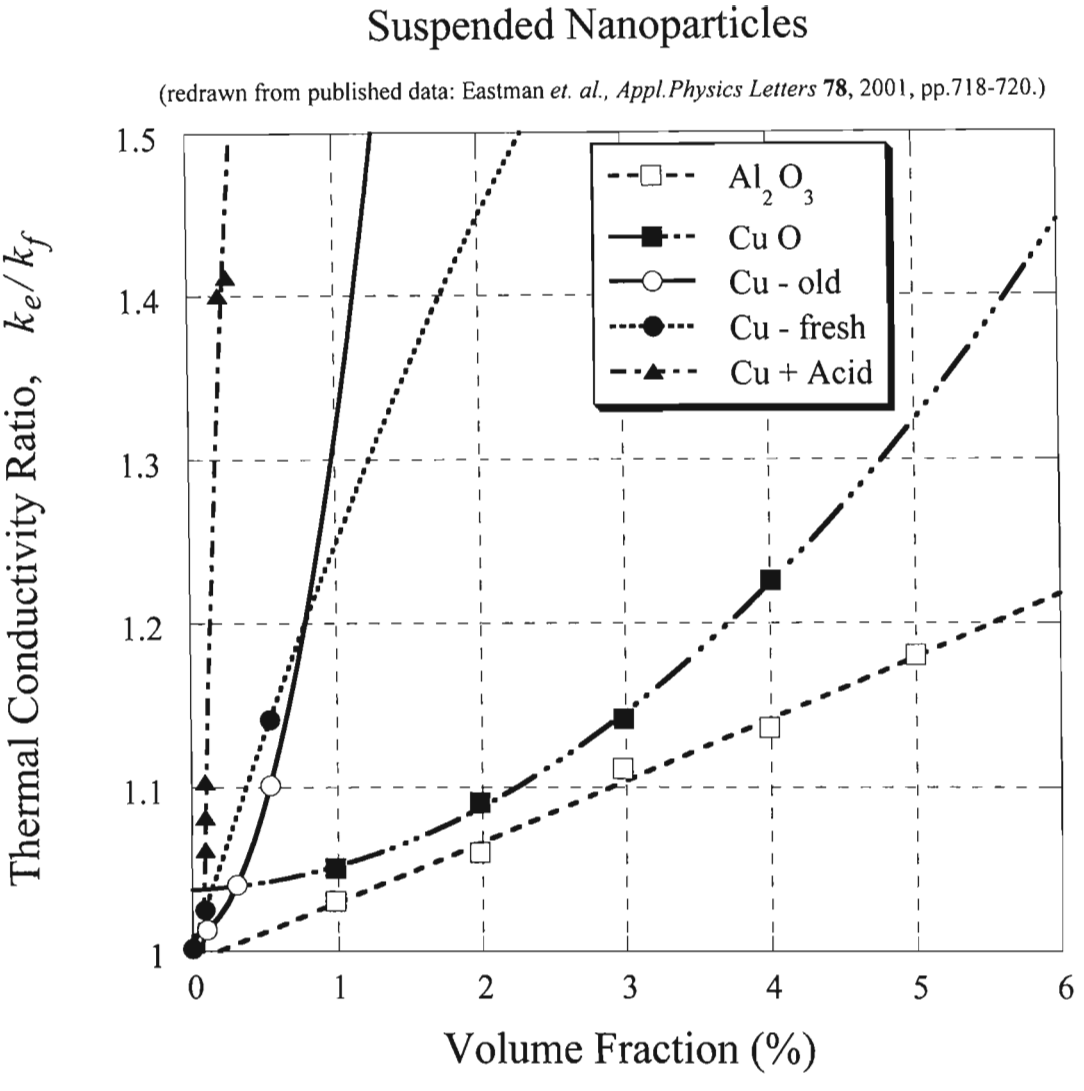

Figure 2-1: Thermal conductivity enhancement in systems consisting of nanoparticles suspended in ethylene glycol as reported by Eastman *et. al.*, 2001. (here redrawn from published data: using a different curve fit than the linear one used by Eastman *et. al.*, 2001).

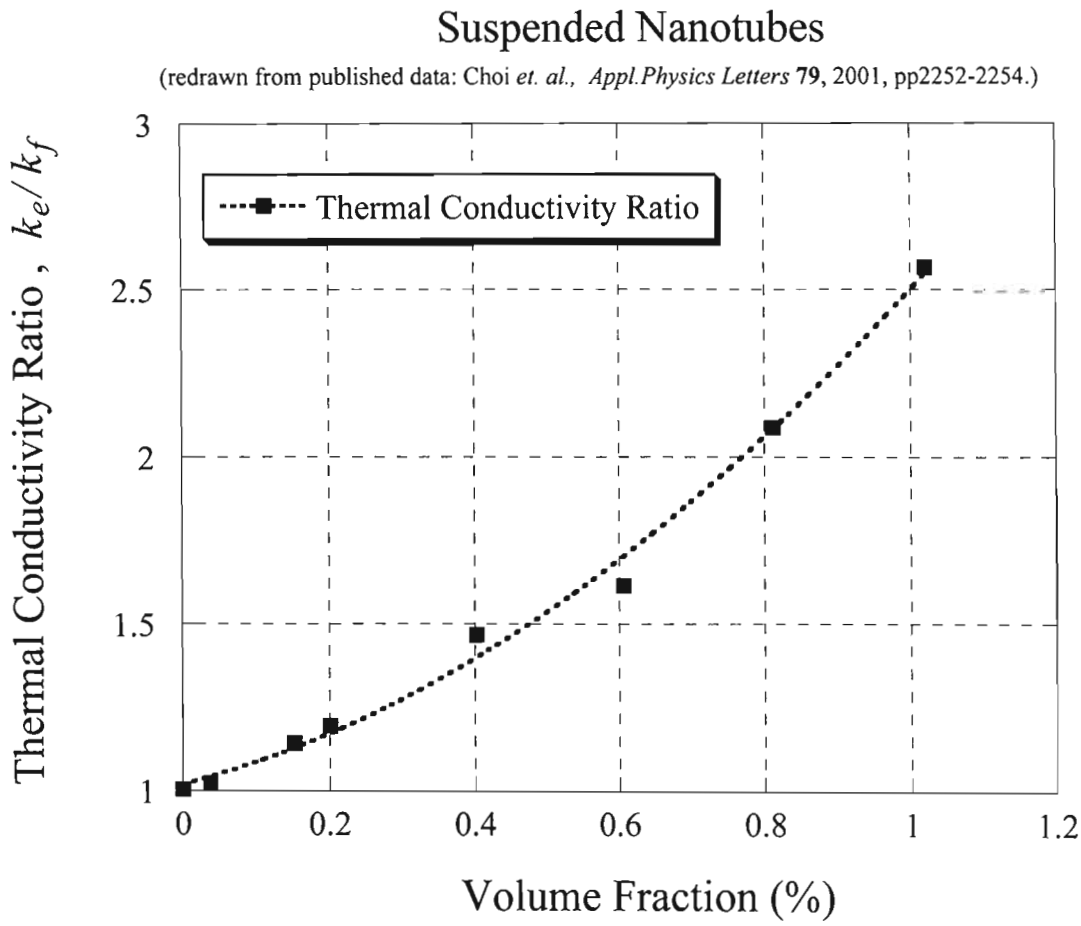

Figure 2-2: Thermal conductivity enhancement in systems consisting of multiwalled carbon nanotubes suspended in oil, as reported by Choi *et. al.*, 2001. (here redrawn from published data: Choi *et.al.*, 2001).

2.2 Transient Hot Wire and Transient Hot Strip Methods of measuring the thermal conductivity

The Transient Hot Wire (THW) method for estimating experimentally the thermal conductivity of solids, Assael *et al.* (2002) and fluids, De Groot, Kestin and Sookiazian (1974), Healy, De Groot and Kestin (1976), Kestin and Wakeham (1978), established itself as the most accurate, reliable and robust technique, Hammerschmidt and Sabuga (2000). It replaced the steady state methods primarily because of the difficulty to determine that steady state conditions haven indeed been established and for fluids the difficulty in preventing the occurrence of natural convection and consequently the difficulty in eliminating the natural convection effects on the heat flux. The method consists in principle of determining the thermal conductivity of a selected material/fluid by observing the rate at which the temperature of a very thin platinum (or tantalum) wire ($5\,\mu$m - $80\,\mu$m) increases with time after a step change in voltage has been applied to it. The platinum wire is embedded vertically in the selected material/fluid and serves as a heat source as well as a thermometer, as presented schematically in Figure 2-3. The temperature of the platinum wire is established by measuring its electrical resistance, the latter being related to the temperature via a well-known relationship. A Wheatstone bridge is used to measure the electrical resistance R_w of the platinum wire (see Figure 2-3). The electrical resistance of the potentiometer R_3 is adjusted until the reading of the galvanometer G shows zero current. When the bridge is balanced as indicated by a zero current reading on the galvanometer G, the value of R_w can be established from the known electrical resistances R_1, R_2 and R_3 by using the balanced Wheatstone bridge relationship $R_w = R_1 R_3 / R_2$. Because of the very small diameter (micrometer size) and high thermal conductivity of the platinum wire the latter can be regarded as a line source in an otherwise infinite cylindrical medium. The rate of heat generated per unit length (l_*) of platinum wire is therefore $\dot{q}_{*l} = iV/l_*$ [W/m], where i is the electric current flowing through the wire and V is the voltage drop across the wire. Solving for the radial heat conduction due to this line heat source as shown in Appendix A leads to a temperature solution in the following closed form that can be expanded in an infinite series as follows:

$$T_* = \frac{\dot{q}_{*l}}{4\pi k_*} Ei\left(\frac{r_*^2}{4\alpha_* t_*}\right)$$
$$= \frac{\dot{q}_{*l}}{4\pi k_*}\left[-\gamma + \ln\left(\frac{4\alpha_* t_*}{r_*^2}\right) + \frac{r_*^2}{4\alpha_* t_*} - \frac{r_*^4}{64\alpha_*^2 t_*^2} + \frac{r_*^6}{1152\alpha_*^3 t_*^3} - \ldots.\right] \quad (2\text{-}1)$$

where $Ei(\bullet)$ represents the exponential integral function, and $\gamma = \ln(\sigma) = 0.5772156649$ is Euler's constant. For a line heat source embedded in a cylindrical cell of infinite radial extent and filled with the test fluid one can use the approximation $r_*^2/4\alpha_* t_* << 1$ in equation (2-1) to truncate the infinite series and yield

$$T_* \approx \frac{\dot{q}_{*l}}{4\pi k_*}\left[-\gamma + \ln\left(\frac{4\alpha_* t_*}{r_*^2}\right) + O\left(\frac{r_*^2}{4\alpha_* t_*}\right)\right] \quad (2\text{-}2)$$

Equation (2-2) reveals a linear relationship, on a logarithmic time scale, between the temperature and time. For $r_* = r_{w*}$, r_{w*} being the radius of the platinum wire, the condition for the series truncation $r_*^2/4\alpha_* t_* << 1$ can be expressed in the following equivalent form that provides the validity condition of the approximation in the form

$$t_* >> \frac{r_{w*}^2}{4\alpha_*} \quad (2\text{-}3)$$

For any two temperature readings T_{1*} and T_{2*} recorded at the times t_{*1} and t_{*2} respectively the temperature difference $(T_{2*} - T_{1*})$ can be approximated by using equation (2-2) in the form

$$(T_{2*} - T_{1*}) \approx \frac{iV}{4\pi k_* l_*}\left[\ln\left(\frac{t_{*2}}{t_{*1}}\right)\right] \quad (2\text{-}4)$$

where the heat source was replaced with its explicit dependence on the i, V and l_*, i.e. $\dot{q}_{*l} = iV/l_*$. From equation (2-4) one can express the thermal conductivity k_* explicitly in the form

$$k_* \approx \frac{iV}{4\pi(T_{2*} - T_{1*})l_*}\left[\ln\left(\frac{t_{*2}}{t_{*1}}\right)\right] \quad (2\text{-}5)$$

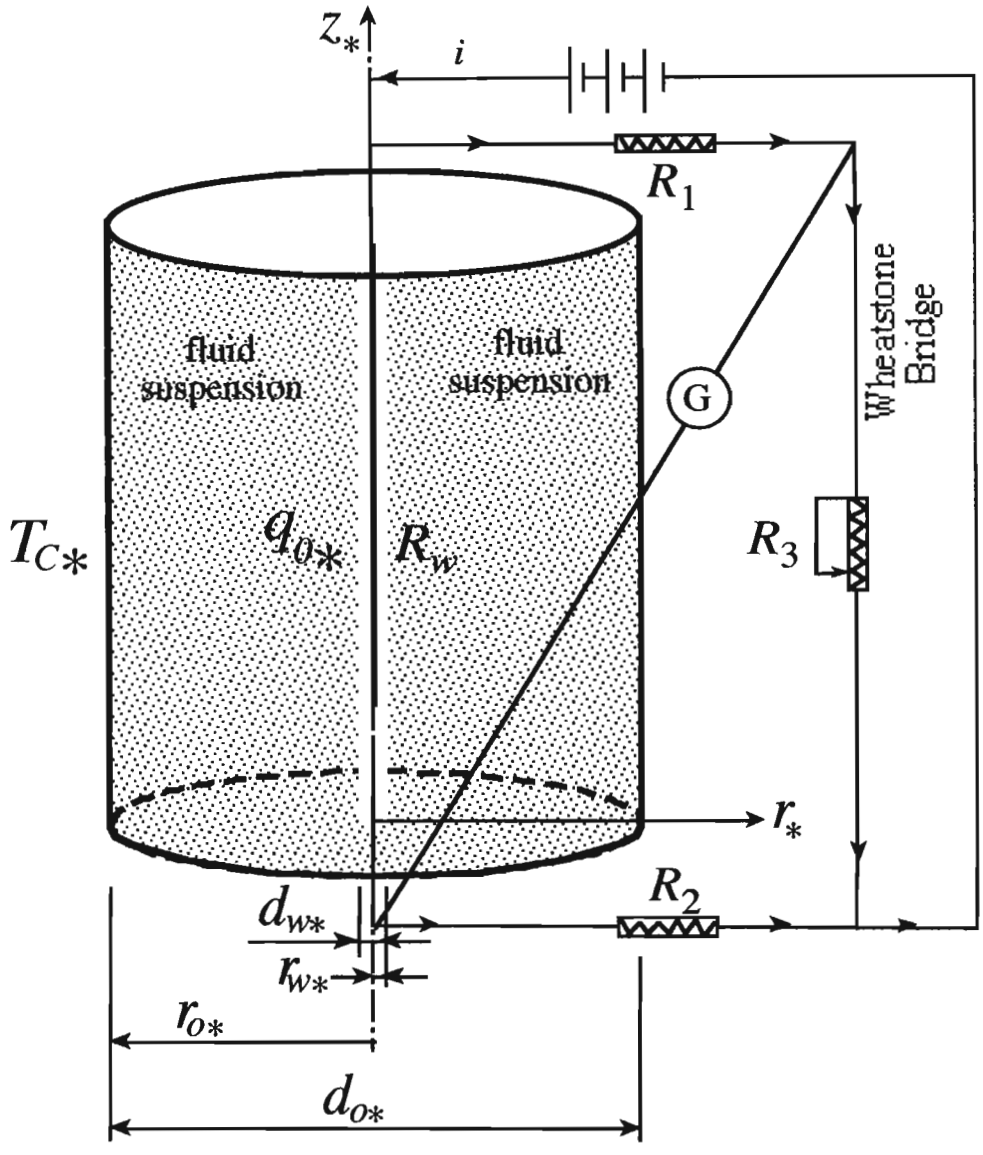

Figure 2-3: An embedded platinum (tantalum) hot wire within a nanofluid suspension in a cylindrical container using the Transient Hot Wire method.

Equation (2-5) is a very accurate way of estimating the thermal conductivity as long as the validity conditions for appropriateness of problem derivations used above are fulfilled. A finite length of the platinum wire, the finite size of the cylindrical container, the heat capacity of the platinum wire, and possibly natural convection effects are examples of possible deviations of any realistic system from the one used in deriving equation (2-5). De Groot, Kestin and Sookiazian (1974), Healy, de Groot and Kestin (1976), and Kestin and Wakeham (1978) introduce an assessment of these deviations and possible corrections to the THW readings to improve the accuracy of the results. In general all the deviations indicated above could be eliminated via the proposed corrections provided the validity condition listed in equation (2-3) is enforced as well as an additional condition that ensures that natural convection is absent. The validity condition (2-3) implies the application of equation (2-5) for long times only. However, when evaluating this condition (2-3) to data used in the nanofluids suspensions experiments considered here one obtains explicitly the following values. For a 76.2 μm diameter of platinum wire used by Eastman *et al.* (2001), Lee *et al.* (1999), Choi *et al.* (2001), the wire radius is $r_{w_*} = 3.81\times10^{-5}$ m leading to $r_{w_*}^2/4\alpha_* = 3.9$ ms for ethylene glycol and $r_{w_*}^2/4\alpha_* = 4.2$ ms for oil, leading to the validity condition $t_* >> 3.9$ ms for ethylene glycol and $t_* >> 4.2$ ms. The long times beyond which the solution (2-5) can be used reliably are therefore of the order of a tens of milliseconds, not so long in the actual practical sense. On the other hand the experimental time range is limited from above as well in order to ensure the lack of natural convection that develops at longer time scales. Xuan and Li (2000) estimate this upper limit for the time that an experiment may last before natural convection develops as about 5 s. They indicate that *"An experiment lasts about 5 s. If the time is longer, the temperature difference between the hot-wire and the sample fluid increases and free convection takes place, which may result in errors"*. Lee *et al.* (1999) while using the THW method and providing experimental data in the time range of 1s to 10 s, indicate in their figure 3 the "*valid range of data reduction*" to be between 3 s to 6 s. The estimations evaluated above confirm these lower limits as a very safe constraint and it is assumed that the upper limits listed by Xuan and Li (2000) and Lee *et al.* (1999) are also good estimates, leading to the validity condition of the experimental results to be within the following estimated

time range of $0.03s < t_* < 5s$. The valid range for data reduction used by Lee *et al.* (1999), i.e. $3s < t_* < 6s$ should also be satisfactory. Within this time range the experimental results should produce a linear relationship, on a logarithmic time scale, between the temperature and time.

While the application of the method to solids and gases is straightforward its corresponding application to electrically conducting liquids needs further attention. The experiments conducted in nanofluids suspensions listed above used a thin electrical insulation coating layer to cover the platinum wire instead of using the bare metallic wire, a technique developed by Nagasaka and Nagashima (1981). The latter is aimed at preventing problems such as electrical current flow through the liquid causing ambiguity of the heat generation in the wire. Alternatively, Assael *et al.* (2004) used tantalum wires, which were anodized in situ to form a coating layer of tantalum pentoxide (Ta_2O_5) which is an electrical insulator.

A Transient Hot Strip (THS) method using a rectangular geometry was developed as an equivalent alternative to the Transient Hot Wire (THW) method that applies to a cylindrical geometry. The Transient Hot Strip (THS) method uses a very thin metal foil instead of the hot wire to undertake identical functions as presented in a review by Gustafsson (1987). It applies therefore to a rectangular geometry and its accuracy, uncertainty, advantages and disadvantages as compared to the THW method were presented by Hammerschmidt and Sabuga (2000).

2.3 Hyperbolic heat conduction and Thermal Wave Effects

The hyperbolic heat conduction equation

$$\frac{1}{c_*^2}\frac{\partial^2 T}{\partial t_*^2}+\frac{1}{\alpha_*}\frac{\partial T_*}{\partial t_*}=\nabla_*^2 T_* \tag{2-6}$$

where c_* is the speed of wave propagation and α_* is the thermal diffusivity is obtained by replacing the Fourier law $\boldsymbol{q}_* = -k_*\nabla_* T_*$ with the Catteneo (1958) and Vernotte (1958, 1961) formulation

$$\tau_*\frac{\partial \boldsymbol{q}_*}{\partial t_*}+\boldsymbol{q}_* = -k_*\nabla_* T_* \tag{2-7}$$

where k_* is the thermal conductivity and τ_* is the relaxation time.

Equation (2-6) is an extension of the thermal diffusion equation obtained via the Fourier law and presented for constant material properties in the form

$$\frac{\partial T_*}{\partial t_*}=\alpha_*\nabla_*^2 T_* \tag{2-8}$$

It can be observed that the hyperbolic heat conduction equation (2-6) reduces to the thermal diffusion equation (2-8) if the speed of wave propagation is infinitely large, i.e. for $c_*^2 \to \infty$ (or $c_*^2 \gg \alpha_*$) making the first term negligibly small. For finite speeds of wave propagation equation (2-6) produces thermal waves as described among others by Özisik and Tzou (1994), Haji-Sheikh, Minkowycz and Sparrow (2002), Wang (2000), Frankel, Vick and Özisik (1985) and Vick and Özisik (1983). The speed of wave propagation, c_*, in equation (2-6) is defined by

$$c_* = \sqrt{\frac{\alpha_*}{\tau_*}} \tag{2-9}$$

The neglect of the first term in equation (2-6) is possible if $c_*^2 = \alpha_*/\tau_* \gg \alpha_*$ leading to the condition $1/\tau_* \gg 1$ s^{-1} or $\tau_* \ll 1$ s, unless short time scales are of interest.

Although no accurate direct measurement of τ_* was reported so far for homogeneous materials, Özisik and Tzou (1994) estimated the relaxation time τ_* to be of magnitude 10^{-10} s for gases at standard conditions, 10^{-14} s for metals and 10^{-12} s for liquids and solid insulators. These values are indeed very small, certainly satisfying the condition $\tau_* \ll 1$ s above, for the neglect of the first term in equation (2-6).

Nevertheless, Kaminski (1990), Mitra et al. (1995), Barletta and Zanchini (1996), Antaki (1998), Tzou (1995) show that experimental values for heterogeneous materials (composite structures, porous media, porous bio-tissues) may be $\tau_* = 10$ s, $\tau_* = 16$ s or even as large as $\tau_* = 100$ s. The latter indicates that heterogeneous materials are particularly expected to exhibit thermal waves when subjected to heat conduction. Clearly, suspension of solid particles in a fluid is a heterogeneous material that qualifies to the latter conclusion.

CHAPTER 3

PROBLEM FORMULATION

3.1 Fourier and Hyperbolic heat conduction in rectangular geometry.

In this chapter the problem formulation for Fourier and Hyperbolic heat conduction in rectangular geometry is shown, which will be separated into four subchapters indicating the different problems, Fourier and Hyperbolic, for the two different types of boundary conditions, Dirichlet and Dirichlet-Neumann.

3.1.1 Fourier with Dirichlet boundary conditions

Consider the slab as described in Figure 3-1 subject to a constant hot temperature T_{H_*} on its right wall, and a constant cold temperature T_{C_*} on the left wall. The energy balance equation for heat conduction is

$$\rho_* c_{p_*} \frac{\partial T_*}{\partial t_*} = -\nabla_* \cdot \boldsymbol{q}_* \tag{3-1}$$

where $\boldsymbol{q}_*$ is the heat flux, ρ_* is density and c_{p_*} is the (constant pressure) specific heat and by the Fourier Law which is a constitutive relationship between the heat flux and temperature gradient

$$\boldsymbol{q}_* = -k_* \nabla_* T_* \tag{3-2}$$

leading to the Fourier heat conduction equation

$$\frac{\partial T_*}{\partial t_*} = \alpha_* \nabla_*^2 T_* \tag{3-3a}$$

where α_* is the thermal diffusivity.

For the one dimensional slab equation (3-3a) becomes

$$\frac{\partial T_*}{\partial t_*} = \alpha_* \frac{\partial^2 T_*}{\partial x_*^2} \tag{3-3b}$$

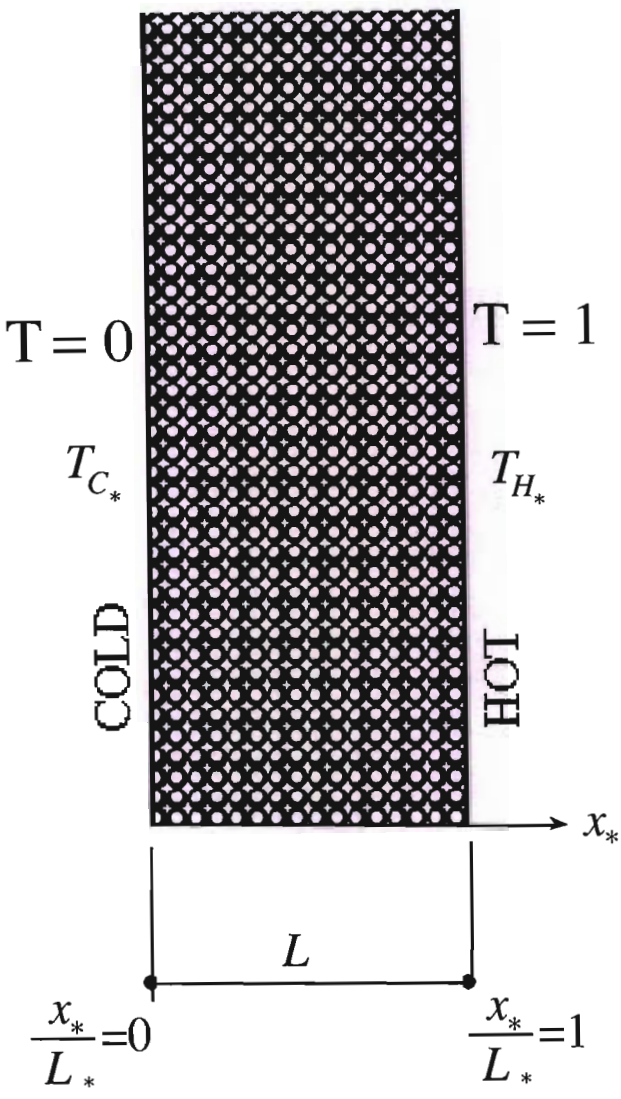

Figure 3-1: Problem formulation of heat conduction in a slab subject to constant temperature (Dirichlet) boundary conditions.

3.1.2 Fourier heat conduction with Dirichlet-Neumann boundary conditions

Consider the slab as described in Figure 3-2 subject to a constant heat flux on its right wall q_{L^*}, representing the heat flux from the hot strip to the fluid due to the uniform Joule heating generated in the thin hot strip by the electric current, and a constant cold temperature T_{C_*} on the left wall. The Fourier conduction phenomenon is governed by the constitutive relationship between the heat flux and temperature gradient in the form shown in equation (3-2) and the energy balance equation (3-1), which lead to the Fourier heat conduction equation (3-3a).

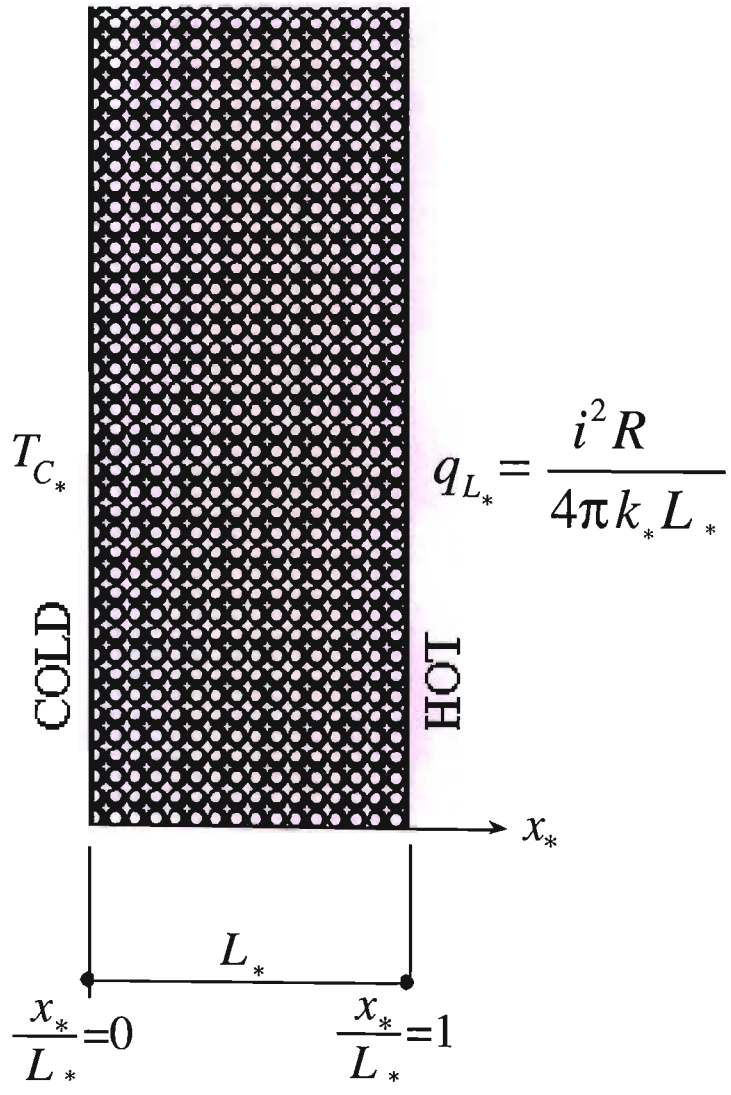

Figure 3-2: Problem formulation of heat conduction in a slab subject to a combination of constant temperature (Dirichlet) and constant heat flux (Neumann) boundary condition.

3.1.3 Hyperbolic heat conduction with Dirichlet boundary conditions

Consider the slab as described in Figure 3-1 subject to a constant temperature T_{H_*} on its right wall, and a constant cold temperature T_C on the left wall. The hyperbolic conduction phenomenon is governed by the constitutive relationship between the heat flux and temperature gradient in the form

$$\tau_* \frac{\partial \boldsymbol{q}_*}{\partial t_*} + \boldsymbol{q}_* = -k_* \nabla_* T_* \tag{3-4}$$

where τ_* is the relaxation time and α_* is the thermal diffusivity, which combined with the energy balance equation (3-1) leads to the hyperbolic heat conduction equation

$$\frac{1}{c_*^2}\frac{\partial^2 T_*}{\partial t_*^2} + \frac{1}{\alpha_*}\frac{\partial T_*}{\partial t_*} = \nabla_*^2 T_* \tag{3-5}$$

where $c_* = \sqrt{\alpha_*/\tau_*}$ is the speed of wave propagation. Equations (3-4) and (3-5) may be transformed into a dimensionless form by introducing the following scales L_*, L_*^2/α_* for the space variable and time variable, respectively. This leads to the following definitions of the dimensionless variables

$$x = \frac{x_*}{L_*}, \quad t = \frac{\alpha_* t_*}{L_*^2}, \quad T = \frac{\left(T_* - T_{C_*}\right)}{\left(T_{H_*} - T_{C_*}\right)} \tag{3-6}$$

that transform equations (3-4) and (3-5) into their corresponding dimensionless form

$$Fo\frac{\partial \boldsymbol{q}}{\partial t} + \boldsymbol{q} = -\nabla T \tag{3-7}$$

$$Fo\frac{\partial^2 T}{\partial t^2} + \frac{\partial T}{\partial t} = \nabla^2 T \tag{3-8}$$

where $Fo = \alpha_* \tau_* / L_*^2$ is the Fourier number. For the one-dimensional slab considered here equations (3-7) and (3-8) take the form

$$Fo\frac{\partial \boldsymbol{q}}{\partial t} + \boldsymbol{q} = -\frac{\partial T}{\partial x} \tag{3-9}$$

$$Fo\frac{\partial^2 T}{\partial t^2} + \frac{\partial T}{\partial t} = \frac{\partial^2 T}{\partial x^2} \tag{3-10}$$

The analysis and investigation of equation (3-10) was extensively covered in excellent papers and reviews, such as Özisik and Tzou (1994), Haji-Sheikh, Minkowycz and Sparrow (2002), Wang (2000), Frankel, Vick and Özisik (1985), and Vick and Özisik (1983), to name only a few. The boundary and initial conditions are expressed in the following dimensionless form

$$\begin{aligned} &x=0: T=0 \\ &x=1: T=1 \end{aligned} \tag{3-11}$$

$$t=0: \begin{cases} T=T_o=const. \\ \dot{T}=\dot{T}_o=const. \end{cases} \tag{3-12}$$

3.1.4 Hyperbolic heat conduction with Dirichlet-Neumann boundary conditions

Consider the slab as described in Figure 3-2 subject to a constant heat flux on its right wall q_{L^*}, representing the heat flux from the hot strip to the fluid due to the uniform Joule heating generated in the thin hot strip by the electric current, and a constant cold temperature T_C on the left wall. The hyperbolic conduction phenomenon is governed by the constitutive relationship between the heat flux and temperature gradient in the form shown in equation (3-4), leading to the hyperbolic heat conduction equation (3-5).

Equations (3-4) and (3-5) may be transferred into a dimensionless form by introducing the following scales L_*, L_*^2/α_*, $|q_{L^*}|$, $|q_{L^*}|L_*/k_*$ for the space variable, time variable, heat flux and temperature difference, respectively. This leads to the following definitions of the dimensionless variables

$$x=\frac{x_*}{L_*}, \quad t=\frac{\alpha_* t_*}{L_*^2}, \quad q=\frac{q_*}{|q_{L^*}|}, \quad T=\frac{(T_*-T_{C^*})\,k_*}{|q_{L^*}|\,L_*} \tag{3-13}$$

that transform equations (3-4) and (3-5) into their corresponding dimensionless form

$$Fo\frac{\partial \boldsymbol{q}}{\partial t}+\boldsymbol{q}=-\nabla T \tag{3-14}$$

$$Fo\frac{\partial^2 T}{\partial t^2}+\frac{\partial T}{\partial t}=\nabla^2 T \tag{3-15}$$

where $Fo = \alpha_* \tau_* / L_*^2$ is the Fourier number. For the one-dimensional slab considered here equations (3-14) and (3-15) take the form

$$Fo \frac{\partial q_x}{\partial t} + q_x = -\frac{\partial T}{\partial x} \tag{3-16}$$

$$Fo \frac{\partial^2 T}{\partial t^2} + \frac{\partial T}{\partial t} = \frac{\partial^2 T}{\partial x^2} \tag{3-17}$$

The analysis and investigation of equation (3-17) was extensively covered in excellent papers and reviews, such as Özisik and Tzou (1994), Haji-Sheikh, Minkowycz and Sparrow (2002), Wang (2000), Frankel, Vick and Özisik (1985), and Vick and Özisik (1983), to name only a few. The boundary and initial conditions are expressed in the following dimensionless form

$$\begin{aligned} &x = 0: \; T = 0 \\ &x = 1: q_L = -1 \;\rightarrow\; \left(\partial T / \partial x\right)_{x=1} = 1 \end{aligned} \tag{3-18}$$

$$t = 0: \begin{cases} T = T_o = const. \\ \dot{T} = \dot{T}_o = const. \end{cases} \tag{3-19}$$

Note that because the boundary heat flux at $x = 1$ is constant, equation (3-16) with $\left(\partial q_x / \partial t\right)_{x=1} = 0$, produces $\left(q_x\right)_{x=1} = -\left(\partial T / \partial x\right)_{x=1}$, a result that is identical to the Fourier boundary condition.

3.2 Fourier and Hyperbolic heat conduction in cylindrical geometry.

In this chapter the problem formulation for Fourier and Hyperbolic heat conduction in cylindrical geometry is shown, which will be separated into two subchapters indicating the different problems, Fourier and Hyperbolic, for the boundary conditions Dirichlet-Neumann.

3.2.1 Fourier heat conduction with Dirichlet-Neumann boundary conditions

Consider the cylinder as described in Figure 3-3 subject to a constant heat flux at r_{w*} q_{L*}, representing the heat flux from the hot wire to the fluid due to the uniform Joule heating generated in the thin hot wire by the electric current, and a constant cold temperature T_{C*} at r_{0*}. The Fourier conduction phenomenon is governed by the constitutive relationship between the heat flux and temperature gradient in the form shown in equation (3-2) and the energy balance equation (3-1), which lead to the Fourier heat conduction equation

$$\frac{\partial^2 T_*}{\partial r_*^2} + \frac{1}{r_*}\frac{\partial T_*}{\partial r_*} = \frac{1}{\alpha_*}\frac{\partial T_*}{\partial t_*} \tag{3-20}$$

where r_* is the independent variable in the radial direction and α_* is the thermal diffusivity.

Equation (3-20) may be transformed into a dimensionless form by introducing the following definitions of dimensionless variables

$$r = \frac{r_*}{r_{o*}} \quad ; \quad t = \frac{\alpha_* t_*}{r_{o*}^2} \tag{3-21}$$

that transform equation (3-20) into its corresponding dimensionless form

$$\frac{\partial^2 T}{\partial r^2} + \frac{1}{r}\frac{\partial T}{\partial r} = \frac{\partial T}{\partial t} \tag{3-22}$$

The boundary and initial conditions are expressed in the following dimensionless form

$$r = r_w : \frac{\partial T}{\partial r} = -1 \qquad (3\text{-}23)$$
$$r = 1 : T = 0$$

$$t = 0 : \begin{cases} T = T_o = const. \\ \dot{T} = \dot{T}_o = const. \end{cases} \qquad (3\text{-}24)$$

3.2.2 Hyperbolic heat conduction with Dirichlet-Neumann boundary conditions

Consider the cylinder as described in Figure 3-3 subject to a constant heat flux at r_{w_*} q_{0_*}, representing the heat flux from the hot wire to the fluid due to the uniform Joule heating generated in the thin hot wire by the electric current, and a constant cold temperature $T_{C,}$ at r_{0_*}. The hyperbolic conduction phenomenon is governed by the constitutive relationship between the heat flux and temperature gradient in the form shown in equation (3-4), leading to the hyperbolic heat conduction equation (3-5). Equations (3-4) and (3-5) may be transferred into a dimensionless form by introducing the following scales r_{0_*}, $r_{0_*}^2/\alpha_*$, q_{0_*}, $q_{0_*}L_*/k_*$ for the space variable, time variable, heat flux and temperature difference, respectively. This leads to the following definitions of the dimensionless variables

$$r = \frac{r_*}{r_{o*}} \quad ; \quad t = \frac{\alpha_* t_*}{r_{o*}^2}, \quad q = \frac{q_*}{q_{0_*}}, \quad T = \frac{(T_* - T_{C*})\, k_*}{q_{0_*}\, L_*} \qquad (3\text{-}25)$$

that transform equations (3-4) and (3-5) into their corresponding dimensionless form

$$Fo\frac{\partial \boldsymbol{q}}{\partial t} + \boldsymbol{q} = -\nabla T \qquad (3\text{-}26)$$

$$Fo\frac{\partial^2 T}{\partial t^2} + \frac{\partial T}{\partial t} = \nabla^2 T \qquad (3\text{-}27)$$

where $Fo = \alpha_* \tau_* / r_{0_*}^2$ is the Fourier number. For the one-dimensional slab considered here equation (3-27) takes the form

$$Fo\frac{\partial^2 T}{\partial t^2}+\frac{\partial T}{\partial t}=\frac{\partial^2 T}{\partial r^2}+\frac{1}{r}\frac{\partial T}{\partial r} \tag{3-28}$$

The boundary and initial conditions are expressed in the following dimensionless form

$$\begin{aligned} &r=r_w:\ \frac{\partial T}{\partial r}=-1 \\ &r=1:T=0 \end{aligned} \tag{3-29}$$

$$t=0:\begin{cases} T=T_o=const. \\ \dot{T}=\dot{T}_o=const. \end{cases} \tag{3-30}$$

Note that because the boundary heat flux at $r=r_w$ is constant, equation (3-26) with $\left(\partial \boldsymbol{q}/\partial t\right)_{r=r_w}=0$, produces $\left(q_r\right)_{r=r_w}=-\left(\partial T/\partial r\right)_{r=r_w}$, a result that is identical to the Fourier boundary condition.

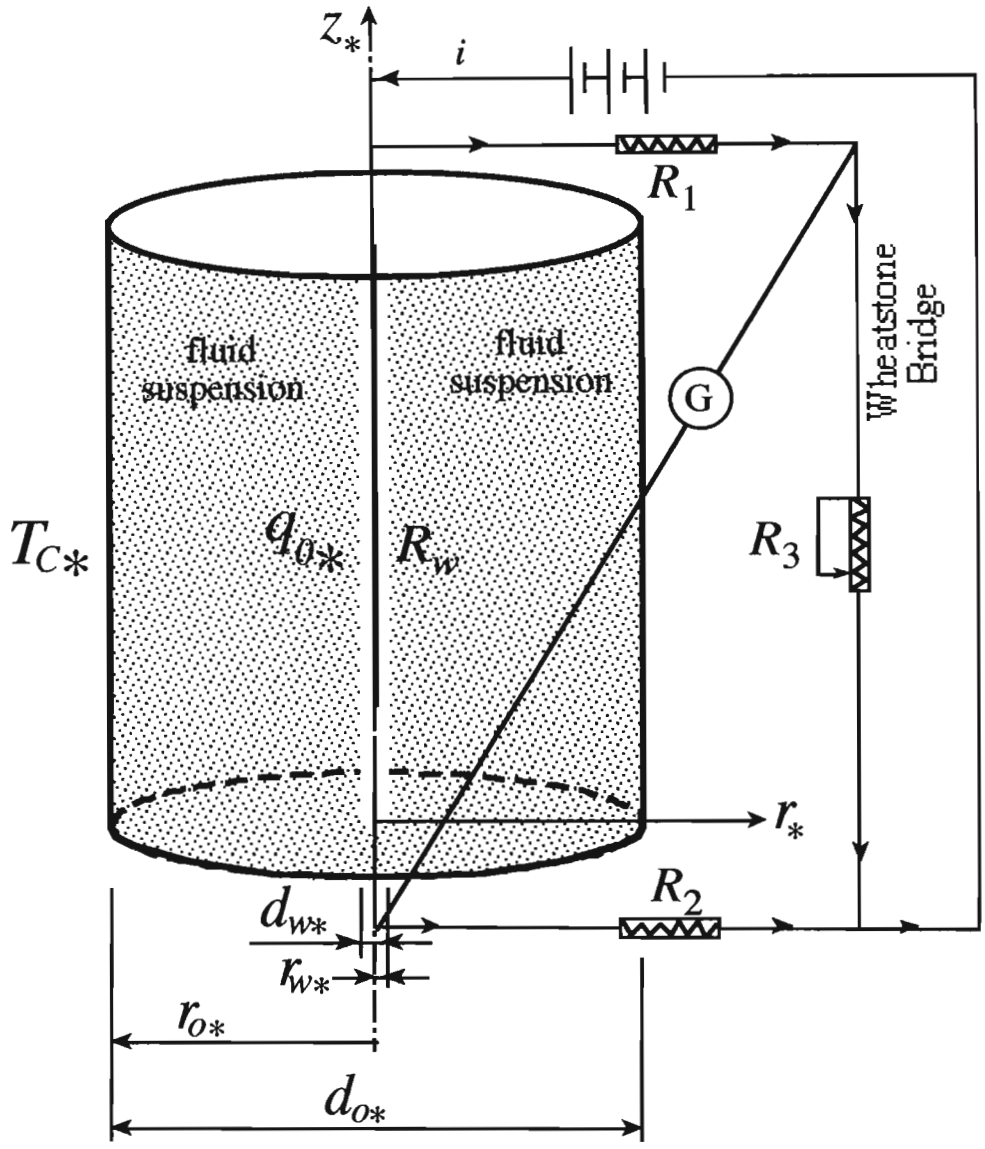

Figure 3-3: Problem formulation of heat conduction in a cylindrical annulus subject to a combination of constant temperature (Dirichlet) and constant heat flux (Neumann) boundary conditions.

CHAPTER 4

SOLUTION TO HYPERBOLIC HEAT CONDUCTION PROBLEM

4.1 Solution to the Heat Conduction Problem in rectangular geometry

In this chapter the solution for Fourier and Hyperbolic heat conduction in rectangular geometry is shown, which will be separated into five subchapters, four indicating the different problems, Fourier and Hyperbolic, for the two different types of boundary conditions, Dirichlet and Dirichlet-Neumann, and one subchapter for the calculation of the time needed by a pulse to cross the gap.

4.1.1 Solution to the Fourier heat conduction problem subject to Dirichlet boundary conditions.

While the objective of this chapter is to present the derivations of the solutions to the hyperbolic heat conduction problem the first step is to show the solution to the corresponding Fourier heat conduction. The reason for the latter is the need to have the reference Fourier solution for comparison purposes as will be shown later.

Equation (3-3b) has a steady state solution as follows

$$T_{S.} = \frac{T_{H.} - T_{C.}}{L_*} x_* + T_{C.} \tag{4-1}$$

Using the following definitions of dimensionless variables

$$x = \frac{x_*}{L_*}, \quad T = \frac{\left(T_{S.} - T_{C*}\right)}{\left(T_{H.} - T_{C.}\right)} \tag{4-2}$$

equation (4-1) can be transformed into its dimensionless form

$$T_s = x \tag{4-3}$$

The transient solution to equation (3-3) is obtained via separation of variables and can be presented as follows

$$T_{t.} = \sum_{m=1}^{\infty} C_m \cdot e^{-\alpha_{.}(m\pi/L_{.})^2 t_{.}} \cdot \sin\left(\frac{m\pi x_*}{L_*}\right) \tag{4-4}$$

where C_m is a constant which is derived from initial conditions in the form

$$C_m = C_n = 2\frac{(-1)^n(1-T_0)+T_0}{n\pi} \tag{4-5}$$

Using the following definitions of dimensionless variables

$$x = \frac{x_*}{L_*}, \quad t = \frac{\alpha_* t_*}{L_*^2} \tag{4-6}$$

equation (4-4) can be transformed into its dimensionless form

$$T_t = \sum_{n=1}^{\infty} C_n \cdot e^{-(n\pi)^2 t} \cdot \sin(\pi x) \tag{4-7}$$

Equations (4-3) and (4-7) now show the temperature profile in space and time as follows

$$T(t,x) = T_s + T_t = x + \sum_{n=1}^{\infty} C_n \cdot e^{-(n\pi)^2 t} \cdot \sin(\pi x) \tag{4-8}$$

4.1.2 Solution to the Fourier heat conduction problem subject to a combination of Dirichlet and Neumann boundary conditions.

As in the previous section equation (3-3b) still applies but with the different boundary conditions. The solutions to steady state, transient and final temperature equations in a dimensionless form are obtained via separation of variables and can be presented as follows

$$T_s = x \tag{4-9}$$

$$T_t = \sum_{n=1}^{\infty} C_n \cdot e^{-\left(\frac{\pi}{2}+n\pi\right)^2 t} \cdot \sin\left[\left(\frac{\pi}{2}+n\pi\right)x\right] \tag{4-10}$$

$$\text{where } C_n = 2\frac{T_0\left(\frac{\pi}{2}+n\pi\right)-(-1)^n}{\left(\frac{\pi}{2}+n\pi\right)^2} \tag{4-10}$$

$$T(t,x) = T_s + T_t = x + \sum_{n=1}^{\infty} C_n \cdot e^{-\left(\frac{\pi}{2}+n\pi\right)^2 t} \cdot \sin\left[\left(\frac{\pi}{2}+n\pi\right)x\right] \tag{4-11}$$

4.1.3 Solution to the Hyperbolic heat conduction problem subject to Dirichlet boundary conditions.

The solution to equation (3-10) subject to the boundary and initial conditions shown by equations (3-11) and (3-12) is expressed in terms of orthogonal eigenfunctions obtained via separation of variables in the form

$$T = x + e^{\lambda_c t}\sum_{n=0}^{M_o}\left[A_n e^{\lambda_{1sn} t} + B_n e^{\lambda_{2sn} t}\right]\sin\left[n\pi x\right] + \left[A_{n,cr} + B_{n,cr} t\right]e^{\lambda_c t}\sin\left[n_{cr}\pi x\right]\,\delta_{n_{cr},j} + e^{\lambda_c t}\sum_{n=M_1}^{\infty}\left\{\frac{A_n}{2}\left[\cos\left(n\pi x - \lambda_{in} t\right) - \cos\left(n\pi x + \lambda_{in} t\right)\right] + \frac{B_n}{2}\left[\sin\left(n\pi x - \lambda_{in} t\right) + \sin\left(n\pi x + \lambda_{in} t\right)\right]\right\} \tag{4-12}$$

where

$$\lambda_{1n} = \lambda_c + \lambda_{1sn}\ ;\ \lambda_{2n} = \lambda_c + \lambda_{2sn}\ ;\ \lambda_c = -\frac{1}{2Fo}\ ; \qquad \forall\, n < n_{cr} \quad \text{(a)}$$

$$\lambda_{1n,cr} = \lambda_{2n,cr} = \lambda_c; \qquad \forall\, n = n_{cr} \quad \text{(b)} \tag{4-13}$$

$$\lambda_{1n} = \lambda_c + i\lambda_{in}\ ;\ \lambda_{2n} = \lambda_c - i\lambda_{in}\ ;\ \lambda_c = -\frac{1}{2Fo}\ ; \qquad \forall\, n > n_{cr} \quad \text{(c)}$$

and where the following notation was introduced

$$\lambda_{1sn} = -\frac{1}{2Fo}\sqrt{1 - 4n^2\pi^2 Fo}\ ;$$

$$\lambda_{2sn} = \frac{1}{2Fo}\sqrt{1 - 4n^2\pi^2 Fo}\ ; \qquad \forall\, n < n_{cr} \tag{a}$$

$$\Delta\lambda = \frac{1}{Fo}\sqrt{1 - 4n^2\pi^2 Fo} \qquad \forall\, n < n_{cr} \quad \text{(b)} \tag{4-14}$$

$$\lambda_{in} = \frac{1}{2Fo}\sqrt{4n^2\pi^2 Fo - 1} \qquad \forall\, n > n_{cr} \quad \text{(c)}$$

while the critical value of n, i.e. n_{cr}, was evaluated and can be expressed in the form

$$n_{cr} = \frac{1}{2\pi\sqrt{Fo}} \tag{4-15}$$

For initial conditions consistent with an initial permanent constant temperature identical to that of the environment, i.e. to T_{C*}, the dimensionless values of the initial

conditions are $T_o = 0, \dot{T}_o = 0$, leading to the following expressions for the coefficients in the series (4-12)

$$A_n = \frac{2\lambda_{2n} I_{1n}}{\Delta\lambda}\ ;\quad B_n = -\frac{2\lambda_{1n} I_{1n}}{\Delta\lambda}\ ; \qquad \forall\ n < n_{cr} \qquad \text{(a)}$$

$$A_{n,cr} = 2I_{1n,cr}\ ;\quad B_n = -2\lambda_c I_{1n,cr}\ ; \qquad \forall\ n = n_{cr} \qquad \text{(b)} \qquad \text{(4-16)}$$

$$A_n = -\frac{2\lambda_c}{\lambda_{in}} I_{1n}\ ;\quad B_n = 2I_{1n}\ ; \qquad \forall\ n > n_{cr} \qquad \text{(c)}$$

where $I_{1n} = (-1)^n / n\pi$.

The infinite series in equation (4-12) consists of three separate contributions dictated by the values of M_o and M_1 defined by

$$M_o = \lfloor n_{cr} \rfloor - \delta_{n_{cr},j} = \begin{cases} (n_{cr} - 1) & \forall\ n_{cr} = j\ , \quad j = 0,1,2,3,.... \\ \lfloor n_{cr} \rfloor & \forall\ n_{cr} \neq j\ , \quad j = 0,1,2,3,.... \end{cases} \qquad \text{(4-17)}$$

$$M_1 = \lfloor n_{cr} \rfloor + 1 = \begin{cases} (n_{cr} + 1) & \forall\ n_{cr} = j\ , \quad j = 0,1,2,3,.... \\ (M_o + 1) & \forall\ n_{cr} \neq j\ , \quad j = 0,1,2,3,.... \end{cases} \qquad \text{(4-18)}$$

where $\delta_{n_{cr},j}$ is the Kronecker delta function defined in the form

$$\delta_{n_{cr},j} = \begin{cases} 1 & \forall\ n_{cr} = j\ , \quad j = 0,1,2,3,.... \\ 0 & \forall\ n_{cr} \neq j\ , \quad j = 0,1,2,3,.... \end{cases} \qquad \text{(4-19)}$$

and $\lfloor n_{cr} \rfloor$ is the *inclusive floor function* representing the largest integer less than or equal to n_{cr}. Therefore M_o is the *exclusive floor function* representing the largest integer less than n_{cr}. The first contribution is a finite series for the terms corresponding to values of $0 < n < n_{cr}$. When $n_{cr} = 0$ corresponding to $Fo = 1/\pi^2$ this contribution is absent. The second contribution is the critical term which is present only if n_{cr} is a non-negative integer. This critical term is absent when n_{cr} is not a non-negative integer, or if $Fo > 1/\pi^2$. The third contribution is an infinite series representing traveling waves that formed via a cascade of frequencies over a wide range of scales. This contribution is present at all times however it may become significantly small if $n_{cr} >> 1$.

The primary interest is the temperature value at $x = 1$, or dimensionally at $x_* = L_*$, i.e. T_L. The latter is obtained by substituting $x = 1$ into the solution (4-12) leading to

$$T_L = 1 + e^{\lambda_c t}\left[\sum_{n=0}^{M_o}\left(a_n e^{\lambda_{1sn} t} + b_n e^{\lambda_{2sn} t}\right) + \left(a_{n,cr} + b_{n,cr} t\right)\delta_{n_{cr},j} + \sum_{n=M_1}^{\infty}\left[a_n \sin(\lambda_{in} t) + b_n \cos(\lambda_{in} t)\right]\right] \tag{4-20}$$

where the coefficients are defined as follows

$$a_n = (-1)^n A_n = \frac{2\lambda_{2n}}{n\pi\Delta\lambda}; \quad b_n = (-1)^n B_n = \frac{-2\lambda_{1n}}{n\pi\Delta\lambda}; \quad \forall\, n < n_{cr} \tag{a}$$

$$a_{n,cr} = (-1)^{n_{cr}} A_{n,cr} = \frac{2}{n\pi}; \quad b_{n,cr} = (-1)^{n_{cr}} B_{n,cr} = \frac{-2\,\lambda_c}{n\pi}; \quad \forall\, n = n_{cr} \tag{b}$$

$$a_n = (-1)^n A_n = \frac{-2\lambda_c}{n\pi\lambda_{in}}; \quad b_n = (-1)^n B_n = \frac{2}{n\pi}; \quad \forall\, n > n_{cr} \tag{c}$$

(4-21)

Therefore the temperature $T_L(t)$ at $x = 1$, or dimensionally at $x_* = L_*$, can be presented following equation (4-20) in the following form

$$T_L(t) = \frac{\left[T_{L*}(t) - T_{C*}\right] k_*}{|q_{L*}|\, L_*} = 1 + h(t) \tag{4-22}$$

where

$$h(t) = e^{\lambda_c t}\left[\sum_{n=0}^{M_o}\left(a_n e^{\lambda_{1sn} t} + b_n e^{\lambda_{2sn} t}\right) + \left(a_{n,cr} + b_{n,cr} t\right)\delta_{n_{cr},j} + \sum_{n=M_1}^{\infty}\left[a_n \sin(\lambda_{in} t) + b_n \cos(\lambda_{in} t)\right]\right] \tag{4-23}$$

which produces the following dimensional solution

$$\left[T_{L*}(t) - T_{C*}\right] = \frac{|q_{L*}|\, L_*}{k_*}\left[1 + h(t)\right] \tag{4-24}$$

4.1.4 The time needed for a pulse to cross the gap in rectangular geometry.

From equation (3-5)

$$c_*^2 = \frac{\alpha_*}{\tau_*} \rightarrow c_* = \sqrt{\frac{\alpha_*}{\tau_*}} \tag{4-25}$$

where c_* is the speed of wave propagation. Any signal (pulse) will propagate in the x_* direction with speed c_*. It will cross the gap traveling a distance $L_* = c_* t_{L*}$, where t_{L*} is the time needed for the wave to cross the gap, and therefore

$$t_{L*} = \frac{L_*}{c_*} = \frac{L_*}{\sqrt{\frac{\alpha_*}{\tau_*}}} = L_* \sqrt{\frac{\tau_*}{\alpha_*}} \tag{4-26}$$

From equation (3-8) the dimensionless speed of wave propagation is $\frac{1}{\sqrt{Fo}}$ and the dimensionless gap length is 1. Therefore, the dimensionless time needed for a pulse to cross the gap is

$$t_L = \frac{1}{\frac{1}{\sqrt{Fo}}} = \sqrt{Fo} \tag{4-27}$$

4.1.5 Solution to the Hyperbolic heat conduction problem subject to a combination of Dirichlet and Neumann boundary conditions.

The solution to equation (3-10) subject to the boundary and initial conditions shown by equations (3-18) and (3-19) is expressed in terms of orthogonal eigenfunctions obtained via separation of variables in the form

$$T = x + e^{\lambda_c t}\sum_{n=0}^{M_o}\left[A_n e^{\lambda_{1sn} t} + B_n e^{\lambda_{2sn} t}\right]\sin\left[\frac{(2n+1)\pi}{2}x\right] +$$

$$\left[A_{n,cr} + B_{n,cr} t\right]e^{\lambda_c t}\sin\left[\frac{(2n_{cr}+1)\pi}{2}x\right]\delta_{n_{cr},j} +$$

$$e^{\lambda_c t}\sum_{n=M_1}^{\infty}\left\{\frac{A_n}{2}\left[\cos\left(\frac{(2n+1)\pi}{2}x - \lambda_{in} t\right) - \cos\left(\frac{(2n+1)\pi}{2}x + \lambda_{in} t\right)\right] +\right. \tag{4-28}$$

$$\left.\frac{B_n}{2}\left[\sin\left(\frac{(2n+1)\pi}{2}x - \lambda_{in} t\right) + \sin\left(\frac{(2n+1)\pi}{2}x + \lambda_{in} t\right)\right]\right\}$$

where

$$\lambda_{1n} = \lambda_c + \lambda_{1sn}\ ;\ \lambda_{2n} = \lambda_c + \lambda_{2sn}\ ;\ \lambda_c = -\frac{1}{2Fo}\ ; \qquad \forall\, n < n_{cr} \qquad \text{(a)}$$

$$\lambda_{1n,cr} = \lambda_{2n,cr} = \lambda_c ; \qquad \forall\, n = n_{cr} \qquad \text{(b)} \tag{4-29}$$

$$\lambda_{1n} = \lambda_c + i\lambda_{in}\ ;\ \lambda_{2n} = \lambda_c - i\lambda_{in}\ ;\ \lambda_c = -\frac{1}{2Fo}\ ; \qquad \forall\, n > n_{cr} \qquad \text{(c)}$$

and where we introduced the notation

$$\lambda_{1sn} = -\frac{1}{2Fo}\sqrt{1-(2n+1)^2\pi^2 Fo}\ ;$$
$$\lambda_{2sn} = \frac{1}{2Fo}\sqrt{1-(2n+1)^2\pi^2 Fo}\ ; \quad \forall\, n < n_{cr} \qquad \text{(a)}$$

$$\Delta\lambda = \frac{1}{Fo}\sqrt{1-(2n+1)^2\pi^2 Fo} \qquad \forall\, n < n_{cr} \qquad \text{(b)} \tag{4-30}$$

$$\lambda_{in} = \frac{1}{2Fo}\sqrt{(2n+1)^2\pi^2 Fo - 1} \qquad \forall\, n > n_{cr} \qquad \text{(c)}$$

while the critical value of n, i.e. n_{cr}, was evaluated and can be expressed in the form

$$n_{cr} = \frac{1}{2}\left(\frac{1}{\pi\sqrt{Fo}} - 1\right) \tag{4-31}$$

For initial conditions consistent with an initial permanent constant temperature identical to that of the environment, i.e. to T_{C*}, the dimensionless values of the initial conditions are $T_o = 0, \dot{T}_o = 0$, leading to the following expressions for the coefficients in the series (4-28)

$$A_n = \frac{2\lambda_{2n} I_{1n}}{\Delta\lambda}\ ;\quad B_n = -\frac{2\lambda_{1n} I_{1n}}{\Delta\lambda}\ ; \qquad \forall\ n < n_{cr} \qquad \text{(a)}$$

$$A_{n,cr} = 2I_{1n,cr}\ ;\quad B_n = -2\lambda_c I_{1n,cr}\ ; \qquad \forall\ n = n_{cr} \qquad \text{(b)} \qquad \text{(4-32)}$$

$$A_n = -\frac{2\lambda_c}{\lambda_{in}} I_{1n}\ ;\quad B_n = 2I_{1n}\ ; \qquad \forall\ n > n_{cr} \qquad \text{(c)}$$

where $I_{1n} = -4(-1)^n / (2n+1)^2 \pi^2$.

The infinite series in equation (4-28) consists of three separate contributions dictated by the values of M_o and M_1 defined by

$$M_o = \lfloor n_{cr} \rfloor - \delta_{n_{cr},j} = \begin{cases} (n_{cr} - 1) & \forall\ n_{cr} = j\ , \quad j = 0,1,2,3,.... \\ \lfloor n_{cr} \rfloor & \forall\ n_{cr} \neq j\ , \quad j = 0,1,2,3,.... \end{cases} \qquad \text{(4-33)}$$

$$M_1 = \lfloor n_{cr} \rfloor + 1 = \begin{cases} (n_{cr} + 1) & \forall\ n_{cr} = j\ , \quad j = 0,1,2,3,.... \\ (M_o + 1) & \forall\ n_{cr} \neq j\ , \quad j = 0,1,2,3,.... \end{cases} \qquad \text{(4-34)}$$

where $\delta_{n_{cr},j}$ is the Kronecker delta function defined in the form

$$\delta_{n_{cr},j} = \begin{cases} 1 & \forall\ n_{cr} = j\ , \quad j = 0,1,2,3,.... \\ 0 & \forall\ n_{cr} \neq j\ , \quad j = 0,1,2,3,.... \end{cases} \qquad \text{(4-35)}$$

and $\lfloor n_{cr} \rfloor$ is the *inclusive floor function* representing the largest integer less than or equal to n_{cr}. Therefore M_o is the *exclusive floor function* representing the largest integer less than n_{cr}. The first contribution is a finite series for the terms corresponding to values of $0 < n < n_{cr}$. When $n_{cr} = 0$ corresponding to $Fo = 1/\pi^2$ (see equation 4-31) this contribution is absent. The second contribution is the critical term which is present only if n_{cr} is a non-negative integer. This critical term is absent when n_{cr} is not a non-negative integer, or if $Fo > 1/\pi^2$. The third contribution is an infinite series representing traveling waves that formed via a cascade of frequencies over a wide range of scales. This contribution is present at all times however it may become significantly small if $n_{cr} >> 1$.

The primary interest is the temperature value at $x = 1$, or dimensionally at $x_* = L_*$, i.e. T_L. The latter is obtained by substituting $x = 1$ into the solution (4-28) leading to

$$T_L = 1 + e^{\lambda_c t}\left[\sum_{n=0}^{M_o}\left(a_n e^{\lambda_{1sn} t} + b_n e^{\lambda_{2sn} t}\right) + \left(a_{n,cr} + b_{n,cr} t\right)\,\delta_{n_{cr},j} + \sum_{n=M_1}^{\infty}\left[a_n \sin\left(\lambda_{in} t\right) + b_n \cos\left(\lambda_{in} t\right)\right]\right] \tag{4-36}$$

where the coefficients are defined as follows

$$a_n = (-1)^n A_n = \frac{-8\,\lambda_{2n}}{(2n+1)^2 \pi^2 \Delta\lambda}\ ; \qquad b_n = (-1)^n B_n = \frac{8\,\lambda_{1n}}{(2n+1)^2 \pi^2 \Delta\lambda}\ ; \quad \forall\, n < n_{cr} \tag{a}$$

$$a_{n,cr} = (-1)^{n_{cr}} A_{n,cr} = \frac{-8}{(2n+1)^2 \pi^2}\ ; \qquad b_{n,cr} = (-1)^{n_{cr}} B_{n,cr} = \frac{8\,\lambda_c}{(2n+1)^2 \pi^2}\ ; \quad \forall\, n = n_{cr} \tag{b}$$

$$a_n = (-1)^n A_n = \frac{8\,\lambda_c}{(2n+1)^2 \pi^2 \lambda_{in}}\ ; \qquad b_n = (-1)^n B_n = \frac{-8}{(2n+1)^2 \pi^2}\ ; \quad \forall\, n > n_{cr} \tag{c}$$

(4-37)

Therefore the temperature $T_L(t)$ at $x = 1$, or dimensionally at $x_* = L_*$, can be presented following equation (4-36) in the following form

$$T_L(t) = \frac{\left[T_{L*}(t) - T_{C*}\right] k_*}{|q_{L*}|\, L_*} = 1 + h(t) \tag{4-38}$$

where

$$h(t) = e^{\lambda_c t}\left[\sum_{n=0}^{M_o}\left(a_n e^{\lambda_{1sn} t} + b_n e^{\lambda_{2sn} t}\right) + \left(a_{n,cr} + b_{n,cr} t\right)\,\delta_{n_{cr},j} + \sum_{n=M_1}^{\infty}\left[a_n \sin\left(\lambda_{in} t\right) + b_n \cos\left(\lambda_{in} t\right)\right]\right] \tag{4-39}$$

which produces the following dimensional solution

$$\left[T_{L*}(t) - T_{C*}\right] = \frac{|q_{L*}|\, L_*}{k_*}\left[1 + h(t)\right] \tag{4-40}$$

4.2 Solution to the Heat Conduction Problem in cylindrical geometry

In this chapter the solution for Fourier and Hyperbolic heat conduction in rectangular geometry is shown, which will be separated into three subchapters, two indicating the different problems, Fourier and Hyperbolic, for the boundary conditions Dirichlet-Neumann, and the last subchapter for the calculation of the time needed by a pulse to cross the gap.

4.2.1 Solution to the Fourier heat conduction problem subject to a combination of Dirichlet and Neumann boundary conditions.

While the objective of this chapter is to present the derivations of the solutions to the hyperbolic heat conduction problem the first step is to show the solution to the corresponding Fourier heat conduction. The reason for the latter is the need to have the reference Fourier solution for comparison purposes as will be shown later.

Equation (3-22) has a steady state dimensionless solution as follows

$$T_s = -r_w \ln r \tag{4-41}$$

and a transient solution obtained via separation of variables in the form

$$T_t = \sum_{n=0}^{\infty} a_n e^{-\beta_n^2 t} R_{0n} \tag{4-42}$$

where a_n is represented by the following equation

$$a_n = \frac{I_1 - I_2}{I_3} \tag{4-43}$$

and I_1, I_2, I_3 are definite integrals with the following solutions

$$I_1 = \frac{T_0}{\beta_n}\left[\frac{2}{\pi\beta_n} - r_w R_0\left(\beta_n, r_w\right)\right] \tag{a}$$

$$I_2 = -\frac{r_w R_{0n}\left(\beta_n, r_w\right)}{\beta_n^2} \tag{b}$$

$$I_3 = N\left(\beta_n\right) = \frac{2}{\pi^2}\frac{J_0'^2\left(\beta_n r_w\right) - J_0^2\left(\beta_n\right)}{\beta_n^2 J_0'^2\left(\beta_n r_w\right)} \tag{c}$$

(4-44)

where R_{0n} is represented by a linear combination of Bessel functions as follows

$$R_{0n}(\beta_n,r)=J_0(\beta_n r)Y_0(\beta_n)-J_0(\beta_n)Y_0(\beta_n r) \tag{4-45}$$

and β_n's are the positive roots of the following

$$J_0'(\beta_n r_w)Y_0(\beta_n)-J_0(\beta_n)Y_0'(\beta_n r_w)=0 \tag{4-46}$$

where J_0 and Y_0 are the order 0 Bessel functions of the first and second kind, respectively.

This leads to the final solution for the temperature as follows

$$T=T_s+T_t=-r_w\ln r+\sum_{n=0}^{\infty}a_n e^{-\beta_n^2 t}R_{0n}(\beta_n,r) \tag{4-47}$$

4.2.2 Solution to the Hyperbolic heat conduction problem subject to a combination of Dirichlet and Neumann boundary conditions.

The solution to equation (3-28) subject to the boundary and initial conditions obtained via separation of variables by equations (3-29) and (3-30) is expressed in terms of orthogonal eigenfunctions in the form

$$\begin{aligned}T=T_s+T_t=&-r_w\ln r+\sum_{n=1}^{n_{cr}-1}A_{n1}\left(e^{\lambda_1 t/Fo}-\lambda_{ND1}e^{\lambda_2 t/Fo}\right)R_0(\beta_n r)+\\&A_{n2}e^{\lambda t/Fo}(1-\lambda t/Fo)R_0(\beta_{n_{cr}}r)+\\&\sum_{n_{cr}+1}^{\infty}A_{n_{cr}}e^{\lambda_r t/Fo}\left[\cos(\lambda_{in}t/Fo)-\lambda_{ND2}\sin(\lambda_{in}t/Fo)\right]R_0(\beta_n r)\end{aligned} \tag{4-48}$$

where

$$\lambda_{1,2}=-\frac{1}{2}\left(1\pm\sqrt{1-4Fo\beta^2}\right) \qquad \forall\ \beta<\beta_{cr} \tag{4-49}$$

$$\lambda=-\frac{1}{2} \qquad \forall\ \beta=\beta_{cr} \tag{4-50}$$

$$\lambda_r=-\frac{1}{2} \qquad \forall\ \beta>\beta_{cr} \tag{4-51}$$

$$\lambda_{in}=\frac{1}{2}\sqrt{4Fo\beta^2-1} \qquad \forall\ \beta>\beta_{cr} \tag{4-52}$$

$$\lambda_{ND1} = \frac{\lambda_1}{\lambda_2} \tag{4-53}$$

$$\lambda_{ND2} = \frac{\lambda_r}{\lambda_{in}} \tag{4-54}$$

$$A_{n1} = \frac{I_1 - I_2}{\left(1 - \frac{\lambda_1}{\lambda_2}\right) I_3} \qquad \forall \ \beta < \beta_{cr} \qquad \text{(a)}$$

$$A_{n2} = A_{n_{cr}} = \frac{I_1 - I_2}{I_3} \qquad \forall \ \beta = \beta_{cr} \qquad \text{(b)} \tag{4-55}$$

$$A_{n3} = A_{n2} = \frac{I_1 - I_2}{I_3} \qquad \forall \ \beta > \beta_{cr} \qquad \text{(c)}$$

and I_1, I_2, I_3 are definite integrals with the following solutions

$$I_1 = \frac{T_0}{\beta_n}\left[\frac{2}{\pi\beta_n} - r_w R_0\left(\beta_n, r_w\right)\right] \qquad \text{(a)}$$

$$I_2 = -\frac{r_w R_{0n}\left(\beta_n, r_w\right)}{\beta_n^2} \qquad \text{(b)} \tag{4-56}$$

$$I_3 = N\left(\beta_n\right) = \frac{2}{\pi^2}\frac{J_0'^2\left(\beta_n r_w\right) - J_0^2\left(\beta_n\right)}{\beta_n^2 J_0'^2\left(\beta_n r_w\right)} \qquad \text{(c)}$$

where R_{0n} is represented by a linear combination of Bessel functions as follows

$$R_{0n}\left(\beta_n, r\right) = J_0\left(\beta_n r\right) Y_0\left(\beta_n\right) - J_0\left(\beta_n\right) Y_0\left(\beta_n r\right) \tag{4-57}$$

and β_n's are the positive roots of the following equation

$$J_0'\left(\beta_n r_w\right) Y_0\left(\beta_n\right) - J_0\left(\beta_n\right) Y_0'\left(\beta_n r_w\right) = 0 \tag{4-58}$$

where J_0 and Y_0 are the order 0 Bessel functions of the first and second kind, respectively.

The critical value of n, i.e. n_{cr}, cannot be evaluated analytically but only numerically. β_{cr} can be expressed by equating the square root in equation (4-49) to zero, as follows

$$\beta_{cr} = \frac{1}{2\sqrt{Fo}} \tag{4-59}$$

4.2.3 The time needed for a pulse to cross the gap in cylindrical geometry.

The dimensionless distance between the wire and the cylinder wall is $(1-r_w)$ and the dimensionless speed of wave propagation from equation (3-8) is $1/\sqrt{Fo}$, hence the dimensionless time needed for the thermal pulse to cross the annulus gap is

$$t_w = \frac{(1-r_w)}{\frac{1}{\sqrt{Fo}}} = (1-r_w)\sqrt{Fo} \tag{4-60}$$

Its corresponding dimensional time is

$$t_{w*} = \left(r_{0*} - r_{w*}\right)\sqrt{\tau_* / \alpha_*} \tag{4-61}$$

CHAPTER 5
RESULTS AND DISCUSSION

5.1 Analytical solution evaluated using Fortran.

All the results of temperature as a function of time and space presented in the previous section were evaluated by Fortran programming. Also the results for the thermal conductivity ratio and wire temperature versus time were derived using Fortran programming. The Fortran computer language programs were written to show results of temperature vs. time and vs. space for Fourier and Hyperbolic heat conduction in rectangular and cylindrical geometries. In the rectangular geometry the space is represented by x and in the cylindrical one by r, where x and r represent the independent variables in each coordinate system respectively. The results were then plotted graphically to observe the outcome. The numerical method used to calculate β is ZBRENT, which is found in the numerical recipes in the Fortran program. ZBRENT is the combination of advantages of the bisection and Ridders methods of root finding. The accuracy of the root is 10^{-7}.

5.2 Results for the Fourier heat conduction problem subject to Dirichlet boundary conditions.

The computed analytical results of temperature vs. x and vs. t for Fourier heat conduction subject to Dirichlet boundary conditions at different t and x values, respectively are being presented in Figures 5-1 and 5-2. As expected the temperature profile moves from right to left with increasing time until steady state is reached at t = 0.5 as shown in Figure 5-1. Figure 5-2 shows the expected temperature profile vs. time at different points in the medium. The results correspond to those in Figure 5-1 which shows that steady state is reached at t = 0.5 as the temperature curves level to a constant line parallel to the time axis.

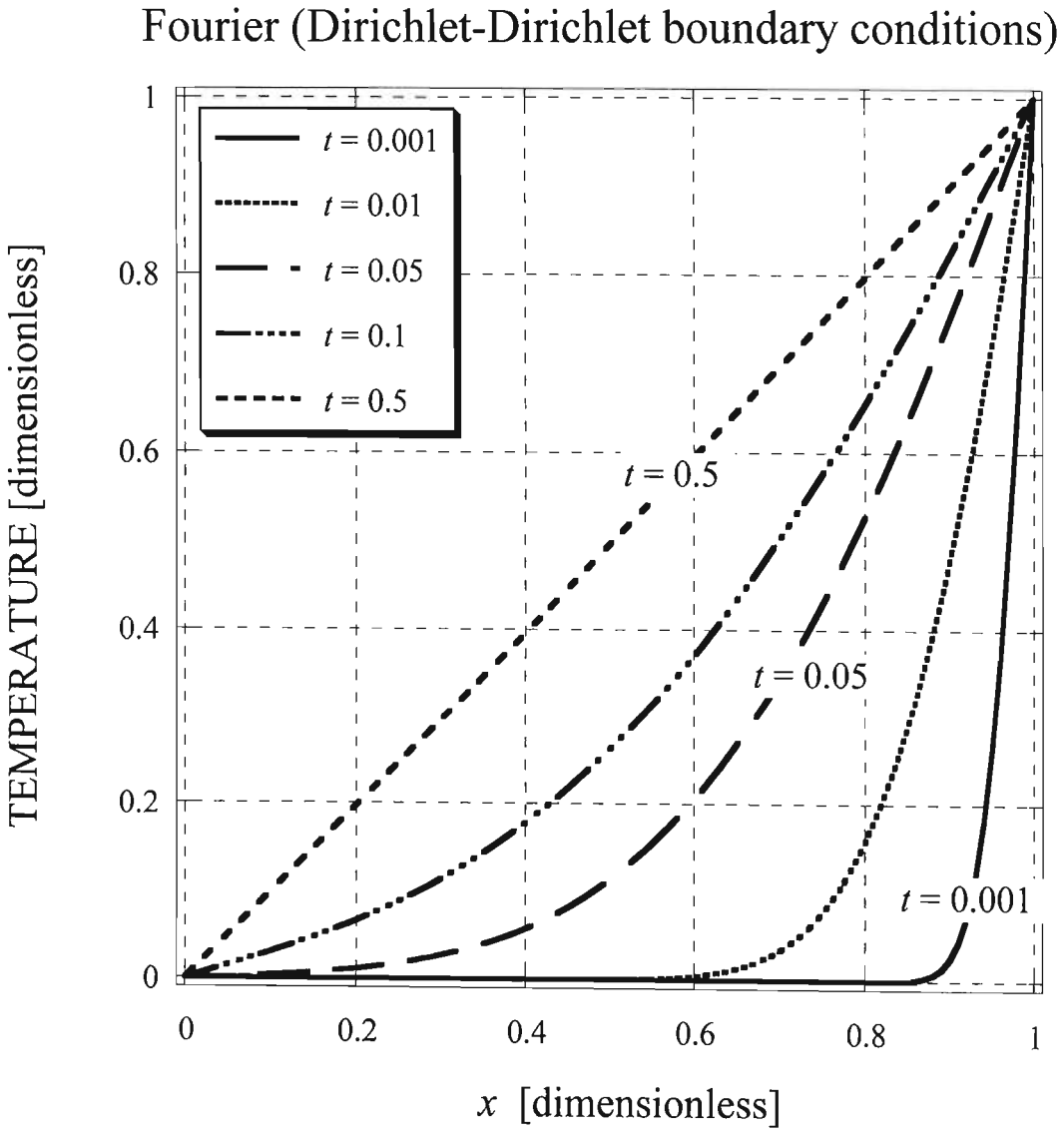

Figure 5-1: Temperature vs. x in dimensionless form using Dirichlet boundary conditions in the Fourier heat conduction problem.

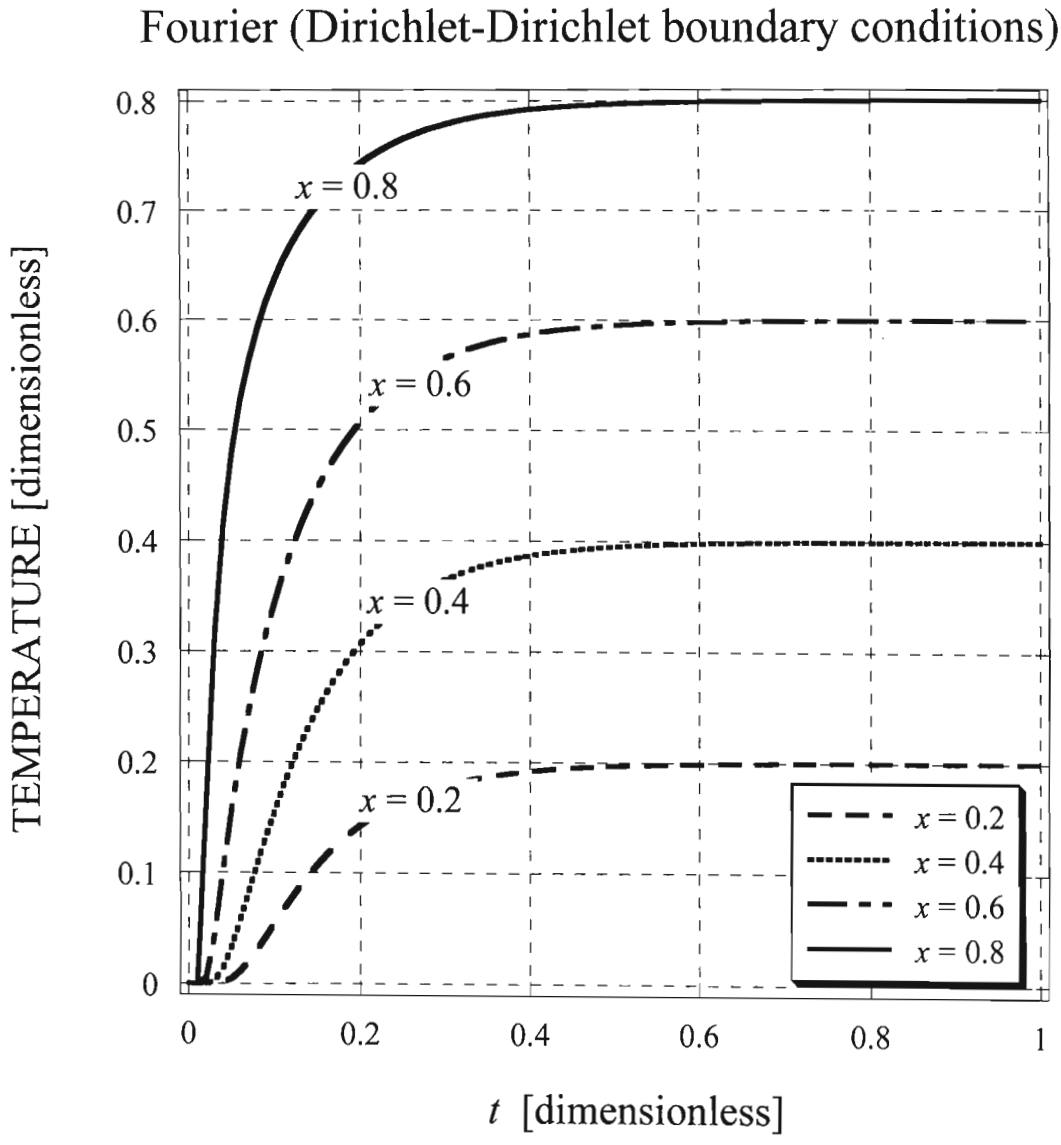

Figure 5-2: Temperature vs. t in dimensionless form using Dirichlet boundary conditions in the Fourier heat conduction problem.

5.3 Results for the Fourier heat conduction problem subject to a combination of Dirichlet and Neumann boundary conditions.

5.3.1 Rectangular geometry.

With the combination of Dirichlet and Neumann boundary conditions Figure 5-3 shows how the temperature reaches steady state as the temperature profile develops moving from right to the left. The difference between this case and that of Dirichlet-Dirichlet boundary conditions is seen at the right wall (boundary). While in Figure 5-1 the temperature at the right boundary is always constant at 1, Figure 5-3 shows how the temperature starts just below 0.2 for a time $t = 0.02$ and rises to 1 at $t = 5$. This is the case since there is a constant heat flux applied to this boundary shown in Figure 5-3 by the constant slope of the curves at $x = 1$ and a constant temperature in Figure 5-1. The constant heat flux would cause a constant temperature gradient at the boundary, which is seen in Figure 5-3. In Figure 5-4 the temperature is plotted versus time at different values for x.

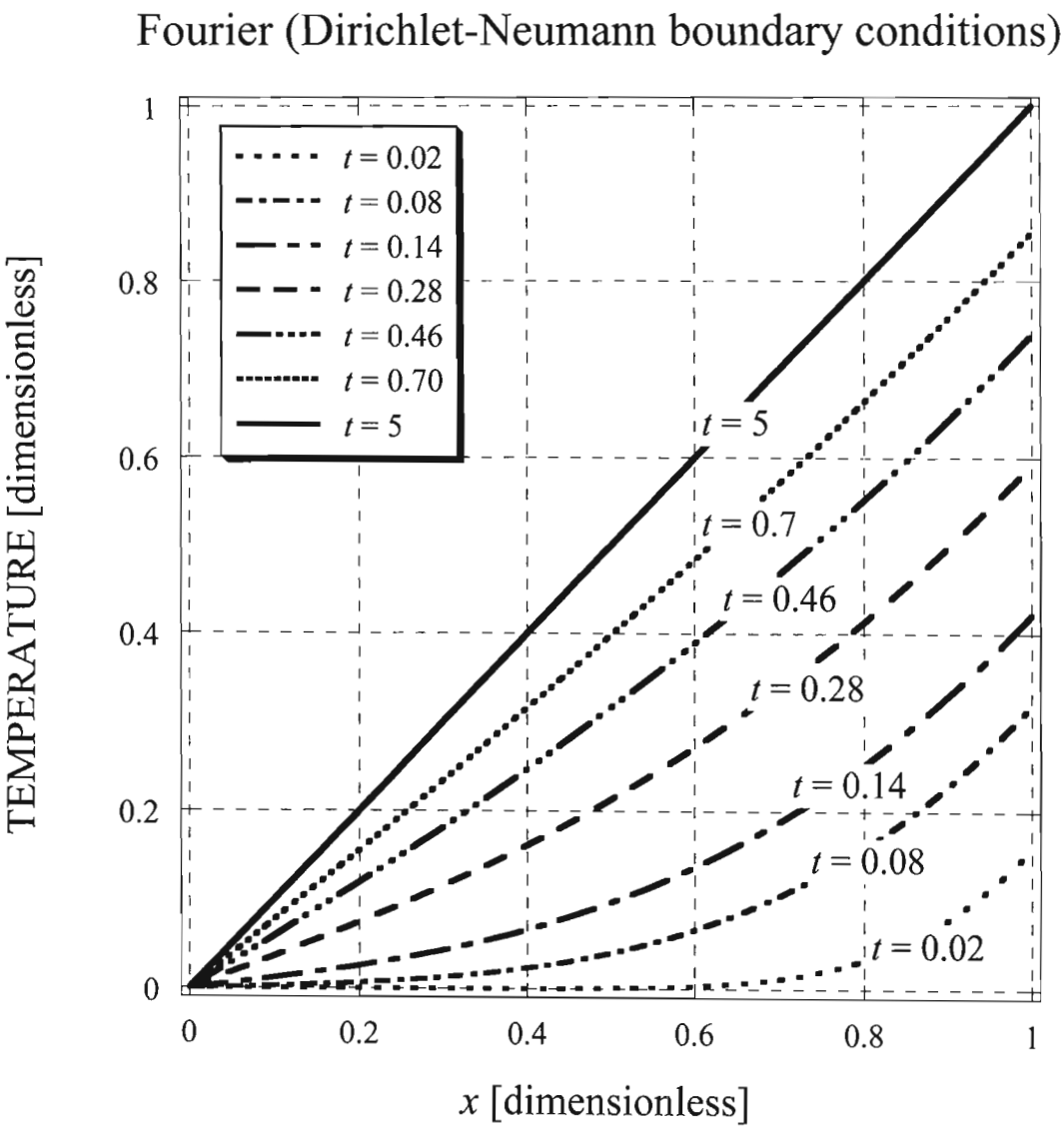

Figure 5-3: Temperature vs. x in dimensionless form using a combination of Dirichlet and Neumann boundary conditions in the Fourier heat conduction problem.

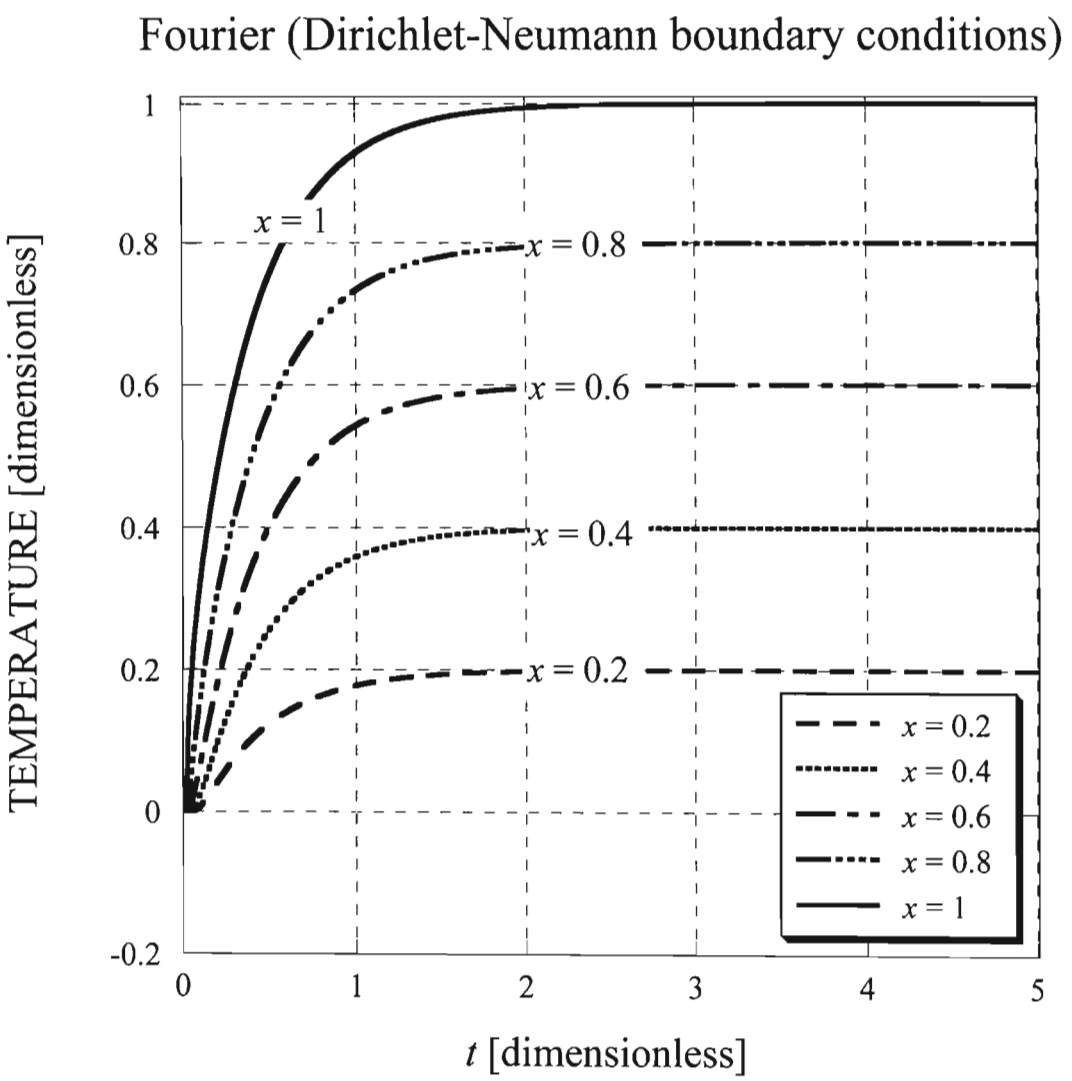

Figure 5-4: Temperature vs. t in dimensionless form using a combination of Dirichlet and Neumann boundary conditions in the Fourier heat conduction problem.

5.3.2 Cylindrical geometry.

The results of temperature vs. r at different values of time are presented in Figure 5-5 for Fourier heat conduction in a cylindrical geometry. Here the steady state is not as easy to recognize because it is logarithmic rather than linear in r, which leads to Figure 5-6, which shows the r axis on a logarithmic scale. This way it is easier to recognize the steady state since a straight line as seen in Figure 5-6 represents it. In Figure 5-7 the temperature is plotted versus time, but now with different values for r, one of which is the inner radius (r_w = 0.002). Since there is a heat flux at this boundary the temperature is not constant as can be seen until steady state is reached.

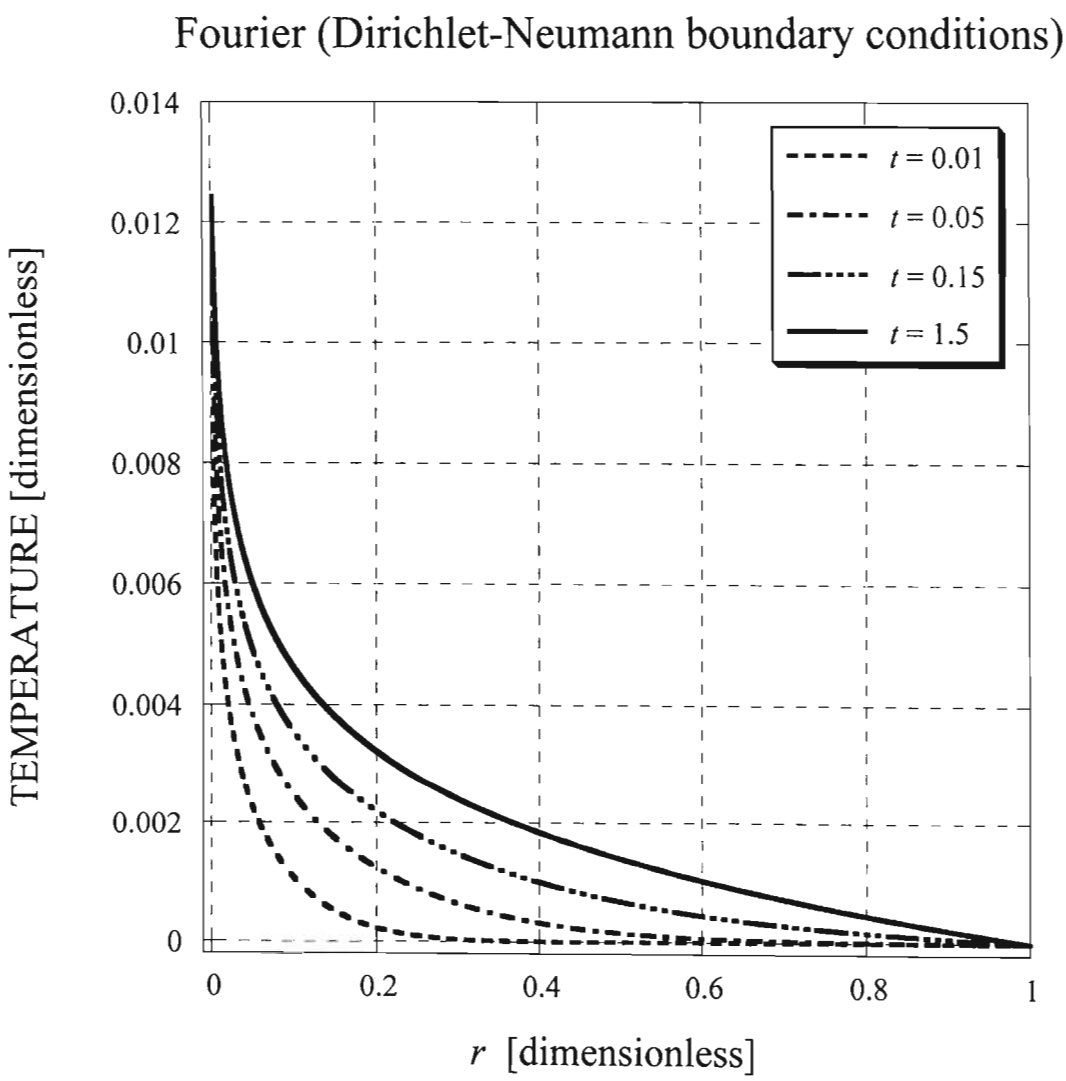

Figure 5-5:Temperature vs. r in dimensionless form using a combination of Dirichlet and Neumann boundary conditions in the Fourier heat conduction problem.

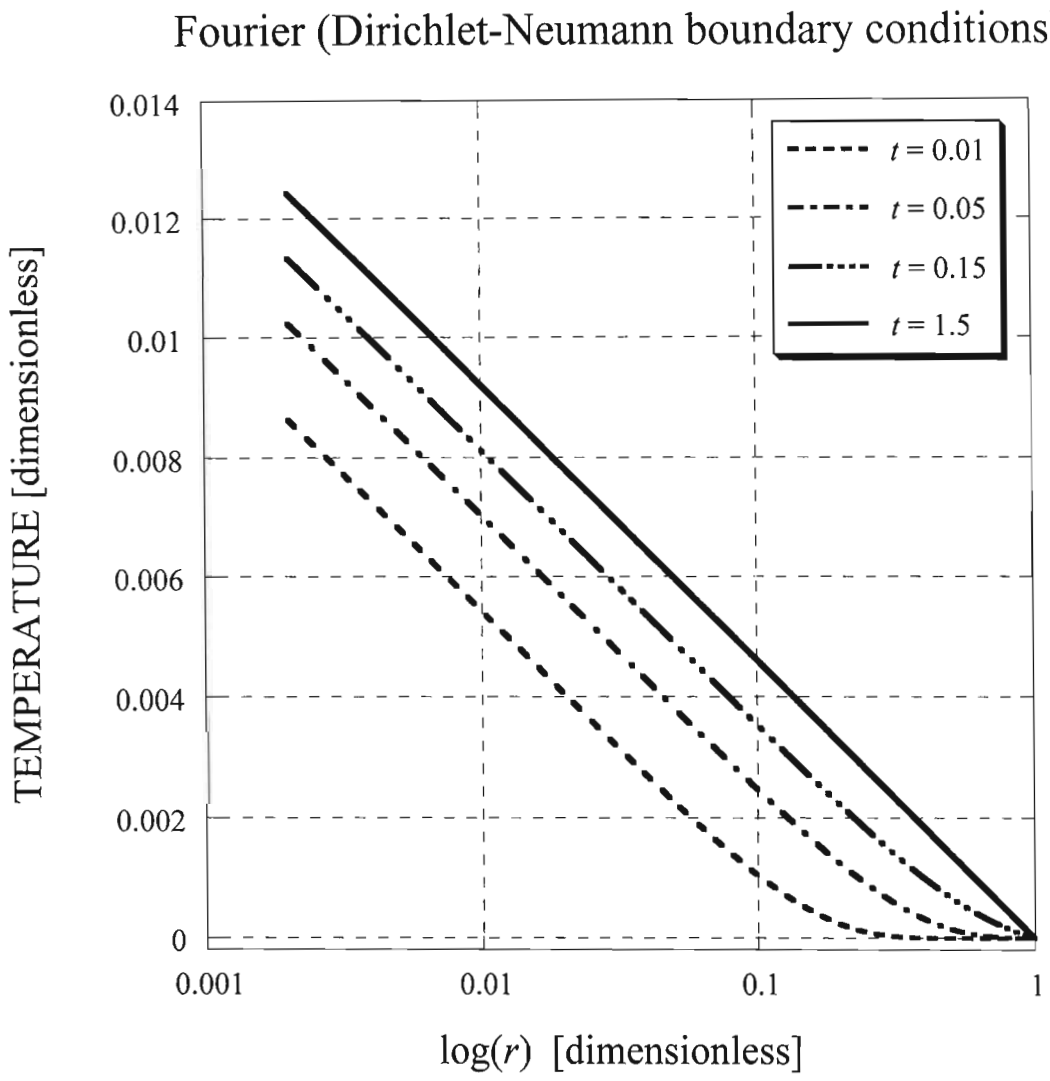

Figure 5-6:Temperature vs. log(*r)* in dimensionless form using a combination of Dirichlet and Neumann boundary conditions in the Fourier heat conduction problem.

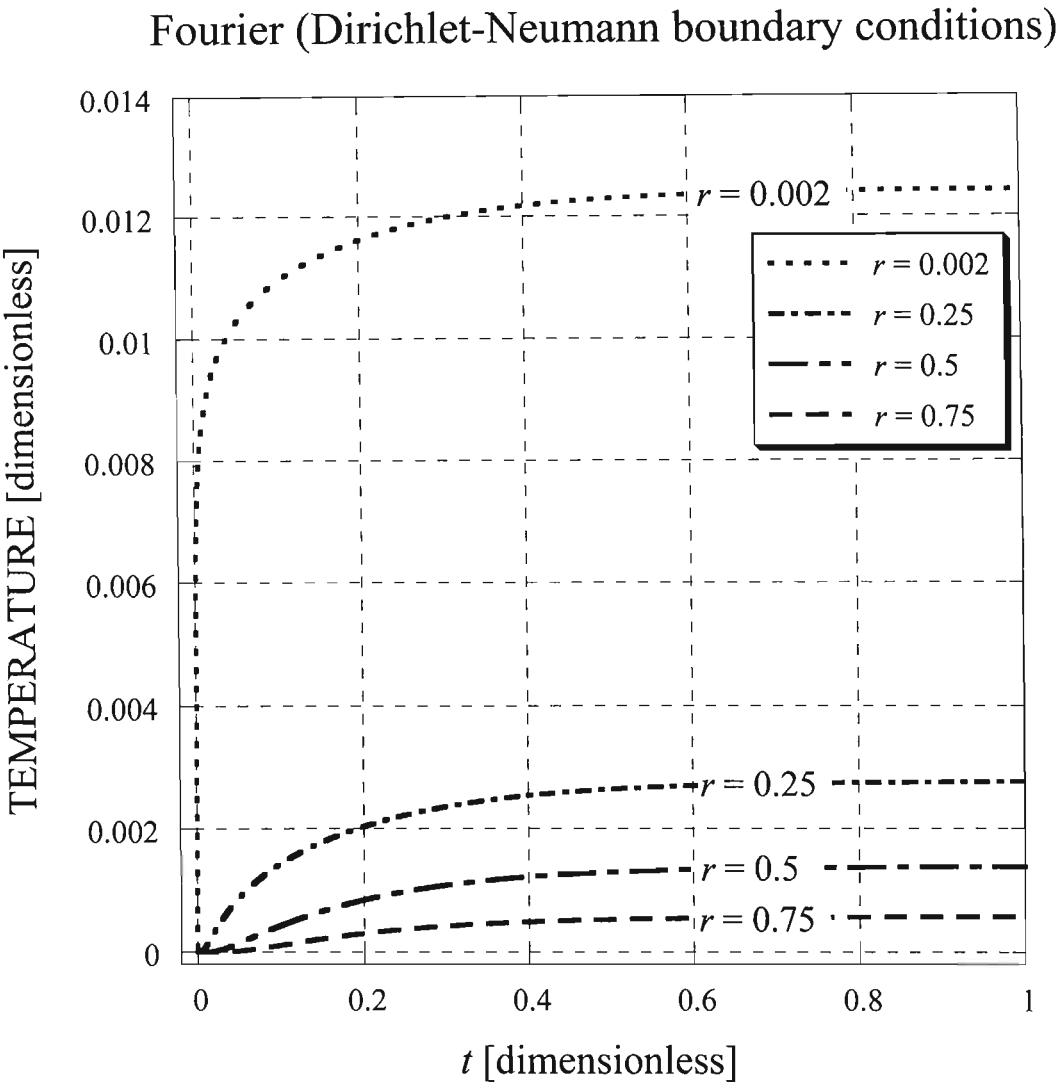

Figure 5-7:Temperature vs. t in dimensionless form using a combination of Dirichlet and Neumann boundary conditions in the Fourier heat conduction problem.

5.4 Results for the hyperbolic heat conduction problem subject to Dirichlet boundary conditions in rectangular geometry.

In hyperbolic heat conduction the Fourier number plays a significant role as it impacts the temperature in space and time. In Figure 5-8 one can see the evolution of the temperature profile towards the steady state for $Fo = 10^{-4}$. It is obvious that for such a small Fourier number the hyperbolic conduction solution is expected to be almost identical to the Fourier conduction solution presented in Figure 5-1. Indeed, Figure 5-8 shows a nearly Fourier conduction result in terms of the evolution of the temperature profile towards steady state. This anticipation is based on the fact that equation (3-17) transforms into the Fourier diffusion equation when $Fo \to 0$ (or $Fo \ll 1$). No wave effects are visible in the results presented in Figure 5-8. Increasing the Fourier number to $Fo = 0.01$ as seen in Figure 5-9 causes discontinuity in the temperature gradient that represents the location of the moving front transferring the boundary temperature "signal" within the domain. This can be seen in Figures 5-10 to 5-12 for $Fo = 0.1$. In Figure 5-10 the front moves from the right boundary to the left with the moving front decreasing in magnitude. Figure 5-11 shows the front moving back to the right boundary from the left (reflected back), while the moving front magnitude decreases further. Finally Figure 5-12 shows the front moving toward the left boundary again with steady state being achieved before the front reaches the left boundary. The time needed for a pulse to cross the gap is calculated using equation (4-27). It is seen that the temperatures reach steady state values for all the x values. The graphs in Figures 5-13 to 5-15 show the temperature versus time at different values for x for $Fo = 0.1$. In all three Figures 5-13 to 5-15 it is seen that the temperature reaches the expected steady state values. The discontinuity in Figures 5-13 to 5-15 before steady state is reached is due to the front propagation mentioned earlier. At each point of discontinuity in Figures 5-13 to 5-15 the wave passes through the corresponding value of x as it bounces back and fourth between the boundaries. Figures 5-16 to 5-22 corresponding to $Fo = 1$ show the front even better as it moves from one boundary to the other and back over and over, until steady state is reached at about $t = 9$ (Figure 5-22). The moving front in Figures 5-16 to 5-22 is also seen better as its amplitude reduces with time. In Figures 5-23 and 5-24 the temperature is plotted versus time at different values for x and for $Fo = 10^{-4}$ and $Fo = 10^{-3}$, respectively. In Figures 5-23 and 5-24 there is no discontinuity as seen in

Figures 5-13 to 5-15 in the temperature. The reason for the lack of discontinuity in temperature in Figures 5-23 and 5-24 is because the solution for such small Fourier number follows almost identically the Fourier conduction solution. As mentioned before, with a small Fourier number the hyperbolic conduction solution is almost the same as for the Fourier conduction.

Figures 5-25 to 5-27 show the front propagation from boundary to boundary most clearly. With Fo = 1 Figures 5-25 to 5-27 show the temperature versus time at different values for x. The oscillatory effect is shown and explains the moving front that starts and decays with time until steady state is reached. The time between peaks shows the bouncing period of the pulse. The period is calculated using equation (4-27) that is $t_p = \sqrt{Fo}$ and is identical to the bouncing period revealed in the graphs plotted in Figures 5-25 to 5-27. To compare the values from equation (4-27) and the graphs plotted for the time needed for a pulse to cross the gap, Figures 5-25 to 5-27 show the clearest comparison. One adjustment needs to be made to equation (4-27) to account for this calculation in each of the Figures 5-25 to 5-27. Equation (4-27) calculates the time for the pulse to cross the whole gap, whereas in Figures 5-25 to 5-27 the pulse is relative to different values of x. Looking at the graphs in Figures 5-25 to 5-27 the time between the beginning of each peak represent the time for the pulse to cross the gap twice. Therefore from the graphs in Figures 5-25 to 5-27 for Fo = 1 the time between each peak is equal to 2. From equation (4-27) with Fo = 1 the time needed for the pulse to cross the gap once is 1. Therefore the graphs in Figures 5-25 to 5-27 yield the expected results from equation (4-27). These results are seen for all values of Fourier number. Looking at the graphs in Figures 5-13 to 5-15 with Fo = 0.1 the time between peaks is approximately 0.63. Substituting Fo = 0.1 into equation (4-27) yields 0.316, which is approximately half of 0.63. This shows that for all values of Fo the expected result from equation (4-27) is obtained from the presented results.

$Fo = 10^{-4}$

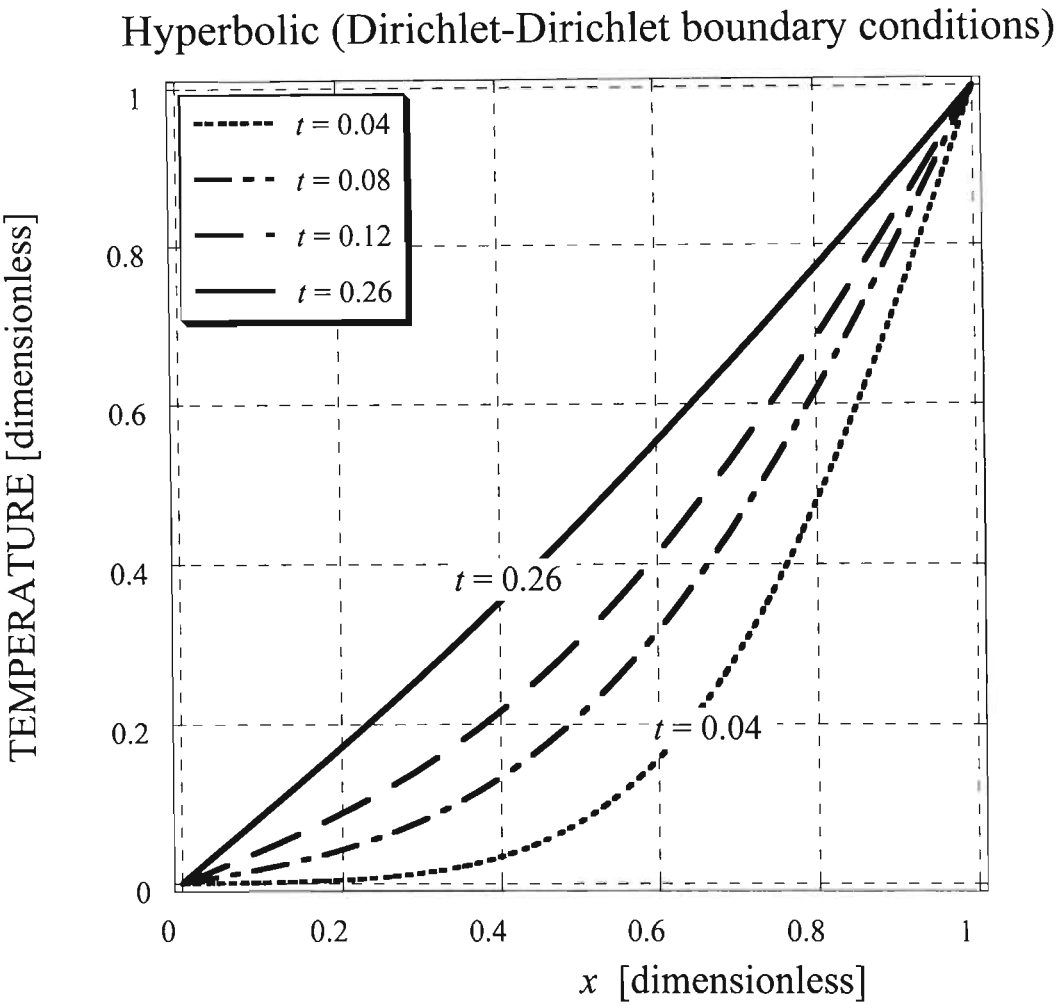

Figure 5-8:Temperature vs. x in dimensionless form using Dirichlet boundary conditions in the Hyperbolic heat conduction problem with Fourier number equal to 10^{-4}.

$Fo = 0.01$

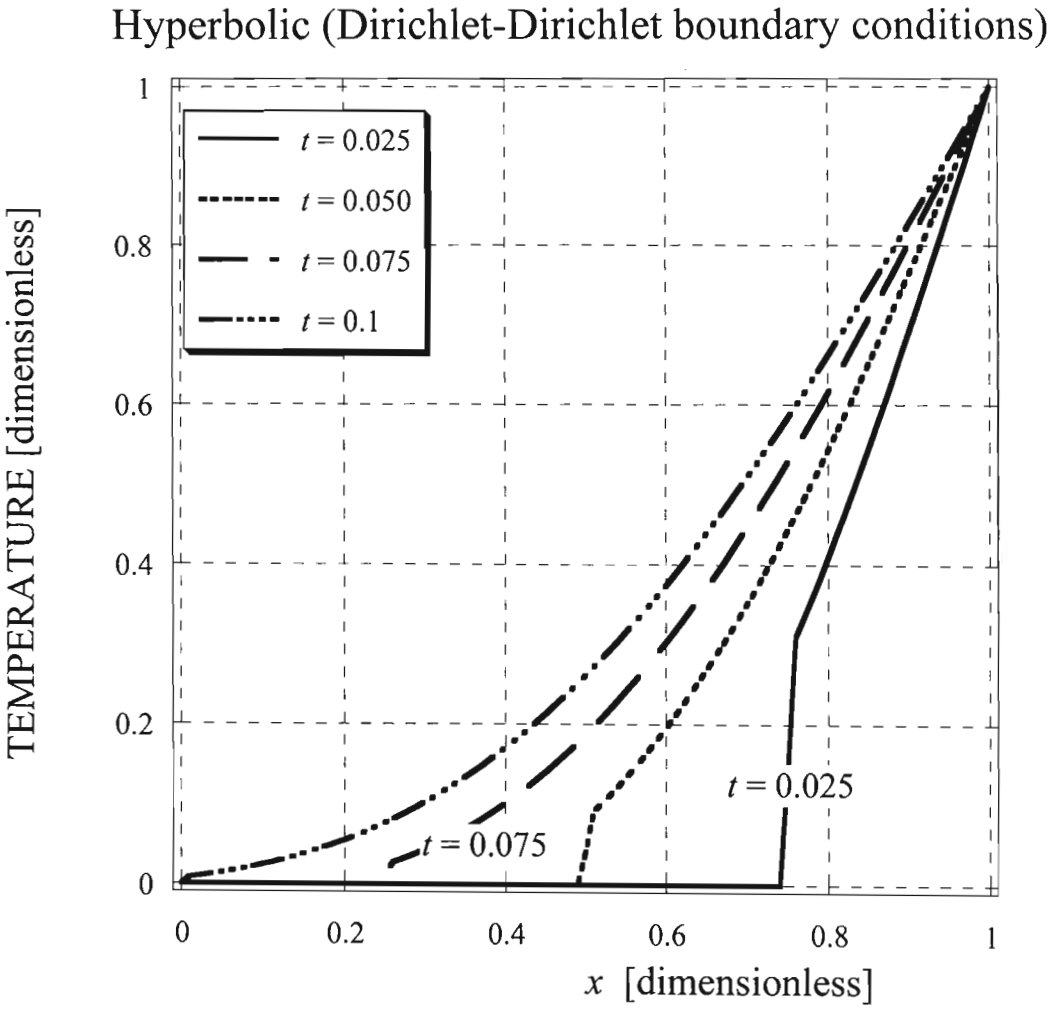

Figure 5-9:Temperature vs. x in dimensionless form using Dirichlet boundary conditions in the Hyperbolic heat conduction problem with Fourier number equal to 0.01.

$Fo = 0.1$

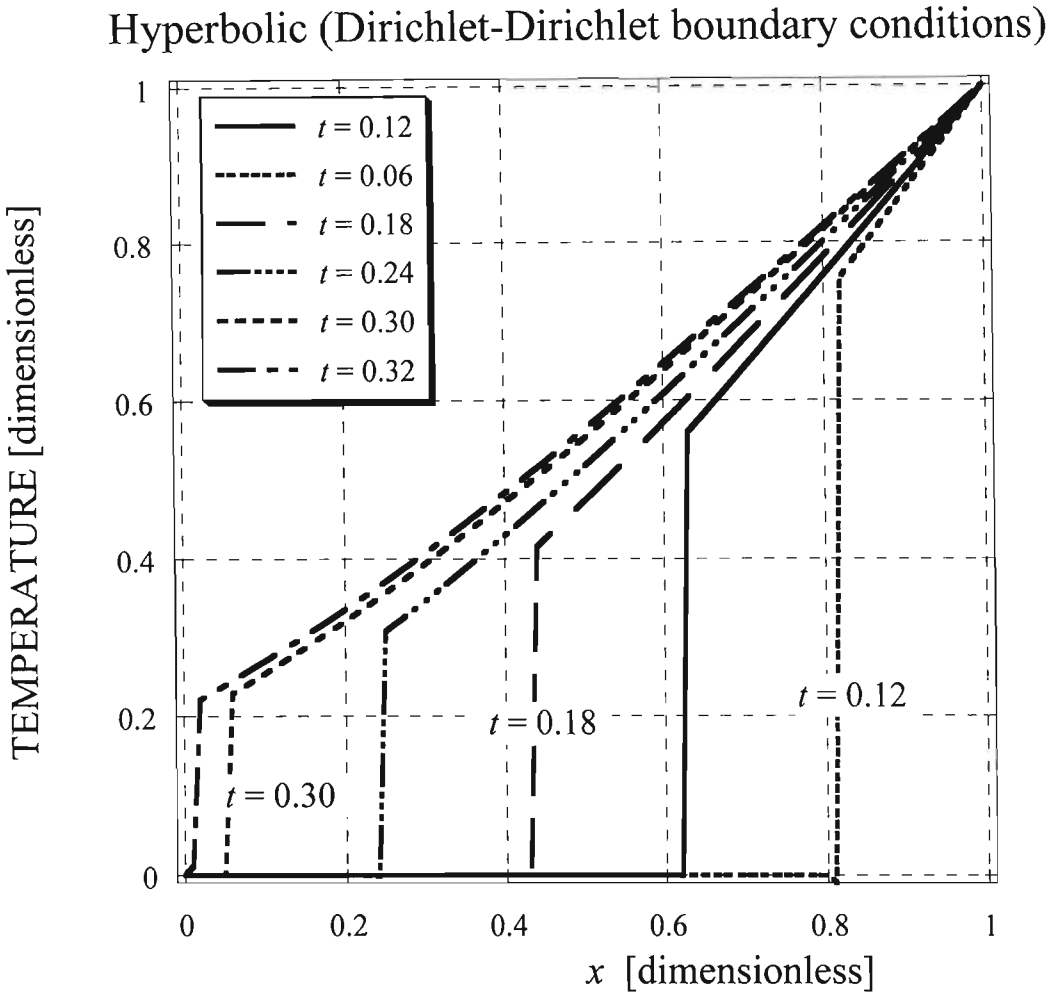

Figure 5-10:Temperature vs. x in dimensionless form using Dirichlet boundary conditions in the Hyperbolic heat conduction problem with Fourier number equal to 0.1.

$Fo = 0.1$

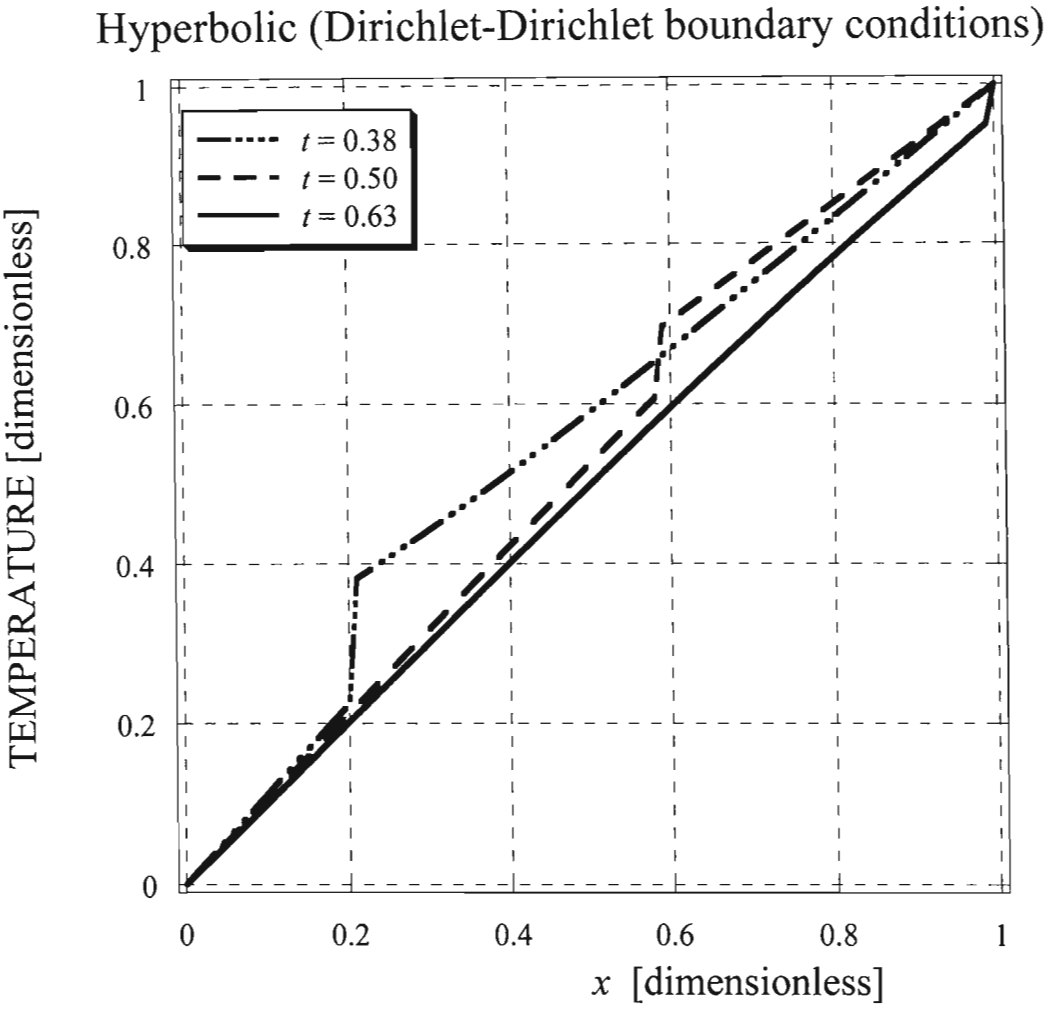

Figure 5-11:Temperature vs. x in dimensionless form using Dirichlet boundary conditions in the Hyperbolic heat conduction problem with Fourier number equal to 0.1.

$Fo = 0.1$

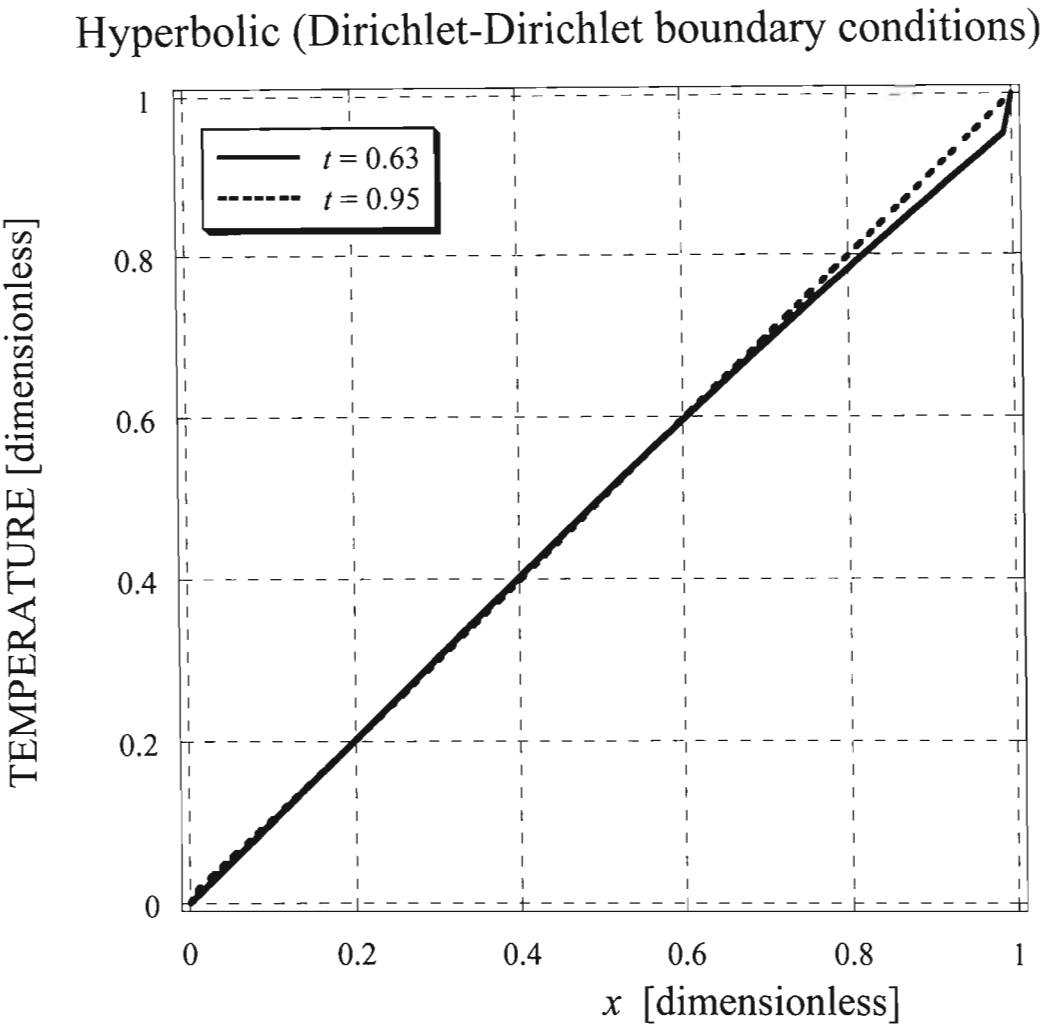

Figure 5-12:Temperature vs. x in dimensionless form using Dirichlet boundary conditions in the Hyperbolic heat conduction problem with Fourier number equal to 0.1.

$Fo = 0.1$

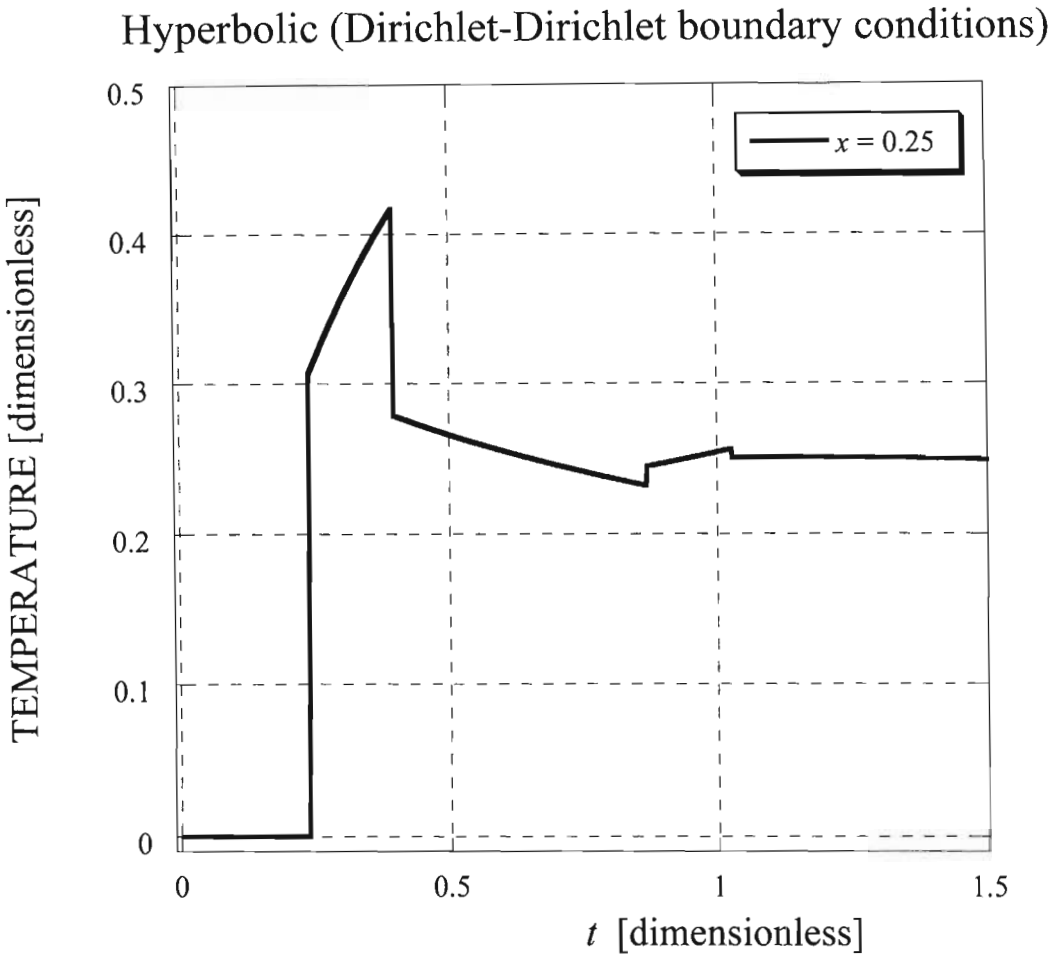

Figure 5-13:Temperature vs. t in dimensionless form using Dirichlet boundary conditions in the Hyperbolic heat conduction problem with Fourier number equal to 0.1.

$Fo = 0.1$

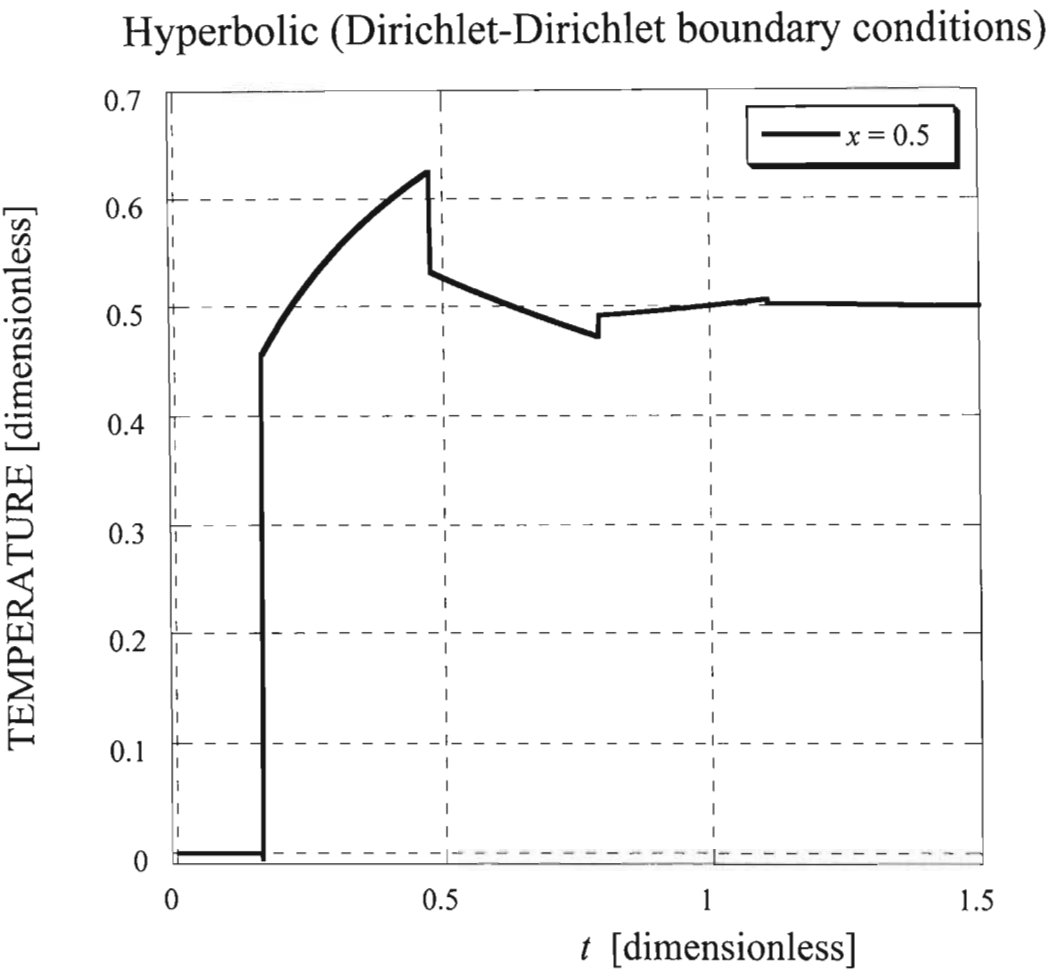

Figure 5-14:Temperature vs. t in dimensionless form using Dirichlet boundary conditions in the Hyperbolic heat conduction problem with Fourier number equal to 0.1.

$Fo = 0.1$

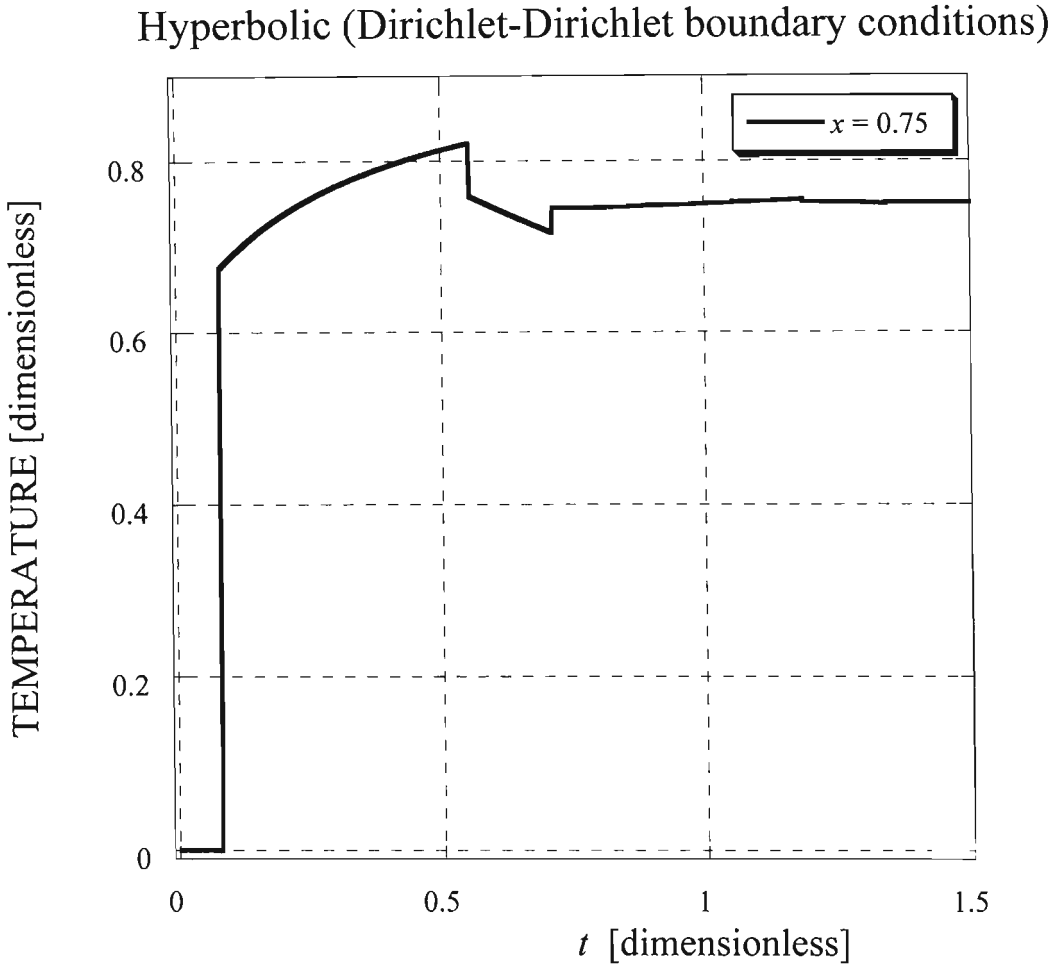

Figure 5-15:Temperature vs. t in dimensionless form using Dirichlet boundary conditions in the Hyperbolic heat conduction problem with Fourier number equal to 0.1.

$Fo = 1$

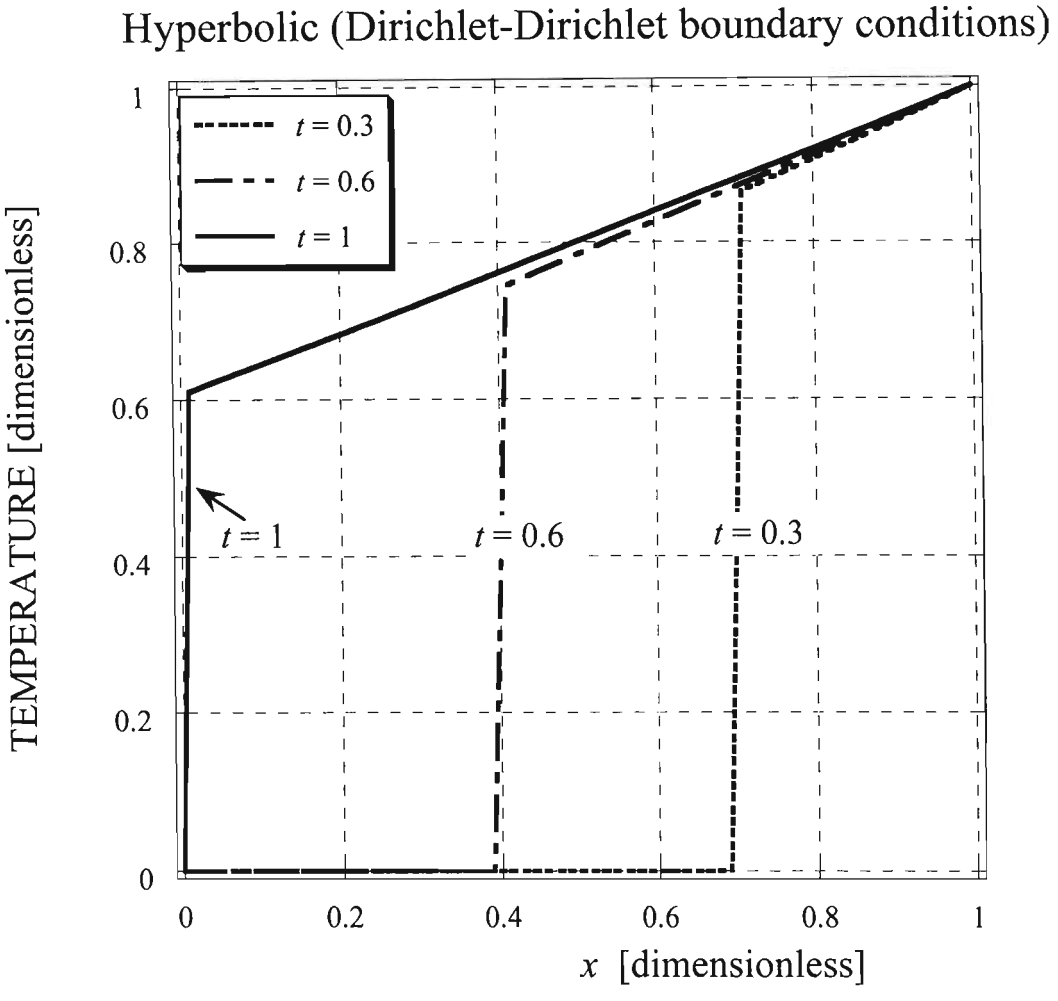

Figure 5-16:Temperature vs. x in dimensionless form using Dirichlet boundary conditions in the Hyperbolic heat conduction problem with Fourier number equal to 1.

$Fo = 1$

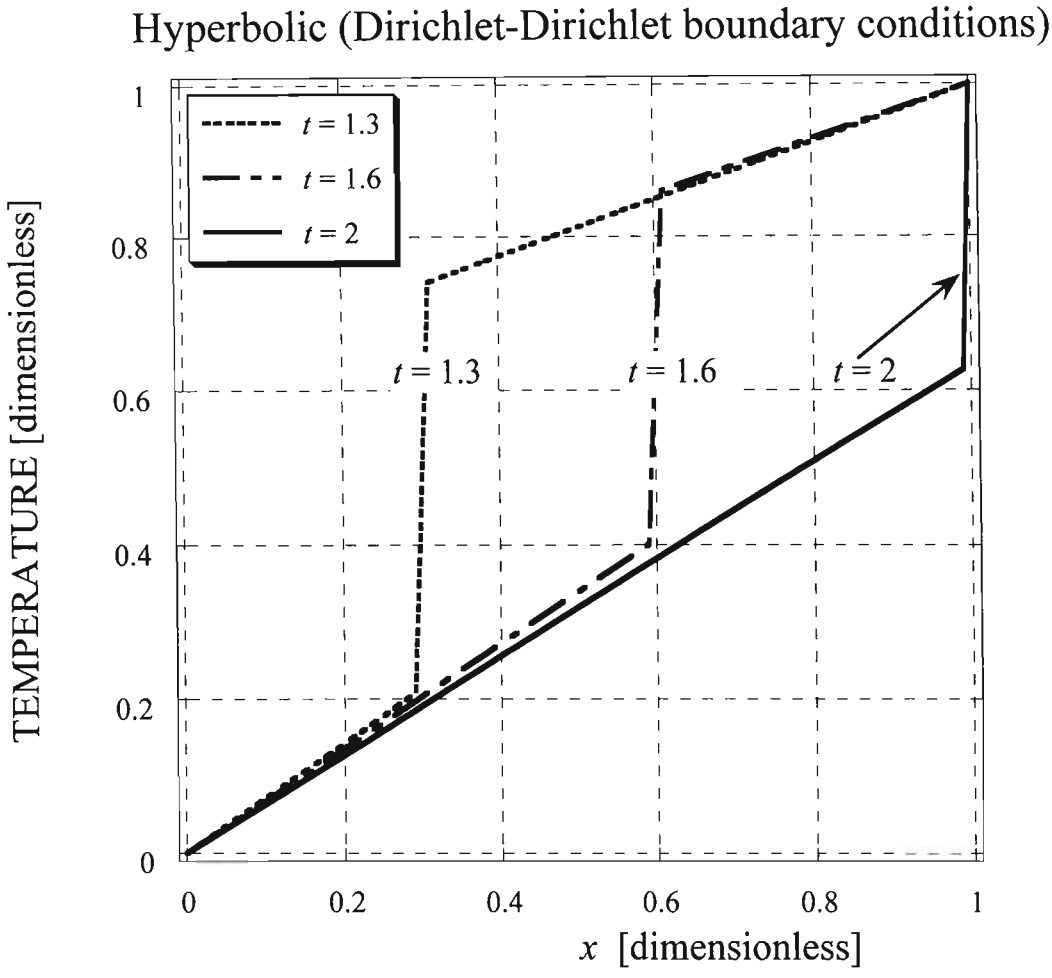

Figure 5-17:Temperature vs. x in dimensionless form using Dirichlet boundary conditions in the Hyperbolic heat conduction problem with Fourier number equal to 1.

$Fo = 1$

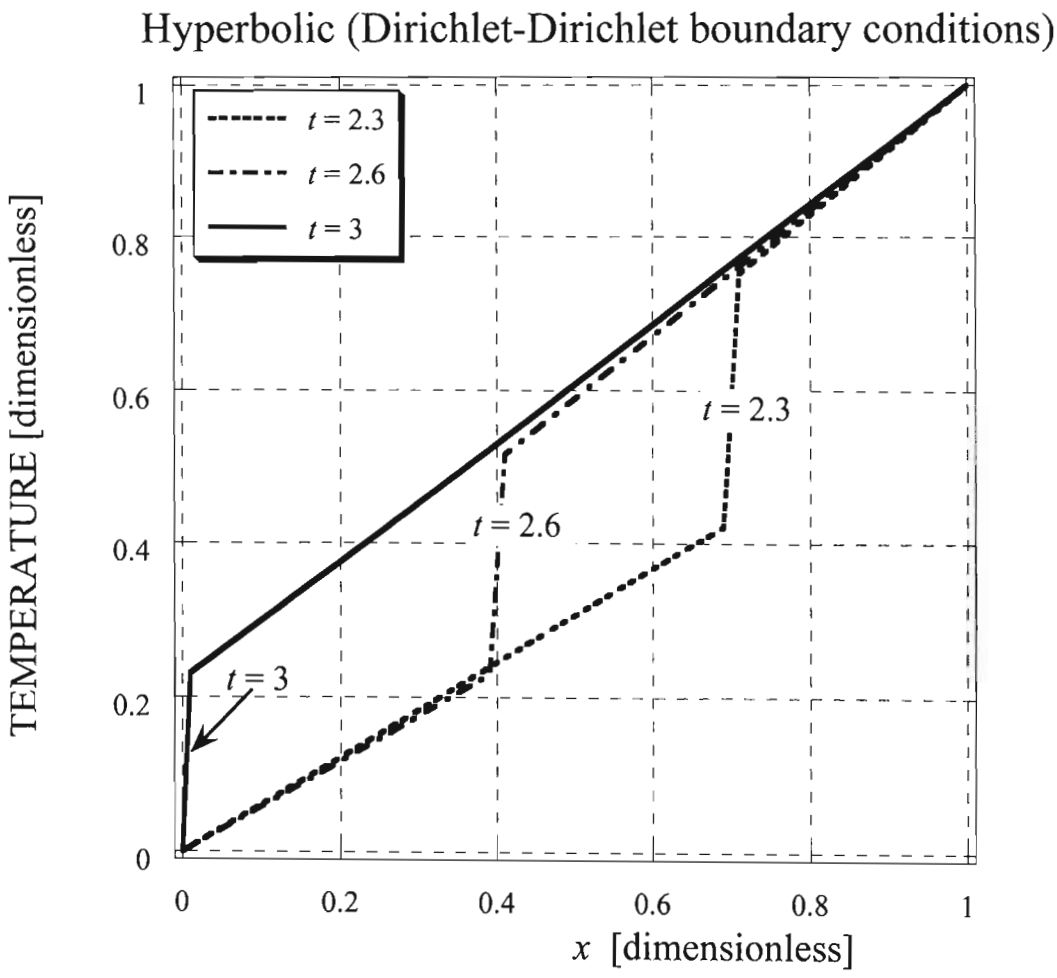

Figure 5-18:Temperature vs. x in dimensionless form using Dirichlet boundary conditions in the Hyperbolic heat conduction problem with Fourier number equal to 1.

$Fo = 1$

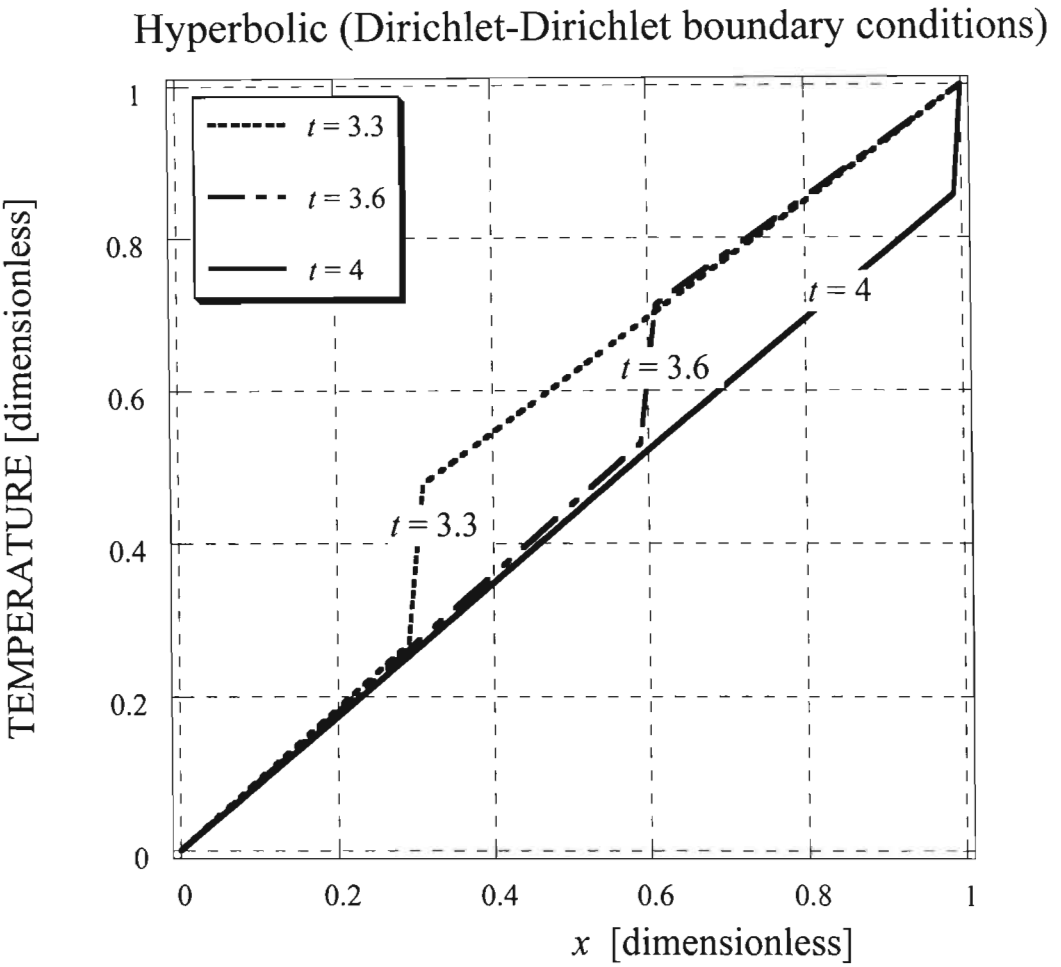

Figure 5-19:Temperature vs. x in dimensionless form using Dirichlet boundary conditions in the Hyperbolic heat conduction problem with Fourier number equal to 1.

$Fo = 1$

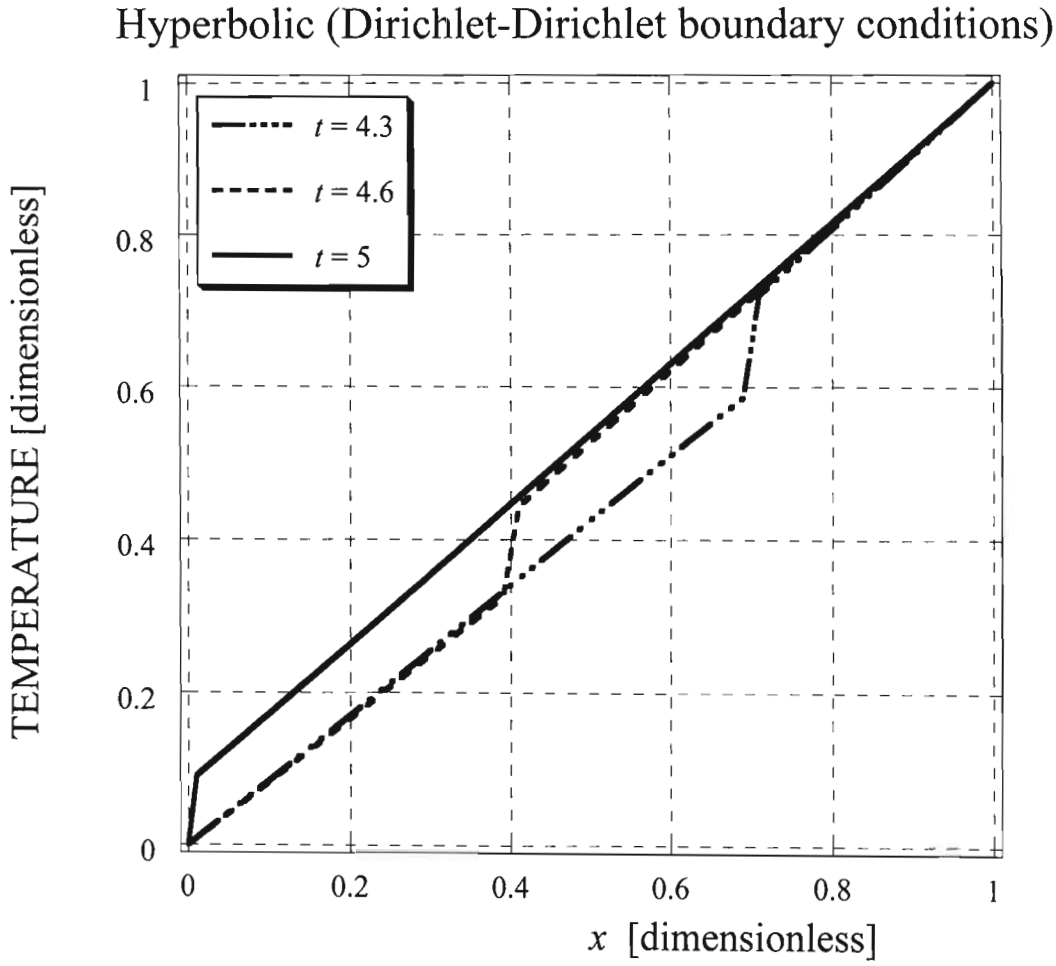

Figure 5-20:Temperature vs. x in dimensionless form using Dirichlet boundary conditions in the Hyperbolic heat conduction problem with Fourier number equal to 1.

$Fo = 1$

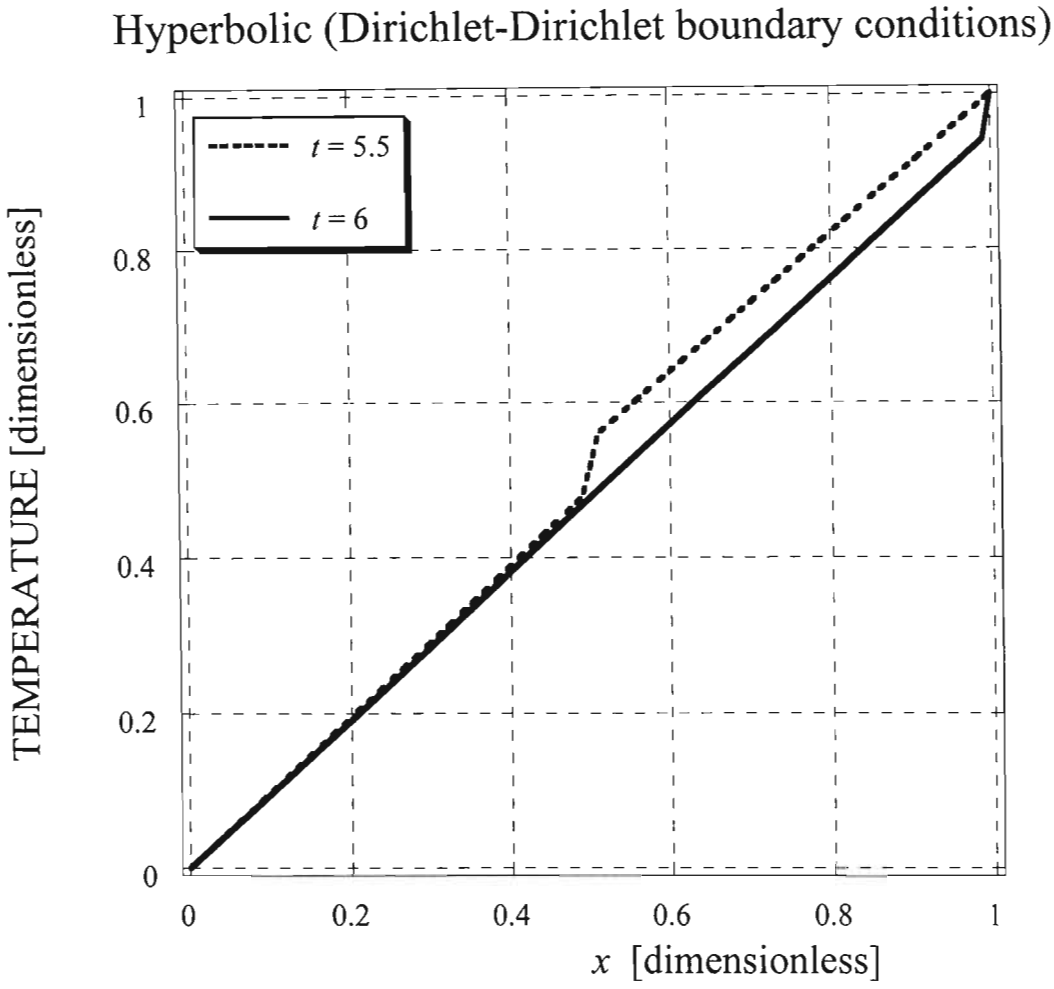

Figure 5-21:Temperature vs. x in dimensionless form using Dirichlet boundary conditions in the Hyperbolic heat conduction problem with Fourier number equal to 1.

$Fo = 1$

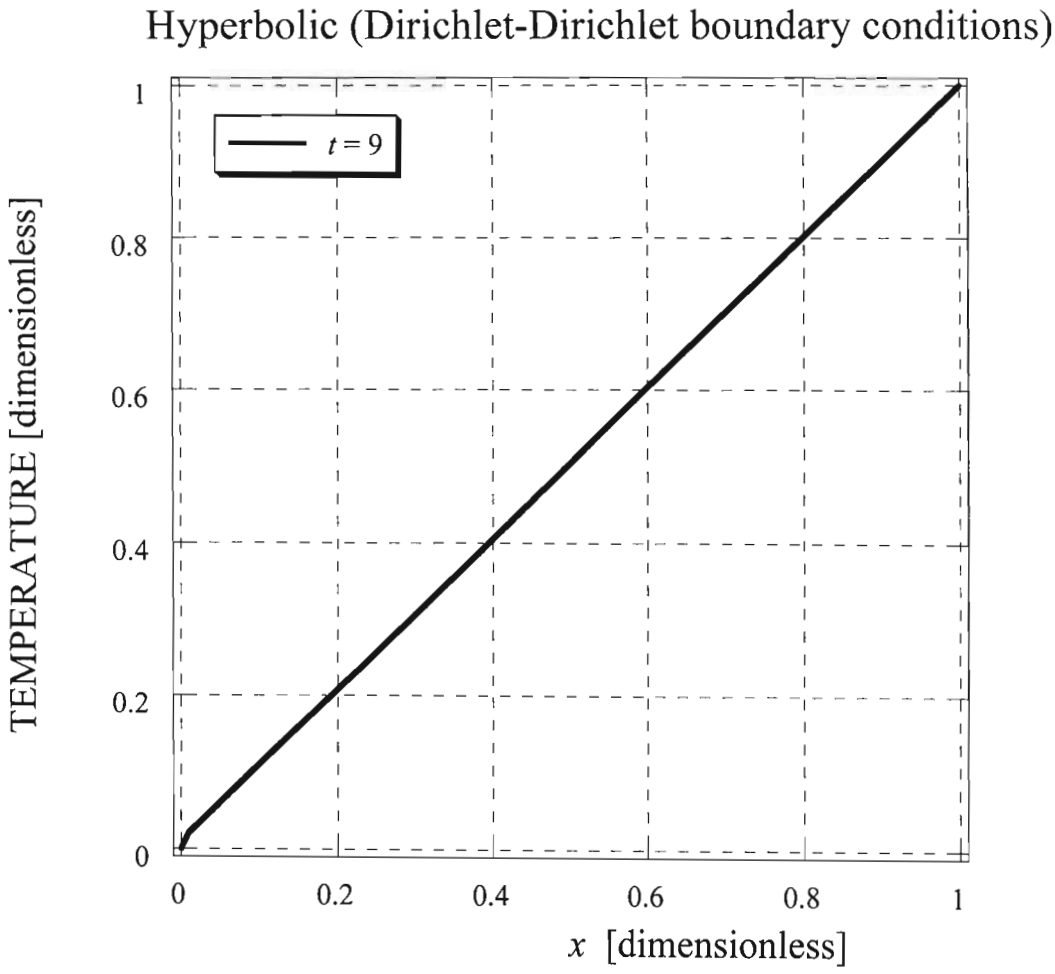

Figure 5-22:Temperature vs. x in dimensionless form using Dirichlet boundary conditions in the Hyperbolic heat conduction problem with Fourier number equal to 1.

$Fo = 10^{-4}$

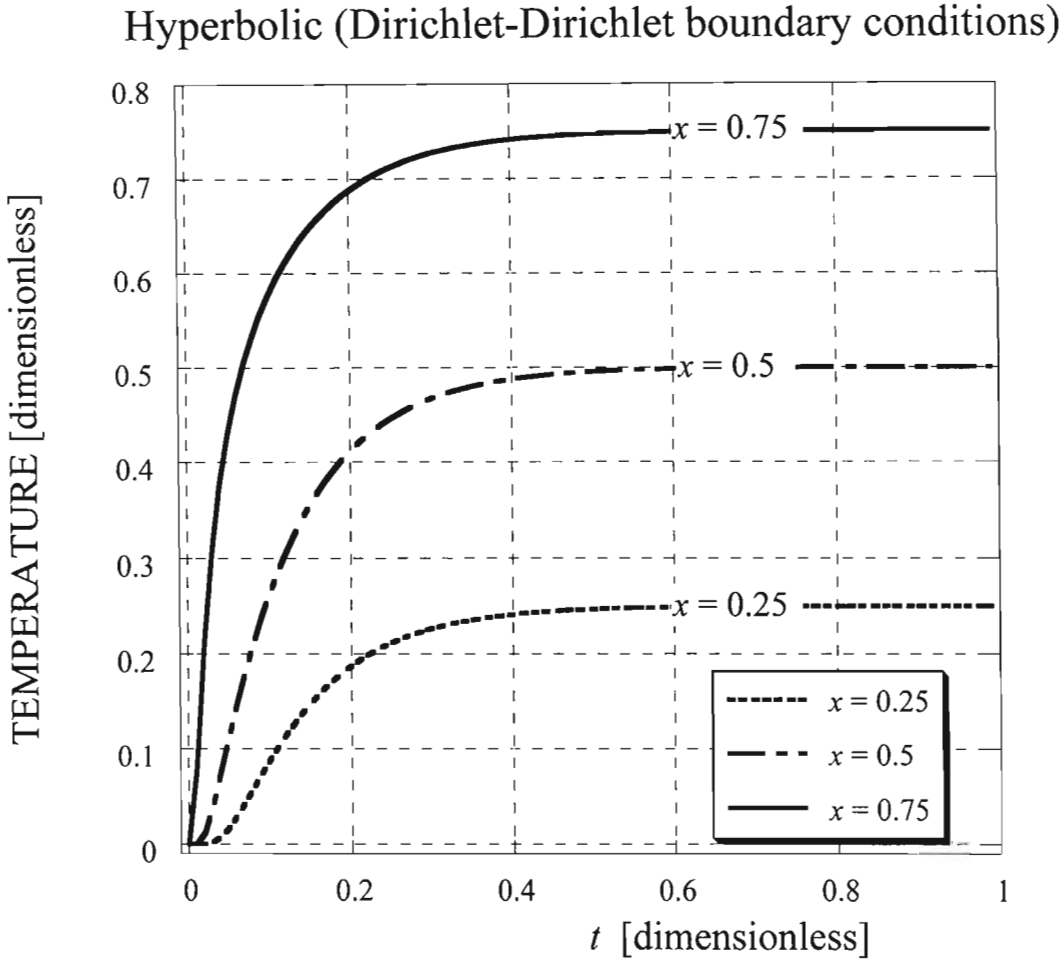

Figure 5-23:Temperature vs. t in dimensionless form using Dirichlet boundary conditions in the Hyperbolic heat conduction problem with Fourier number equal to 10^{-4}.

$Fo = 0.01$

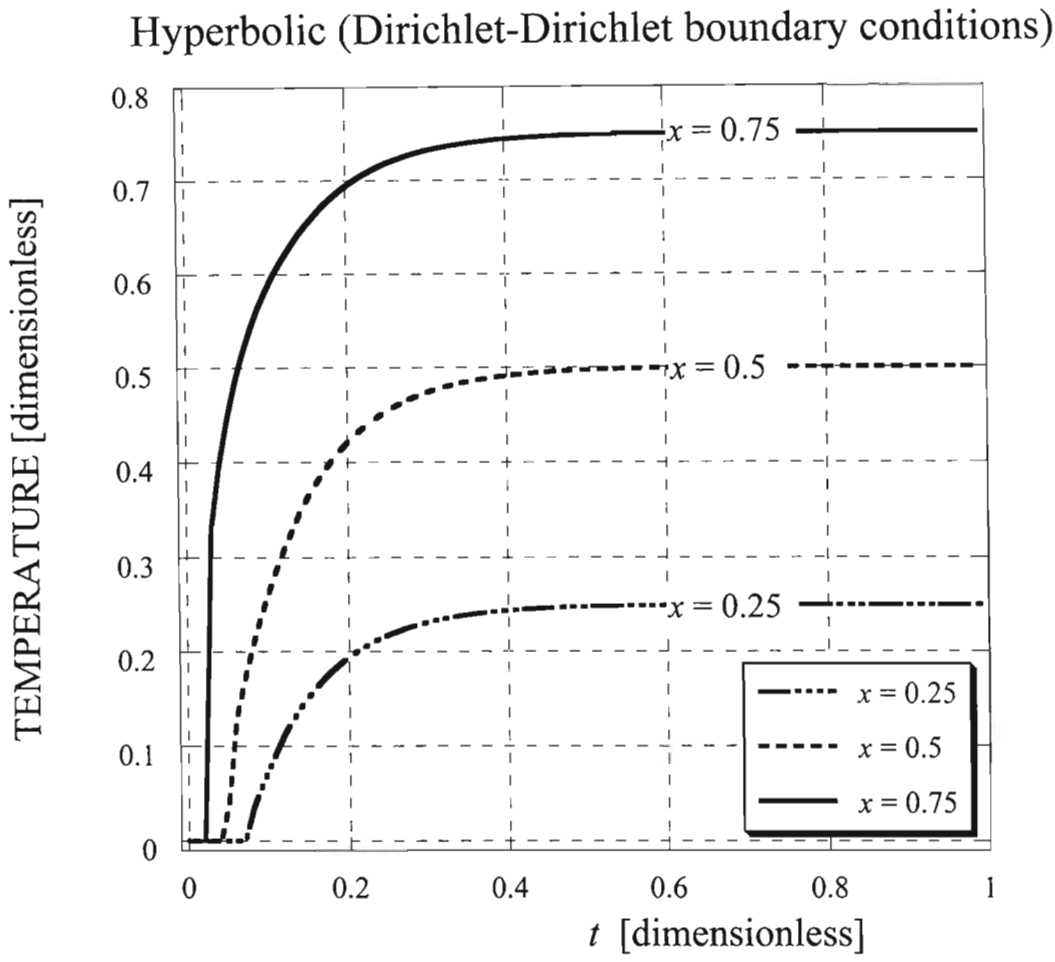

Figure 5-24:Temperature vs. t in dimensionless form using Dirichlet boundary conditions in the Hyperbolic heat conduction problem with Fourier number equal to 0.01.

$Fo = 1$

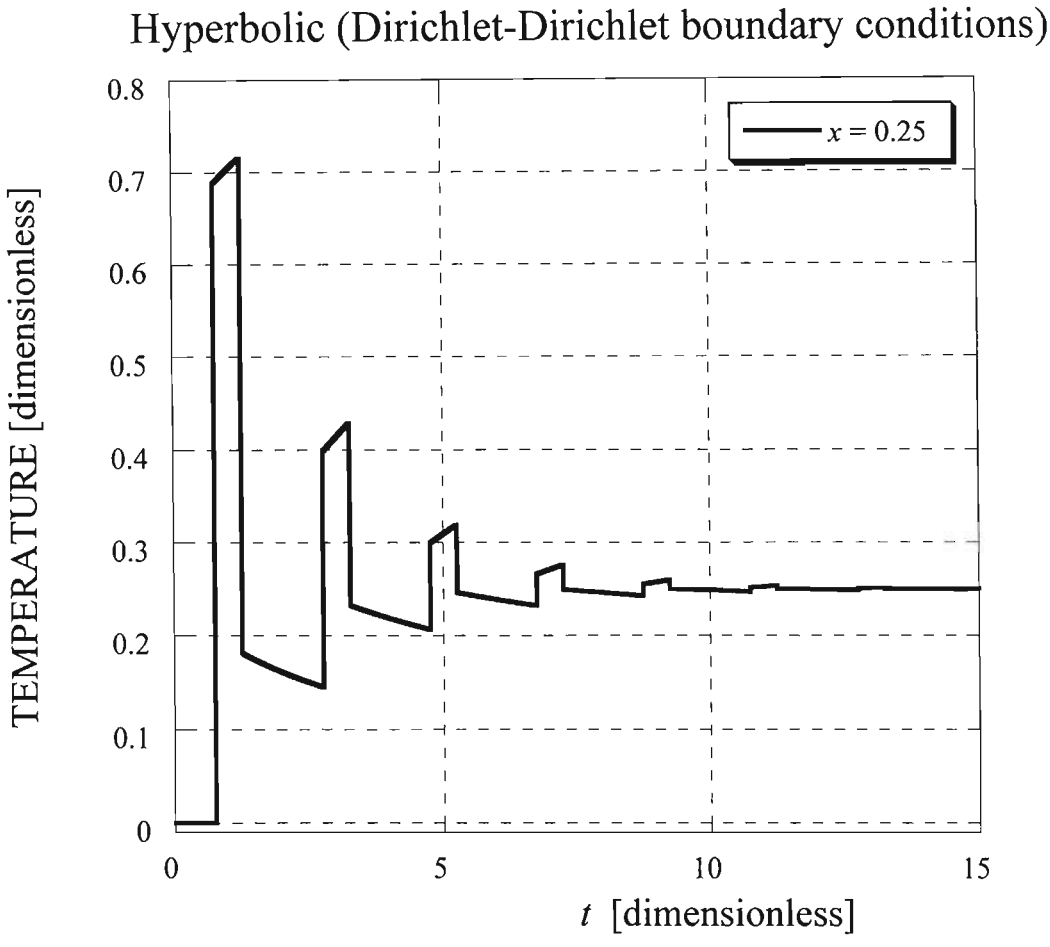

Figure 5-25:Temperature vs. t in dimensionless form using Dirichlet boundary conditions in the Hyperbolic heat conduction problem with Fourier number equal to 1.

$Fo = 1$

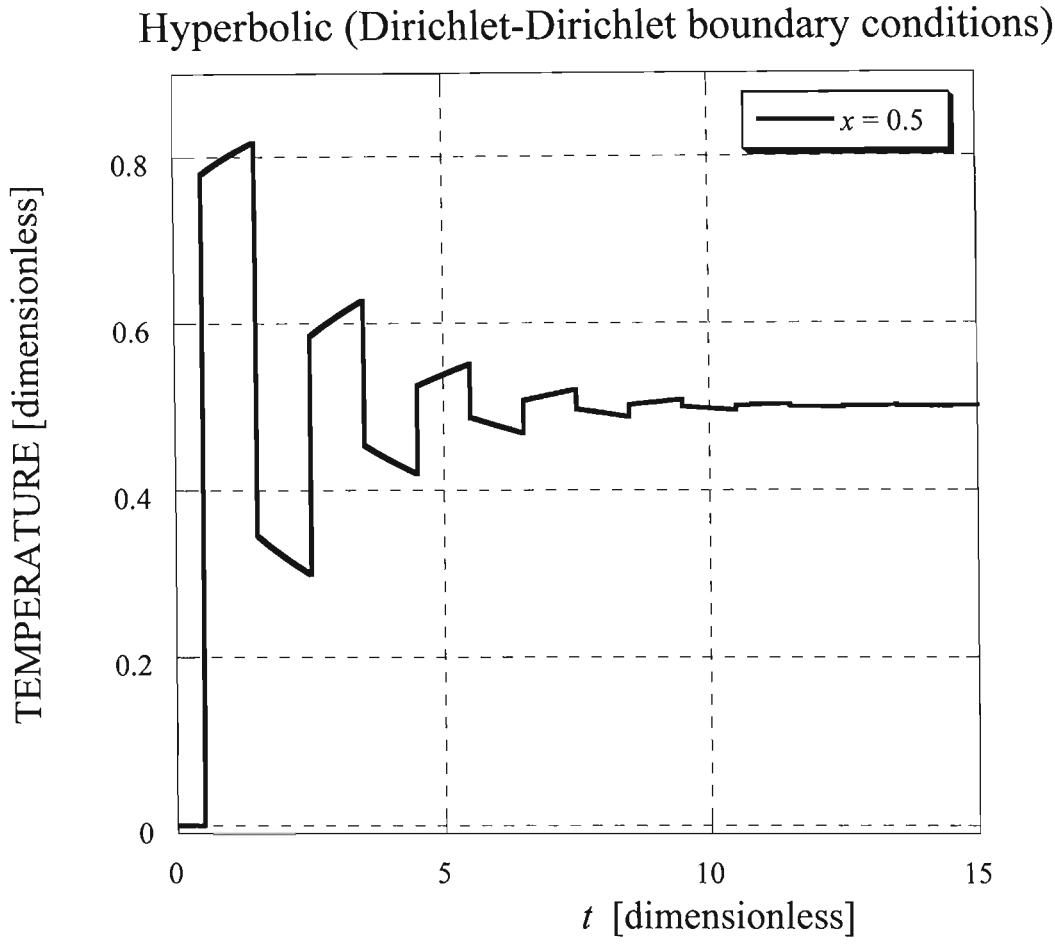

Figure 5-26:Temperature vs. t in dimensionless form using Dirichlet boundary conditions in the Hyperbolic heat conduction problem with Fourier number equal to 1.

$Fo = 1$

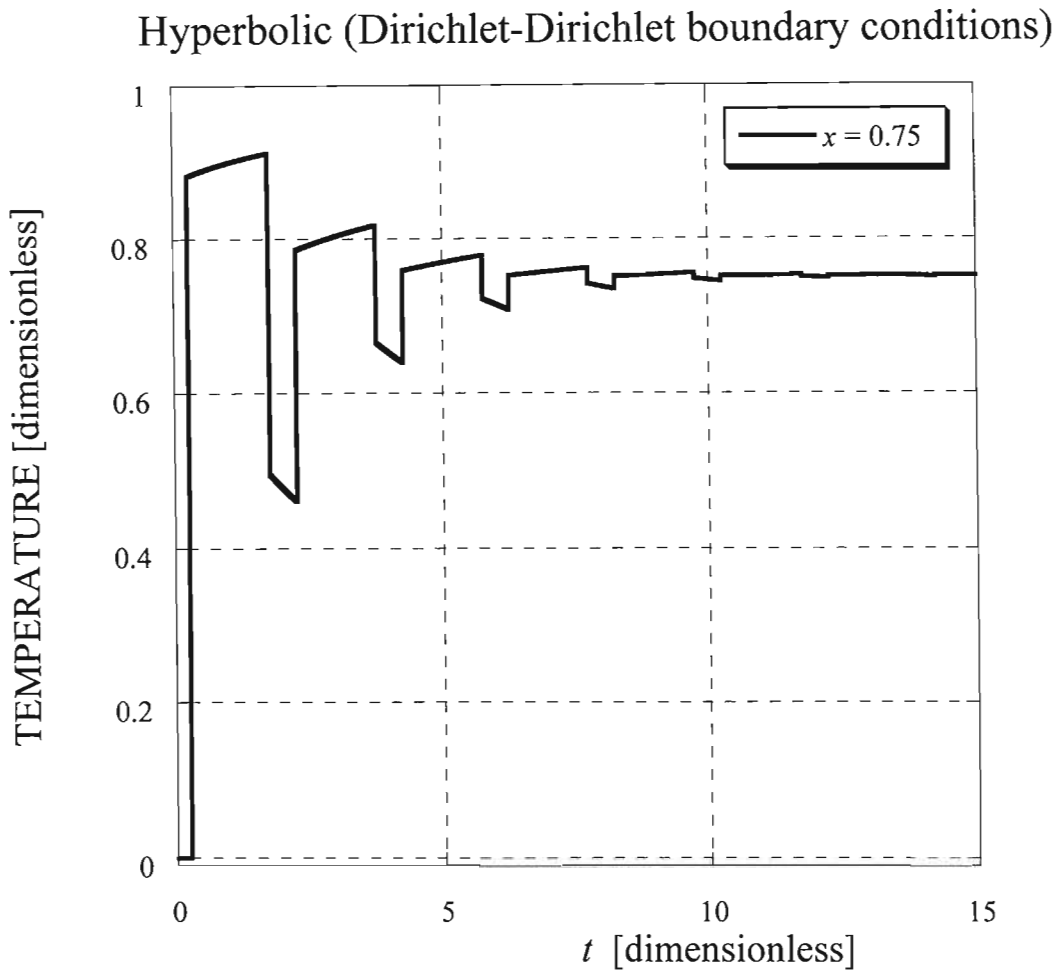

Figure 5-27:Temperature vs. t in dimensionless form using Dirichlet boundary conditions in the Hyperbolic heat conduction problem with Fourier number equal to 1.

5.5 Results for the Hyperbolic heat conduction problem subject to a combination of Dirichlet and Neumann boundary conditions.

5.5.1 Rectangular geometry.

In Figures 5-28 and 5-29 the graphs show the relationship between temperature and x in a dimensionless form. With $Fo = 10^{-4}$ in hyperbolic conduction it is shown that the graphs are almost identical to that of the Fourier conduction. As seen previously with a small value $Fo = 10^{-4}$ the wave effects are negligible, so Figures 5-28 and 5-29 show almost identical results as for Fourier conduction in Figure 5-3. Figures 5-30 and 5-31 represent the dimensionless Temperature versus x graphs for $Fo = 0.01$. The wave effects are seen as the wave propagates until steady state is reached. Figures 5-32 to 5-34 represent the dimensionless temperature versus x for $Fo = 0.1$. Again the wave effects are seen even better as the Fourier number is increased. Figures 5-35 to 5-39 represent the dimensionless temperature versus x for $Fo = 1$. In these graphs the wave propagation is seen best as the Fourier number is increased even further. Figure 5-40 shows the dimensionless temperature versus time for $Fo = 10^{-4}$. Since $Fo = 10^{-4}$ is small, the wave effects are not seen and the graph follows the Fourier solution almost identically. Figure 5-41 shows the dimensionless temperature versus time for $Fo = 0.01$, however the Fourier number is still too small for these effects to be observed. The graph in Figure 5-41 follows the Fourier solution almost identically. Figure 5-42 shows the dimensionless temperature versus time for $Fo = 0.1$. The wave effects can only be seen up to approximately a dimensionless time $t = 0.63$. Figure 5-43 shows the dimensionless temperature versus time graph for $Fo = 1$. In this graph the wave effects are seen very clearly. The dimensionless time for the wave to pass the gap twice is the dimensionless time between a peak and a trough in the graph shown in Figure 5-43 for $x = 1$. For all other values of x except $x = 0$ the dimensionless time for the wave to pass the gap twice is also represented on the graph in Figure 5-43 clearly by the peaks and troughs.

$Fo = 10^{-4}$

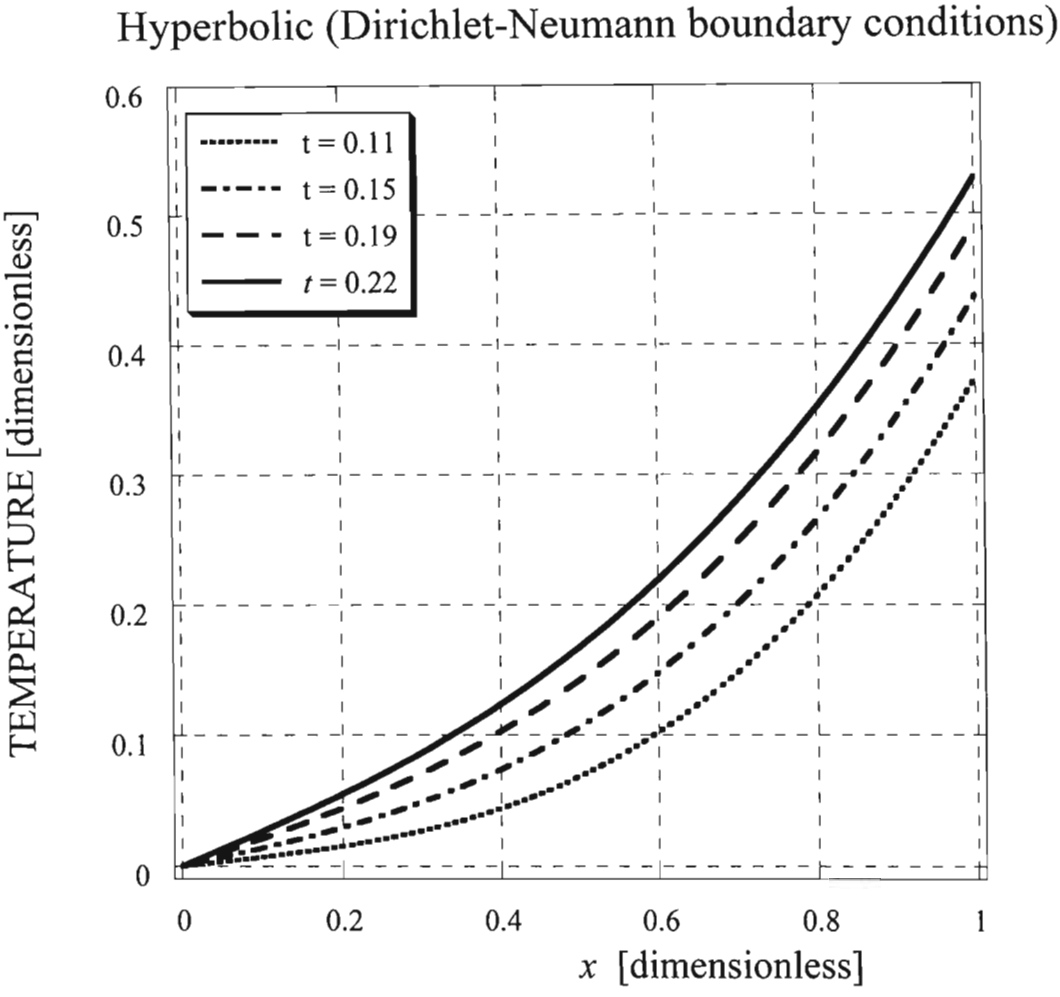

Figure 5-28:Temperature vs. x in dimensionless form using a combination of Dirichlet and Neumann boundary conditions in the Hyperbolic heat conduction problem with Fourier number equal to 10^{-4}.

$Fo = 10^{-4}$

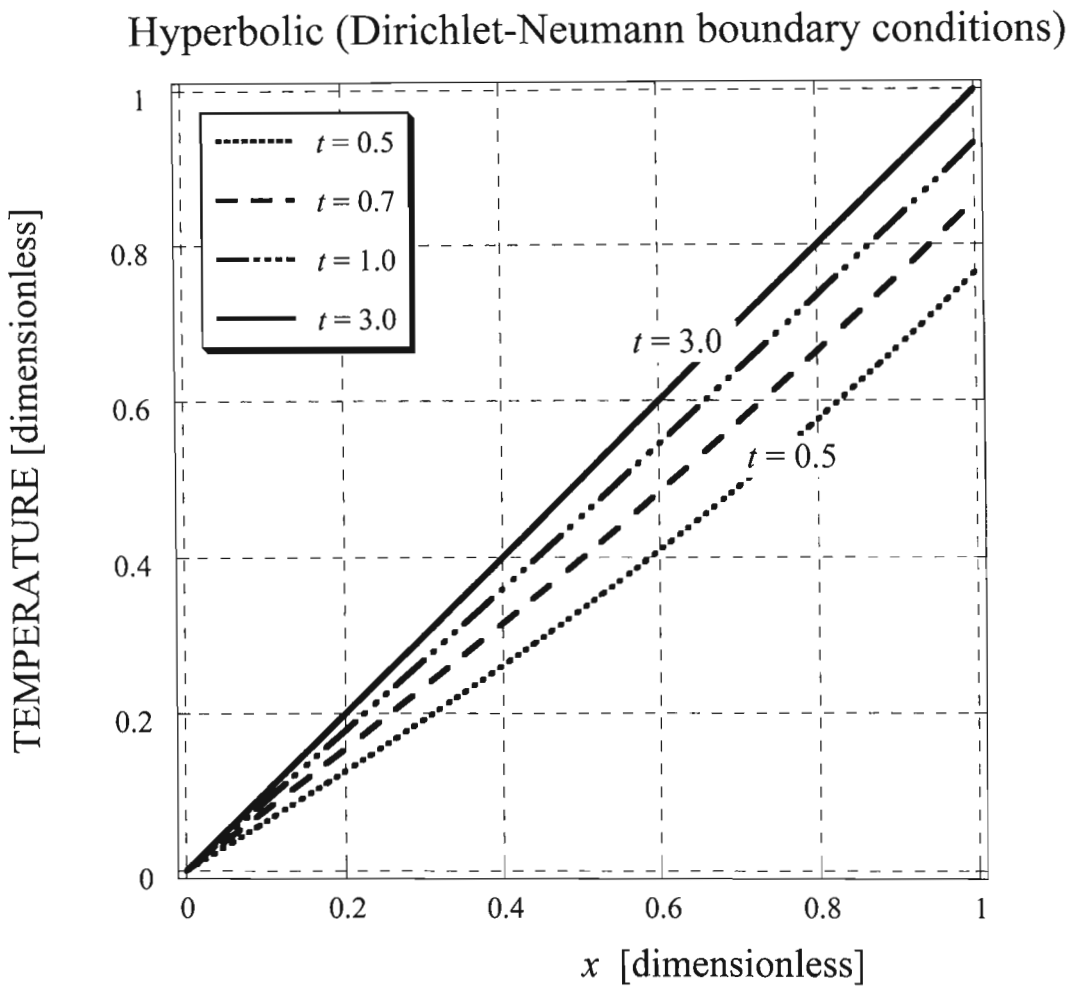

Figure 5-29:Temperature vs. x in dimensionless form using a combination of Dirichlet and Neumann boundary conditions in the Hyperbolic heat conduction problem with Fourier number equal to 10^{-4}.

$Fo = 0.01$

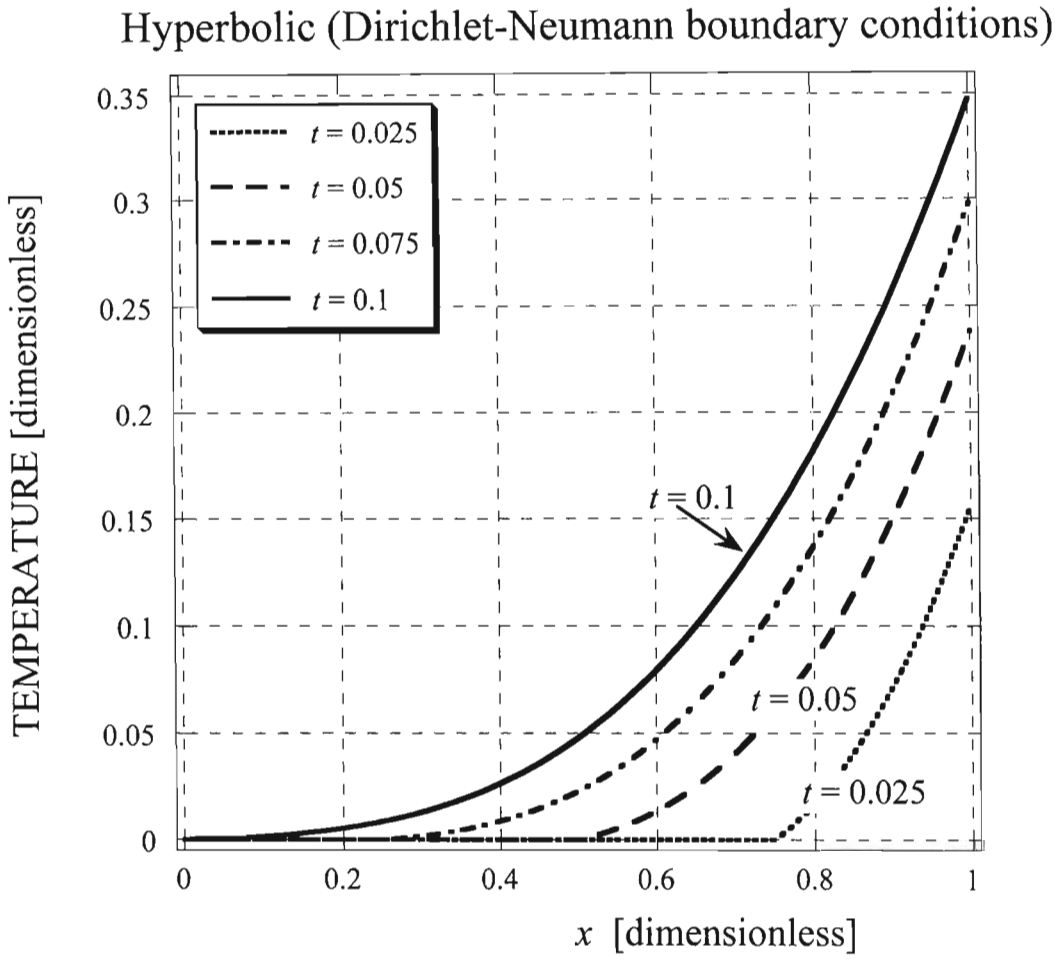

Figure 5-30:Temperature vs. x in dimensionless form using a combination of Dirichlet and Neumann boundary conditions in the Hyperbolic heat conduction problem with Fourier number equal to 0.01.

$Fo = 0.01$

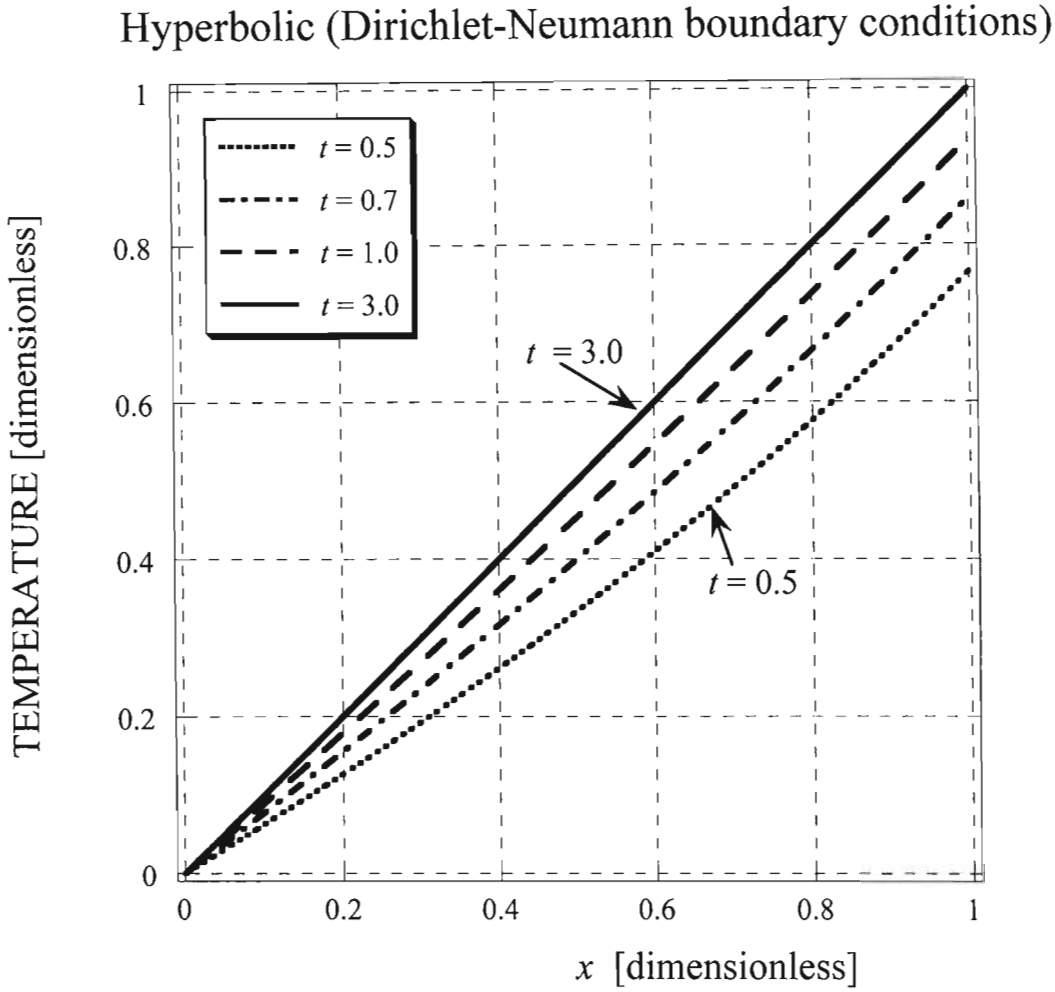

Figure 5-31:Temperature vs. x in dimensionless form using a combination of Dirichlet and Neumann boundary conditions in the Hyperbolic heat conduction problem with Fourier number equal to 0.01.

$Fo = 0.1$

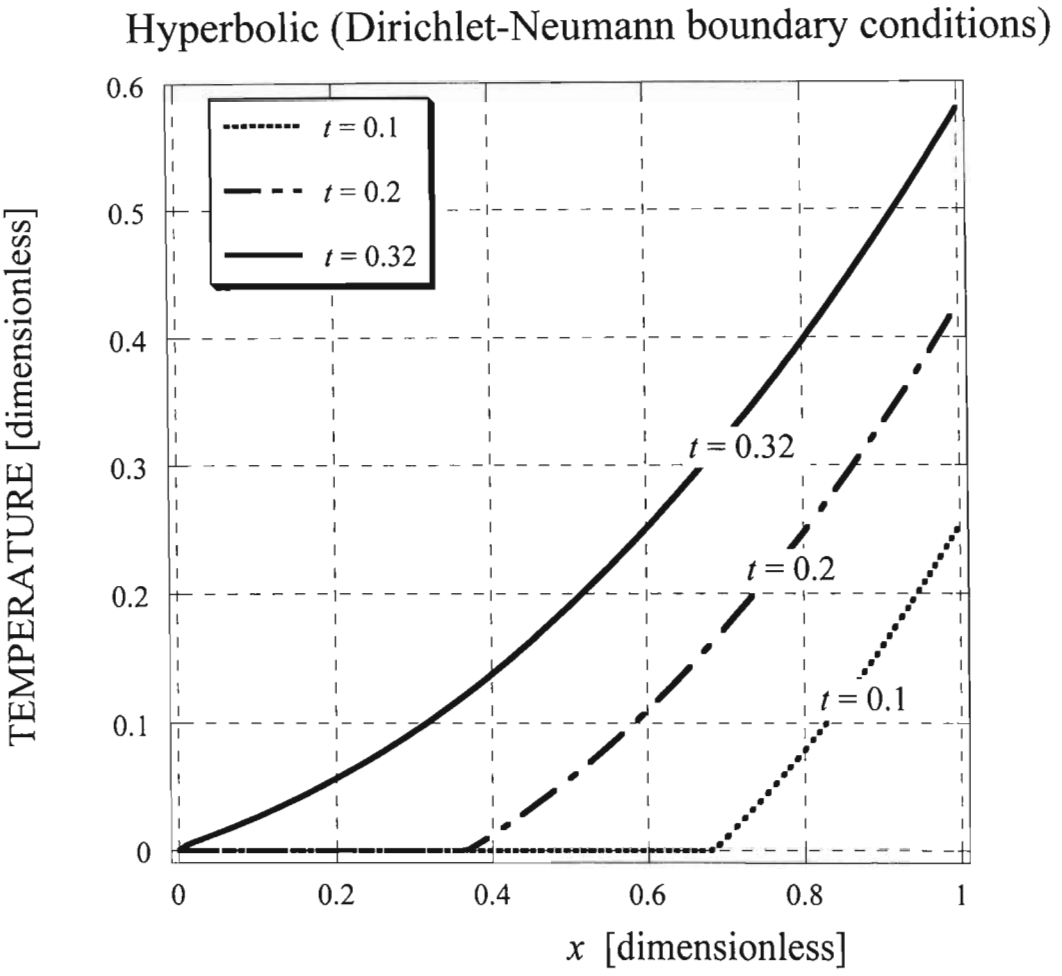

Figure 5-32:Temperature vs. x in dimensionless form using a combination of Dirichlet and Neumann boundary conditions in the Hyperbolic heat conduction problem with Fourier number equal to 0.1.

$Fo = 0.1$

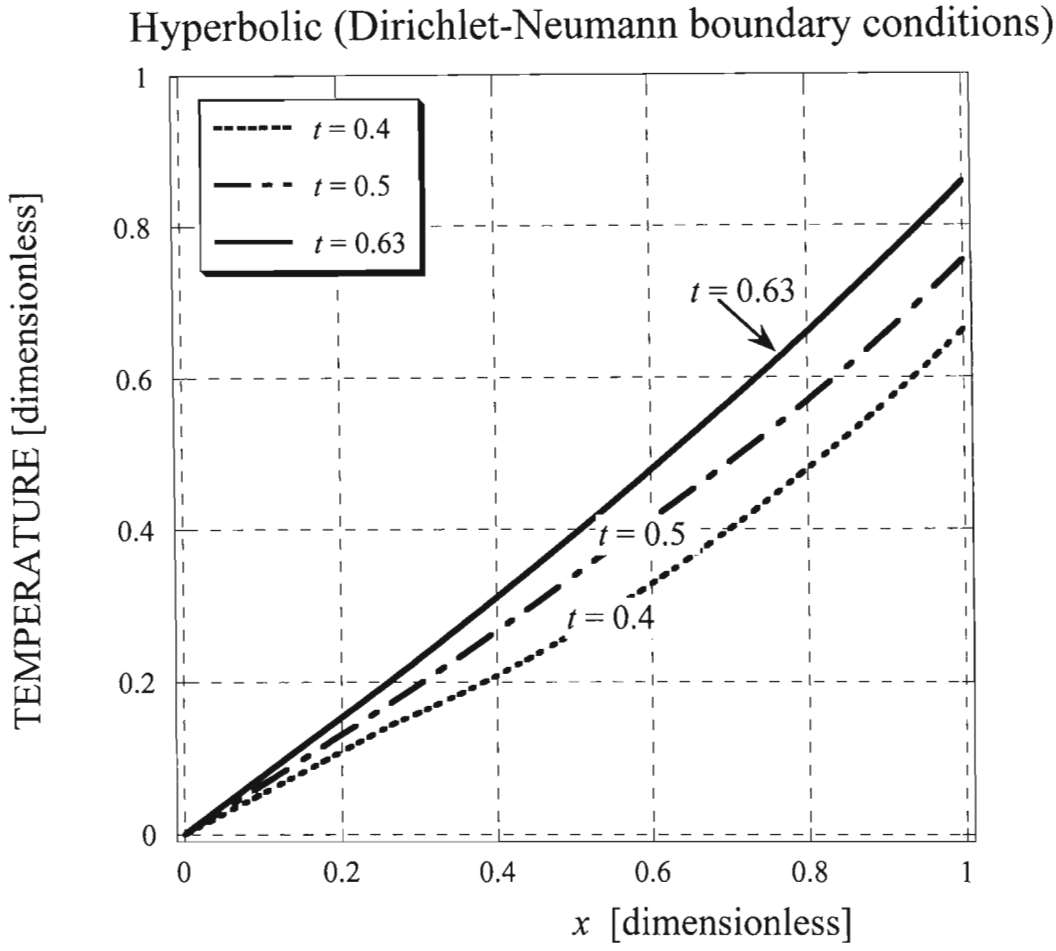

Figure 5-33:Temperature vs. x in dimensionless form using a combination of Dirichlet and Neumann boundary conditions in the Hyperbolic heat conduction problem with Fourier number equal to 0.1.

$Fo = 0.1$

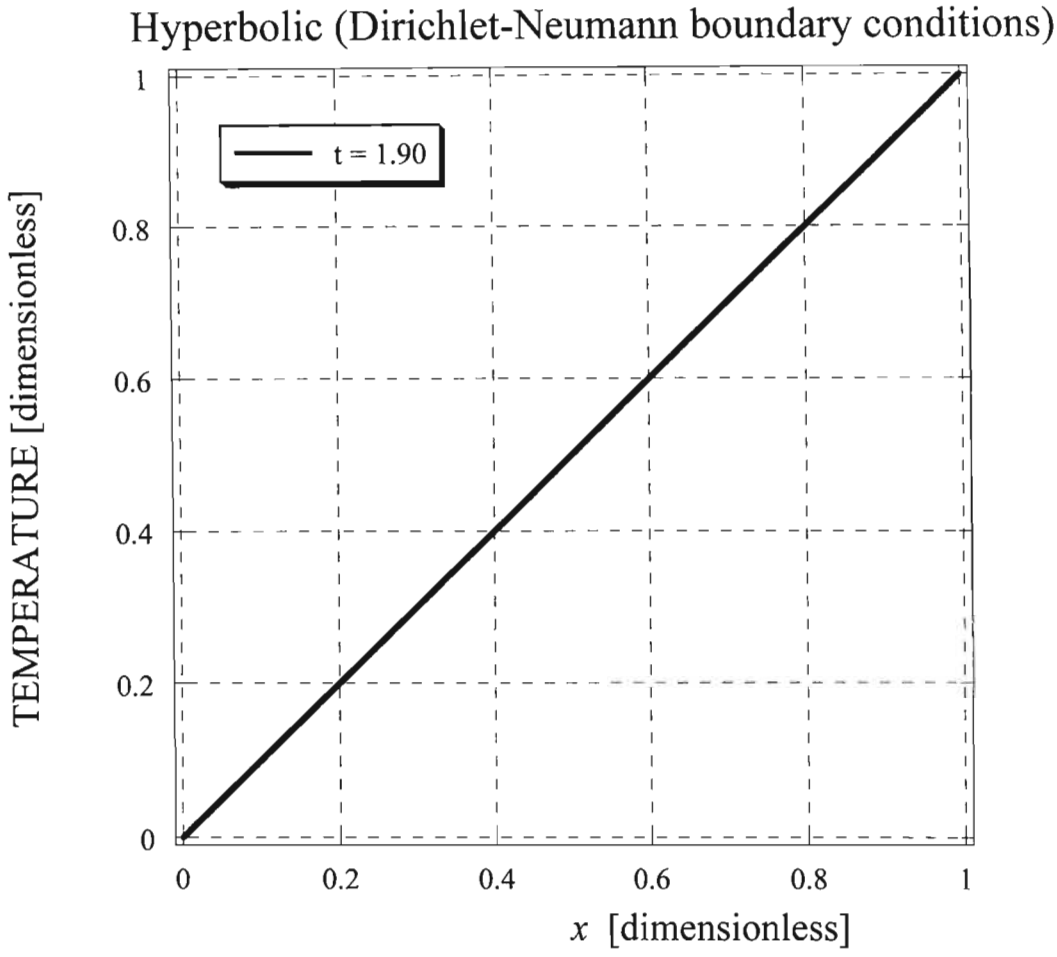

Figure 5-34:Temperature vs. x in dimensionless form using a combination of Dirichlet and Neumann boundary conditions in the Hyperbolic heat conduction problem with Fourier number equal to 0.1.

$Fo = 1$

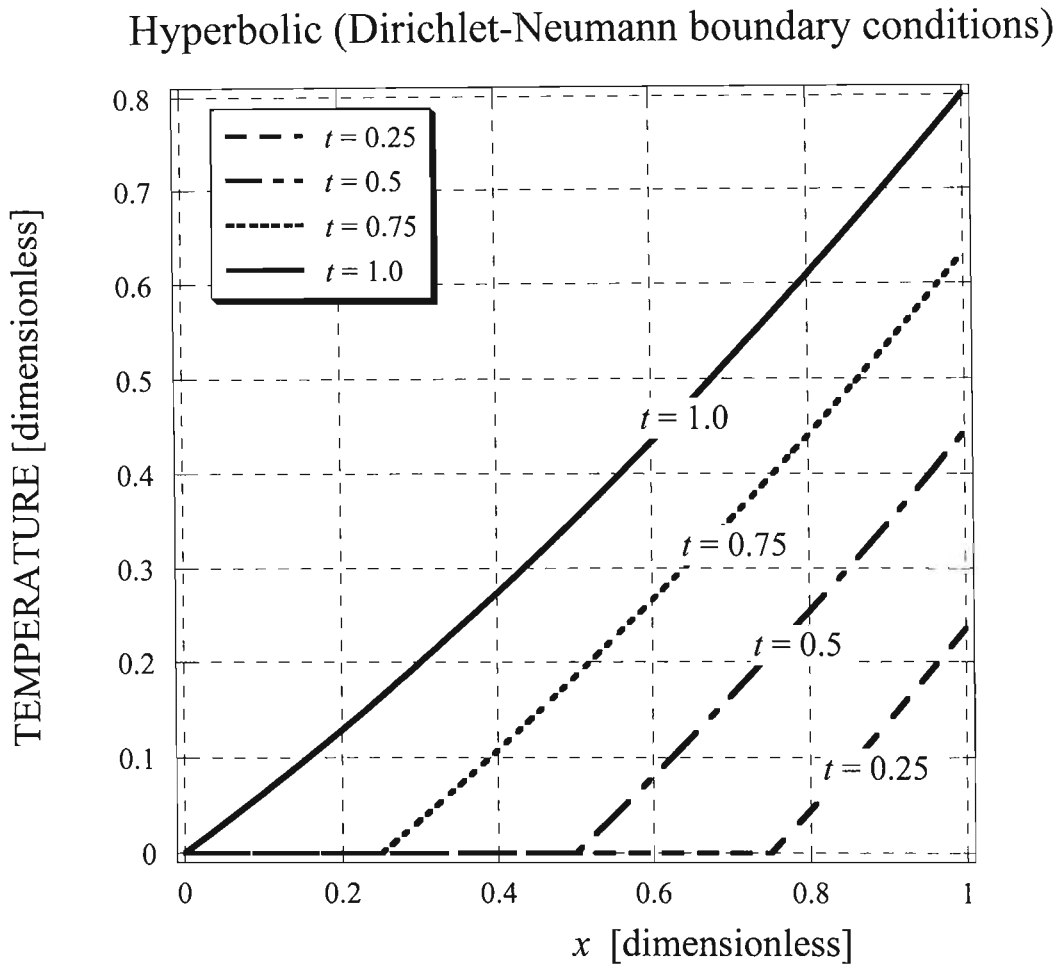

Figure 5-35:Temperature vs. x in dimensionless form using a combination of Dirichlet and Neumann boundary conditions in the Hyperbolic heat conduction problem with Fourier number equal to 1.

$Fo = 1$

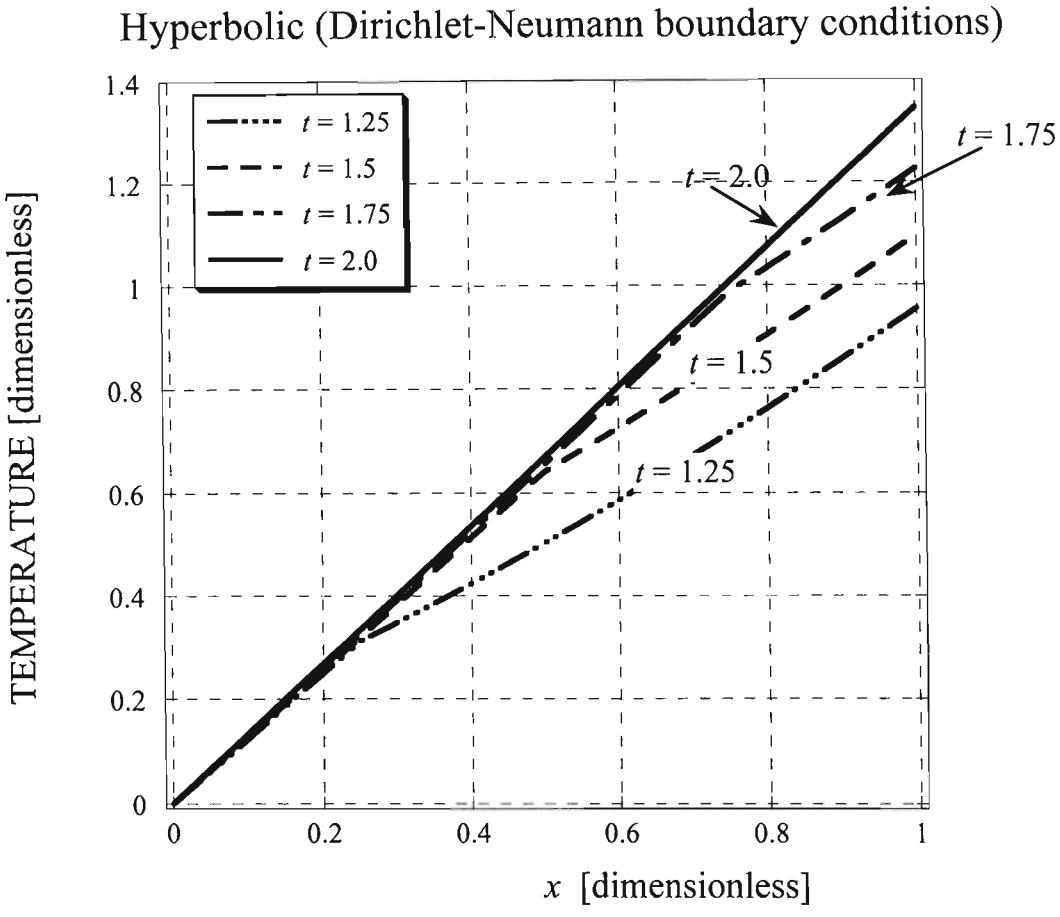

Figure 5-36:Temperature vs. x in dimensionless form using a combination of Dirichlet and Neumann boundary conditions in the Hyperbolic heat conduction problem with Fourier number equal to 1.

$Fo = 1$

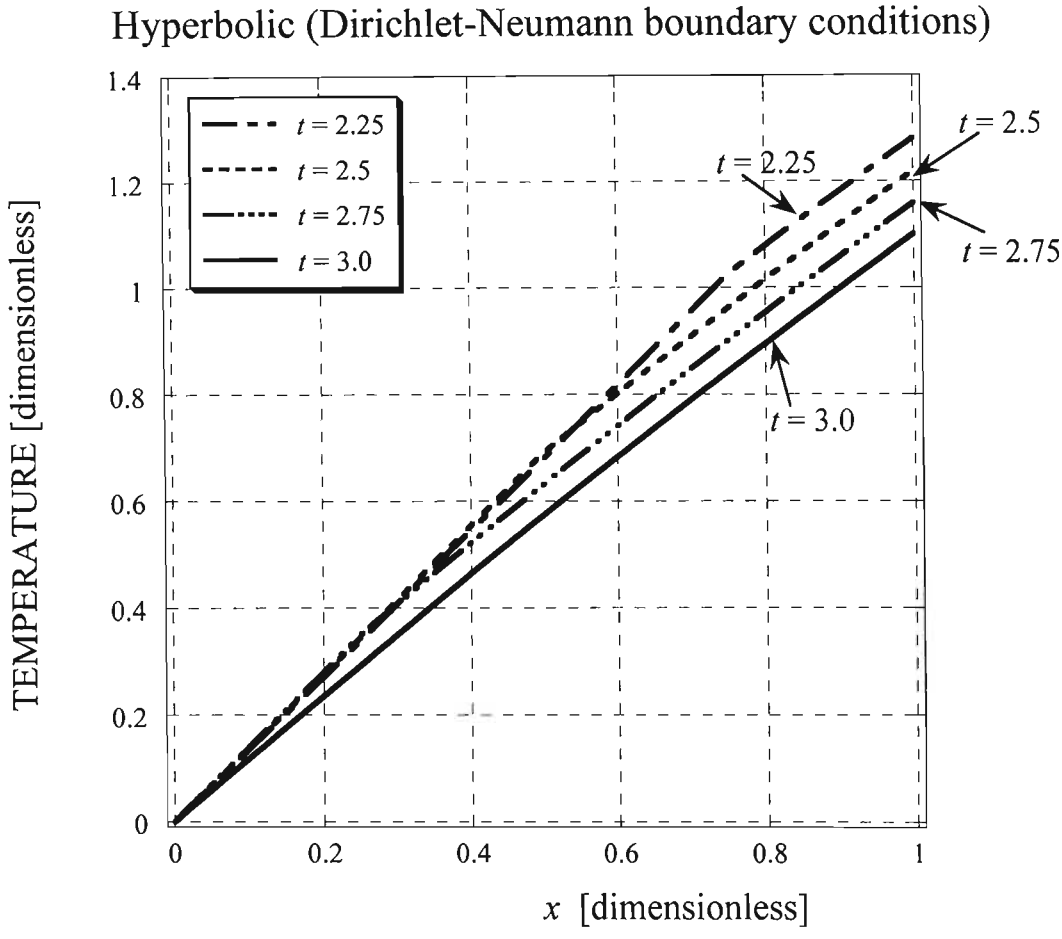

Figure 5-37:Temperature vs. x in dimensionless form using a combination of Dirichlet and Neumann boundary conditions in the Hyperbolic heat conduction problem with Fourier number equal to 1.

$Fo = 1$

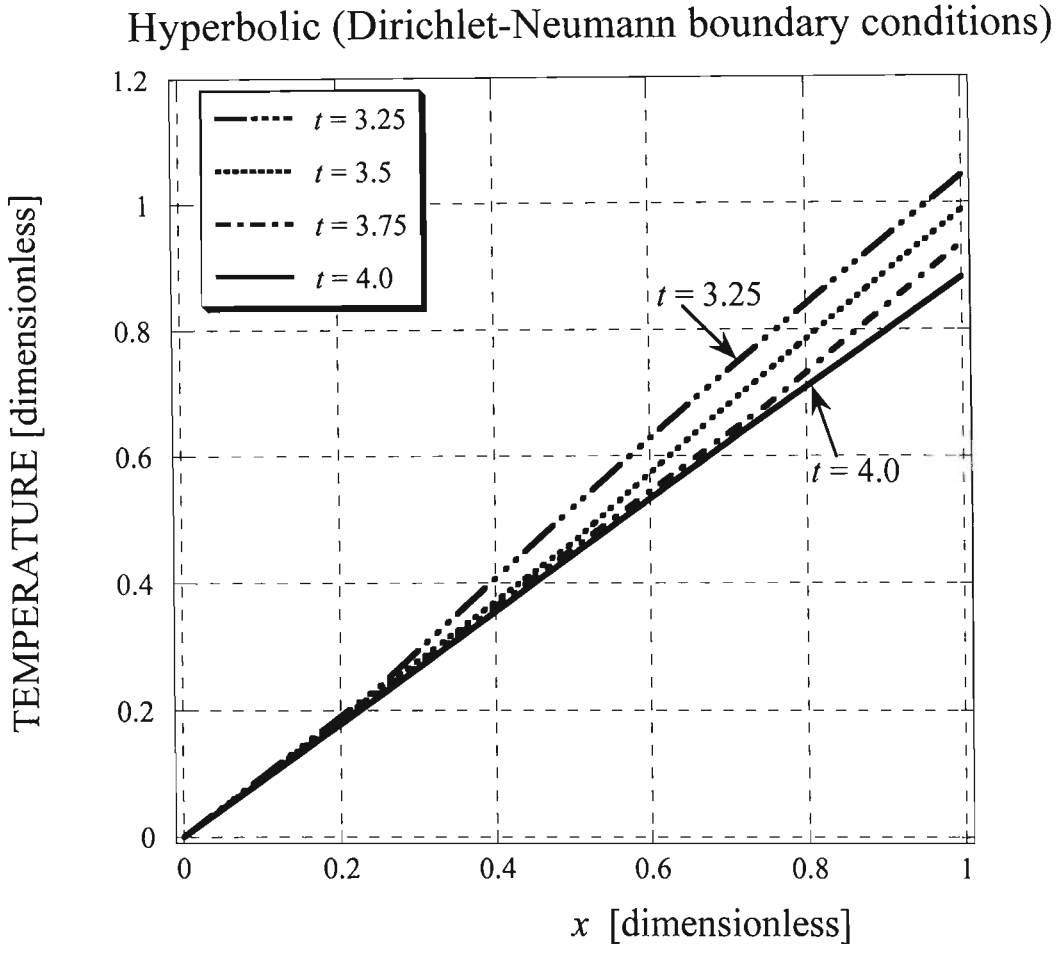

Figure 5-38:Temperature vs. x in dimensionless form using a combination of Dirichlet and Neumann boundary conditions in the Hyperbolic heat conduction problem with Fourier number equal to 1.

$Fo = 1$

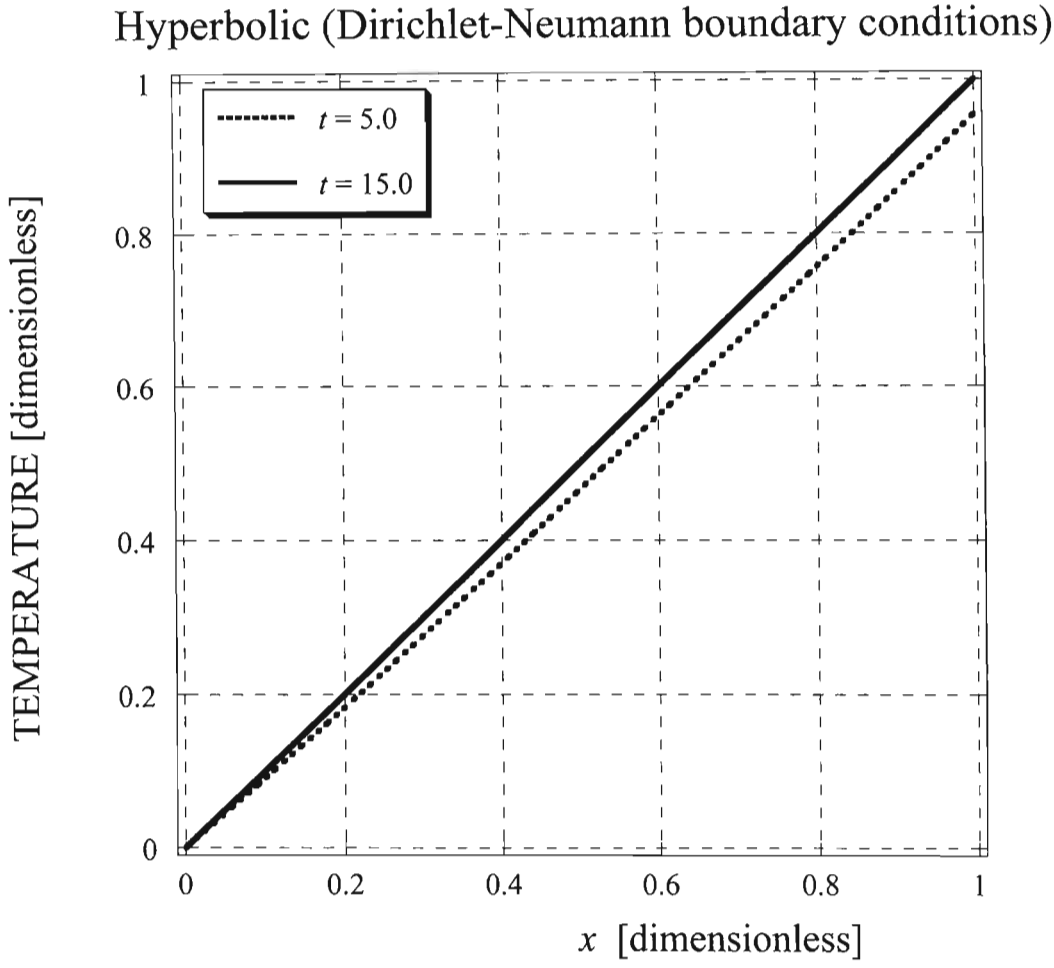

Figure 5-39:Temperature vs. x in dimensionless form using a combination of Dirichlet and Neumann boundary conditions in the Hyperbolic heat conduction problem with Fourier number equal to 1.

$Fo = 10^{-4}$

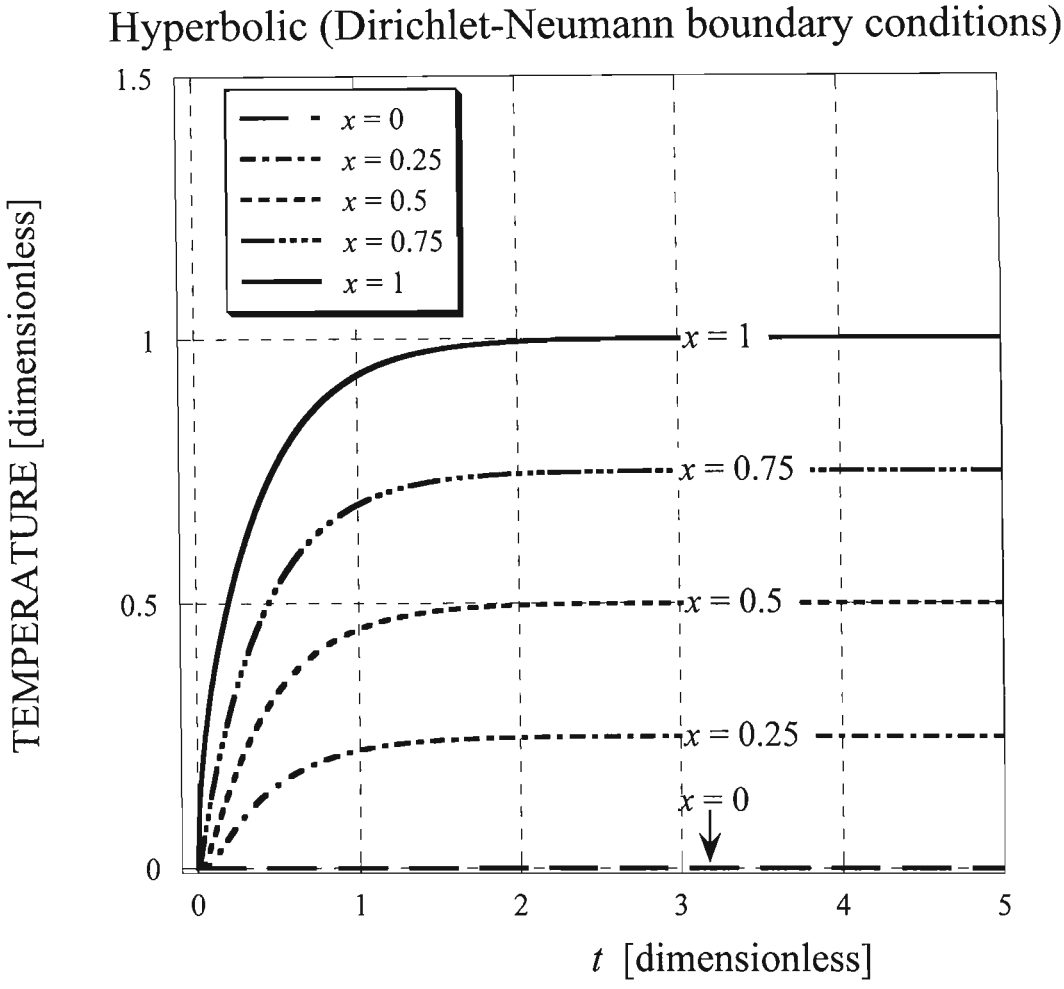

Figure 5-40:Temperature vs. t in dimensionless form using a combination of Dirichlet and Neumann boundary conditions in the Hyperbolic heat conduction problem with Fourier number equal to 10^{-4}.

$Fo = 0.01$

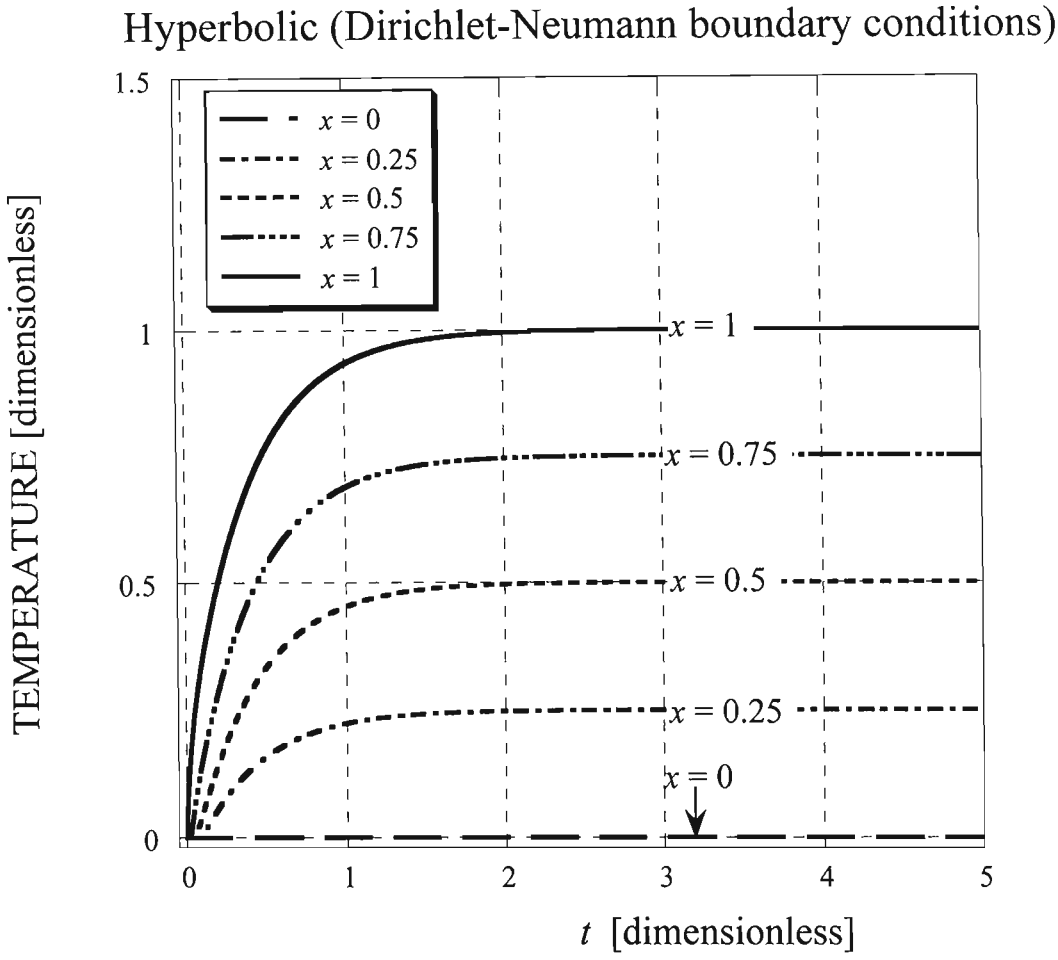

Figure 5-41:Temperature vs. t in dimensionless form using a combination of Dirichlet and Neumann boundary conditions in the Hyperbolic heat conduction problem with Fourier number equal to 0.01.

$Fo = 0.1$

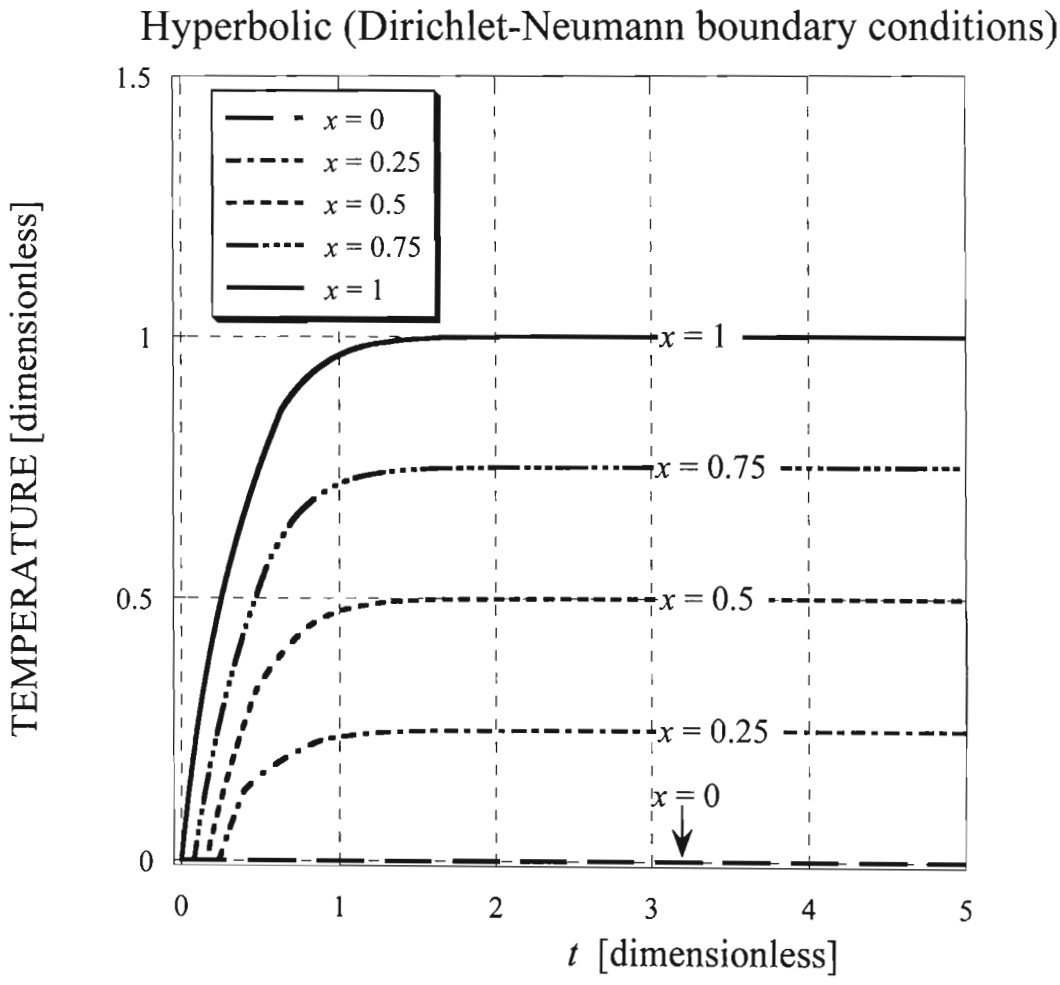

Figure 5-42:Temperature vs. t in dimensionless form using a combination of Dirichlet and Neumann boundary conditions in the Hyperbolic heat conduction problem with Fourier number equal to 0.1.

$Fo = 1$

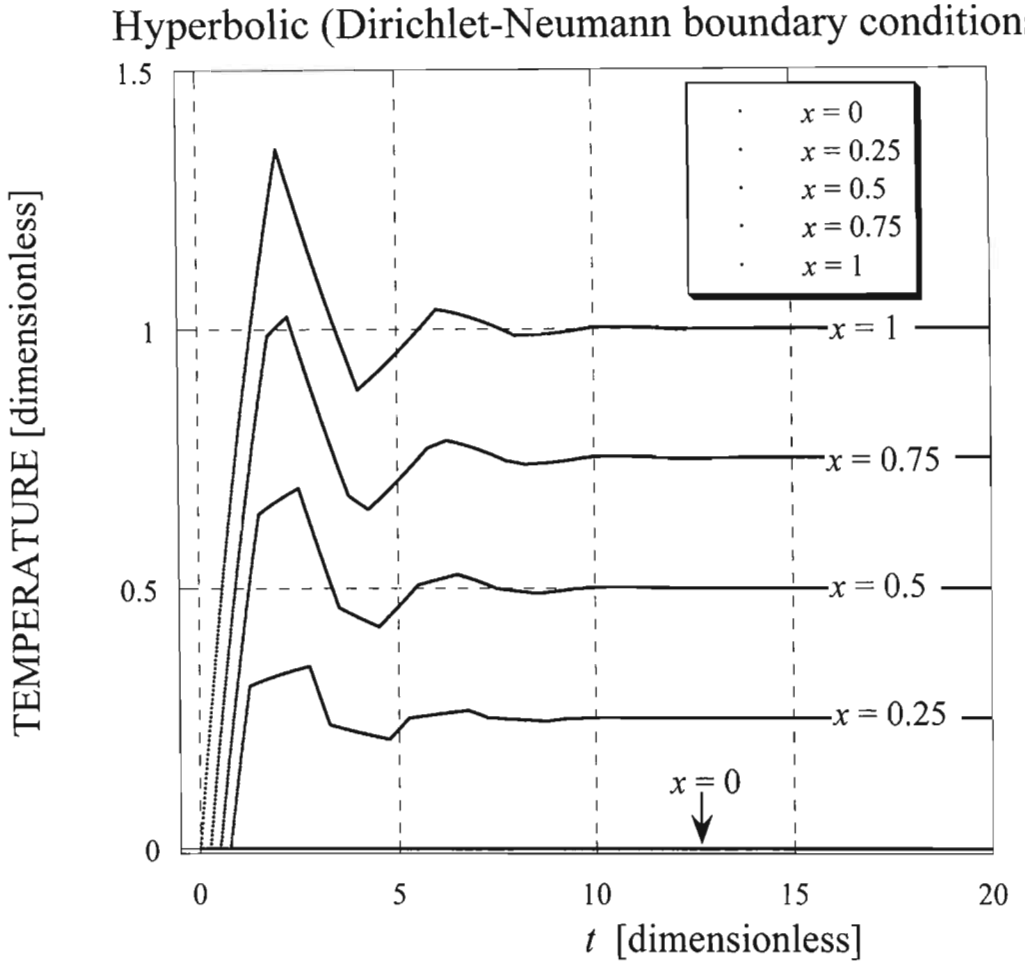

Figure 5-43:Temperature vs. t in dimensionless form using a combination of Dirichlet and Neumann boundary conditions in the Hyperbolic heat conduction problem with Fourier number equal to 1.

5.5.2 Cylindrical geometry.

Figure 5-44 shows the dimensionless temperature versus r for $Fo = 10^{-4}$. The wave effects are not seen due to the small Fourier number. The graph in Figure 5-44 follows almost identically to the Fourier solution shown in Figure 5-5. Figure 5-45 shows the dimensionless temperature versus log(r) for the same $Fo = 10^{-4}$. Again this graph follows almost identically to the Fourier solution shown by Figure 5-6. Figures 5-46 and 5-48 show the dimensionless temperature versus r for $Fo = 0.01$. Figures 5-47 and 5-49 show the dimensionless temperature versus log(r) for the same $Fo = 0.01$. The graphs in Figures 5-46 to 5-49 show the wave propagation until steady state is reached. Figures 5-50 and 5-52 show the dimensionless temperature versus r for $Fo = 0.1$. Figures 5-51 and 5-53 show the dimensionless temperature versus log(r) for $Fo = 0.1$. The graphs in Figures 5-50 to 5-53 show the wave propagation until steady state is reached. Figures 5-54, 5-56 and 5-58 show the dimensionless temperature versus r for $Fo = 1$. Figures 5-55, 5-57 and 5-59 show the dimensionless temperature versus log(r) for $Fo = 1$. The wave propagation is evident in Figures 5-54 to 5-59. With $Fo = 1$ the wave effects are seen most clearly as it takes longer to reach steady state. Figure 5-60 shows the dimensionless temperature versus time for $Fo = 10^{-4}$. The wave effects are not seen in the graph in Figure 5-60 due to the small value for the Fourier number. The graph in Figure 5-60 follows almost identically the Fourier solution shown in Figure 5-7. Figure 5-61 shows the dimensionless temperature versus time for $Fo = 0.01$. The wave effects are only seen up to an approximate dimensionless time $t = 0.1$. For this reason the wave effects are not seen in Figure 5-61 very clearly. Figure 5-61 follows the Fourier solution almost identically since the wave effects are only seen for small values of dimensionless time. Figure 5-62 shows the dimensionless temperature versus time for $Fo = 0.1$. The wave propagation can be seen more clearly in Figure 5-62 and is best seen in Figure 5-63. Figure 5-63 shows the dimensionless temperature versus time for a Fourier number $Fo = 1$. The dimensionless time for the wave to pass the gap is represented by equation (4-60) $t_L = \left(1 - r_w\right)\sqrt{Fo}$. For $Fo = 1$, the dimensionless time to pass the gap is approximately $t_L \simeq 1$ (because $r_w = 0.002 \ll 1$). In Figure 5-63 the dimensionless time for the wave to pass the gap twice is represented by the dimensionless time between peaks which is approximately $t = 2$. This corresponds to equation (4-60) where twice t_L is 2. For larger values of r shown on the graph in

Figure 5-63 the peaks are a little harder to see but the dimensionless bouncing period still corresponds to that of equation (4-60).

$Fo = 10^{-4}$

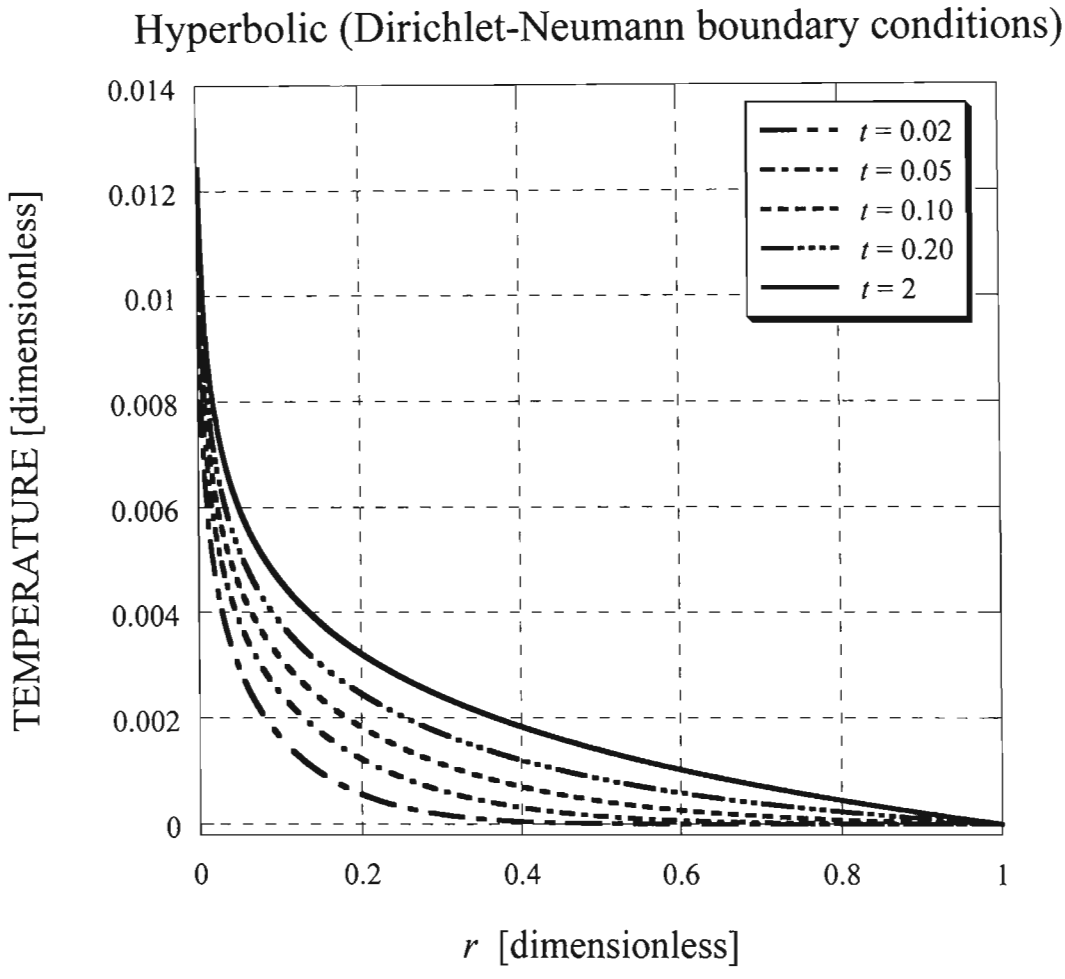

Figure 5-44:Temperature vs. r in dimensionless form using a combination of Dirichlet and Neumann boundary conditions in the Hyperbolic heat conduction problem with Fourier number equal to 10^{-4}.

$Fo = 10^{-4}$

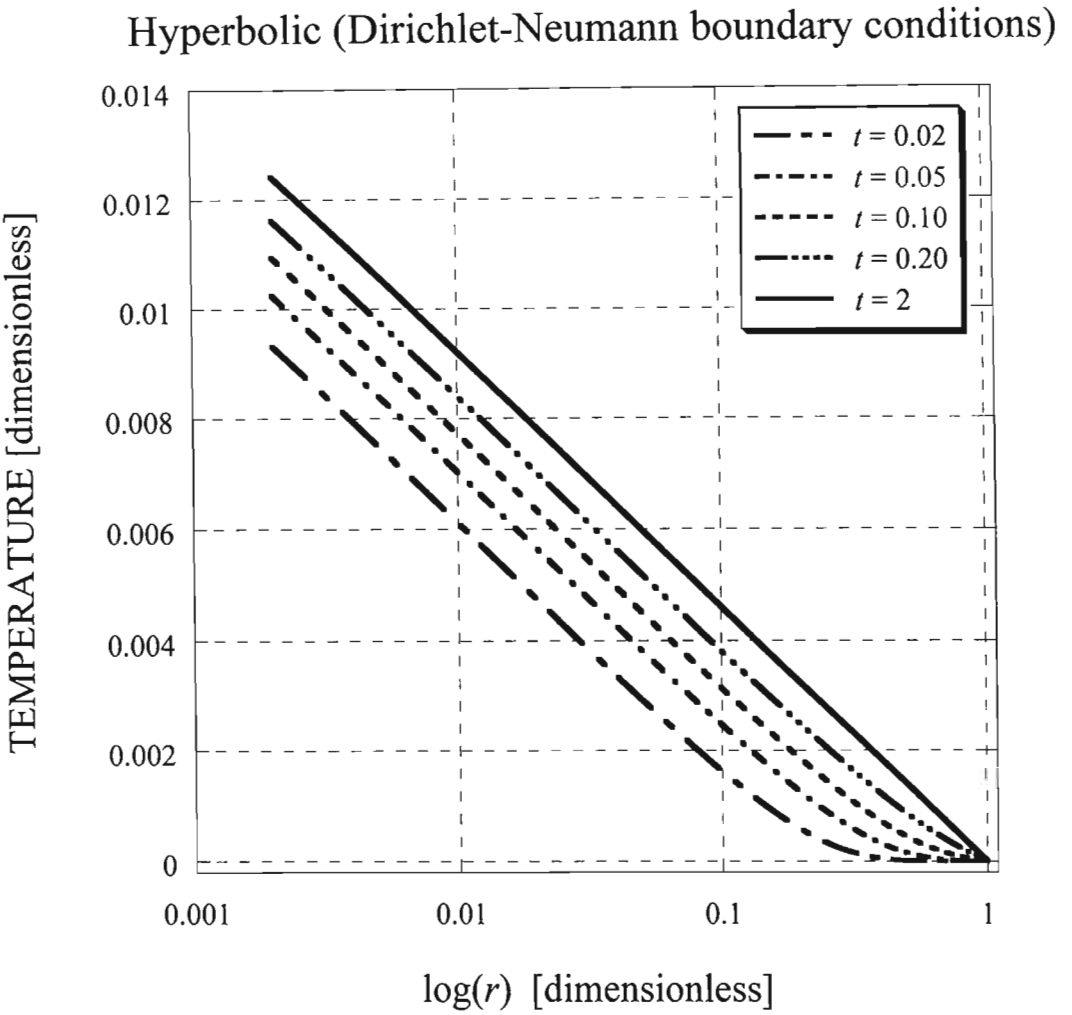

Figure 5-45:Temperature vs. log(r) in dimensionless form using a combination of Dirichlet and Neumann boundary conditions in the Hyperbolic heat conduction problem with Fourier number equal to 10^{-4}.

$Fo = 0.01$

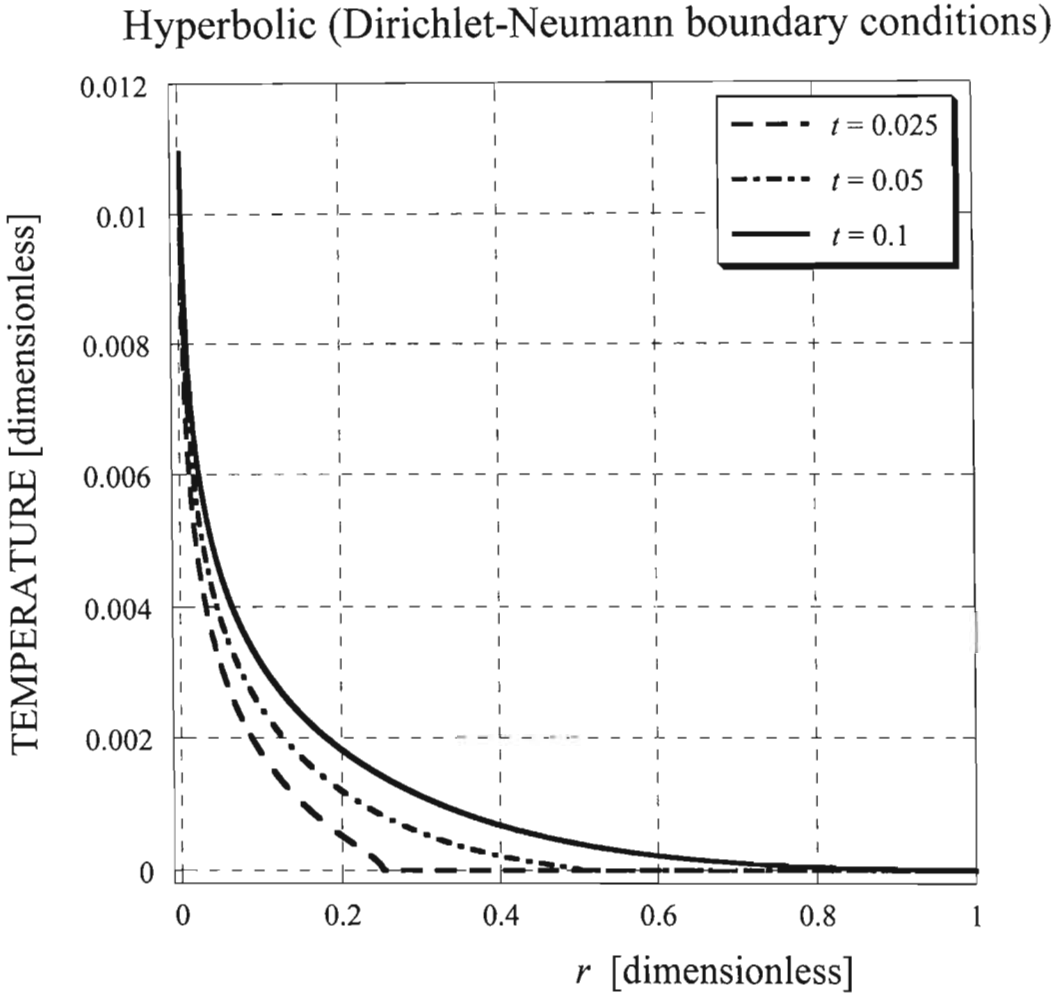

Figure 5-46:Temperature vs. r in dimensionless form using a combination of Dirichlet and Neumann boundary conditions in the Hyperbolic heat conduction problem with Fourier number equal to 0.01.

$Fo = 0.01$

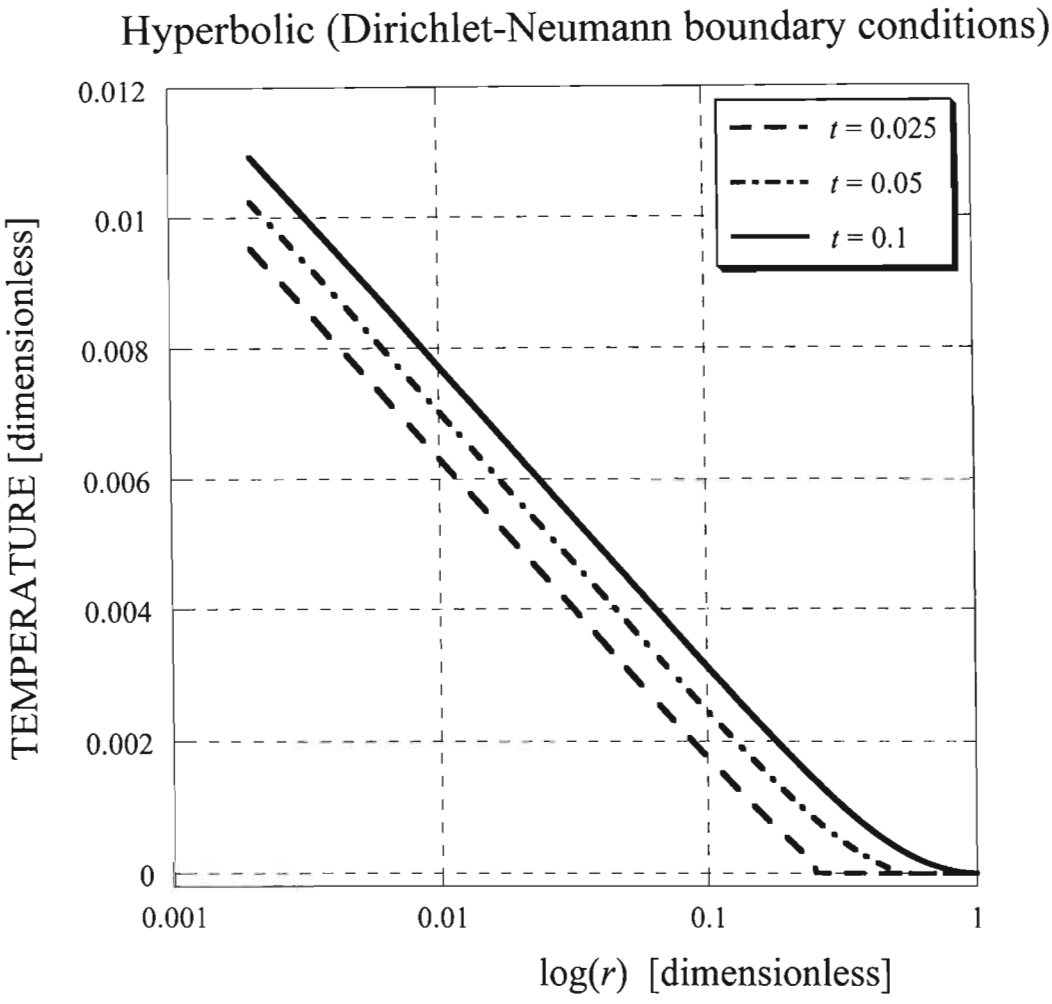

Figure 5-47:Temperature vs. log(r) in dimensionless form using a combination of Dirichlet and Neumann boundary conditions in the Hyperbolic heat conduction problem with Fourier number equal to 0.01.

$Fo = 0.01$

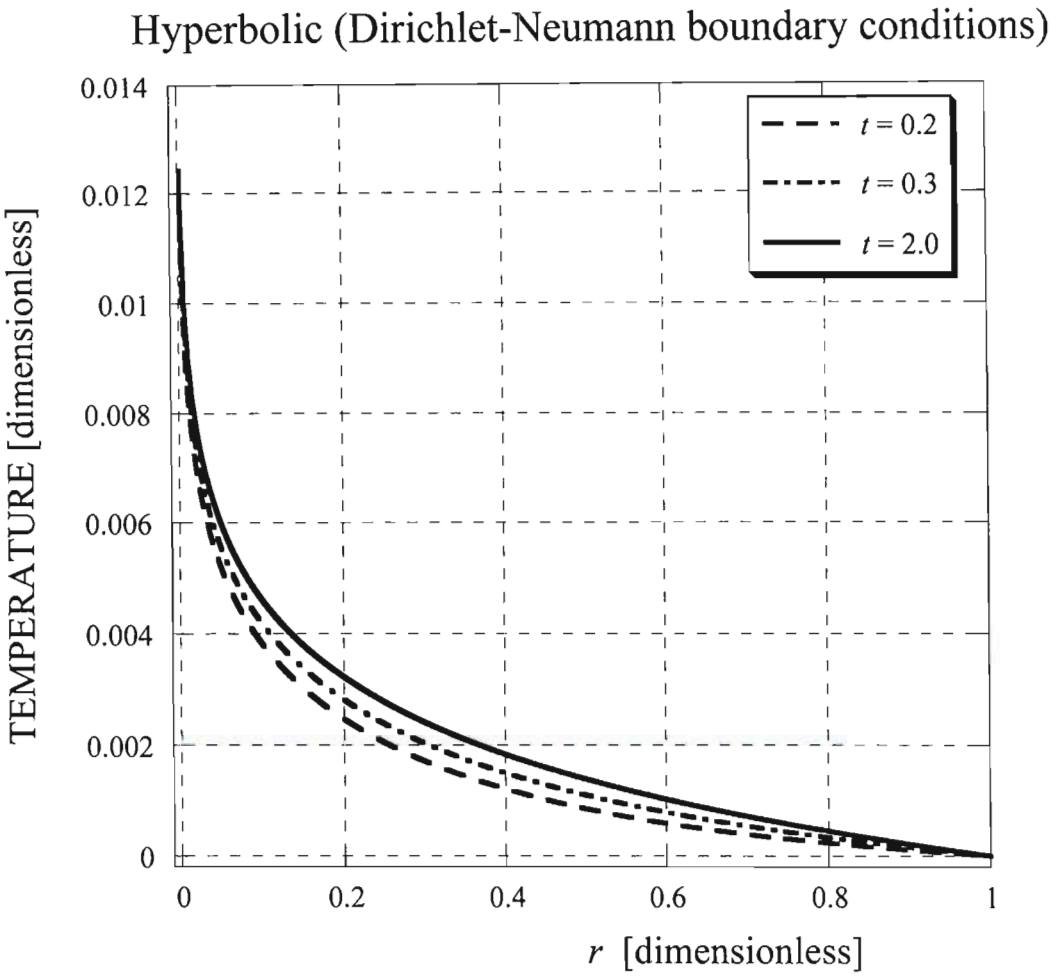

Figure 5-48:Temperature vs. r in dimensionless form using a combination of Dirichlet and Neumann boundary conditions in the Hyperbolic heat conduction problem with Fourier number equal to 0.01.

$Fo = 0.01$

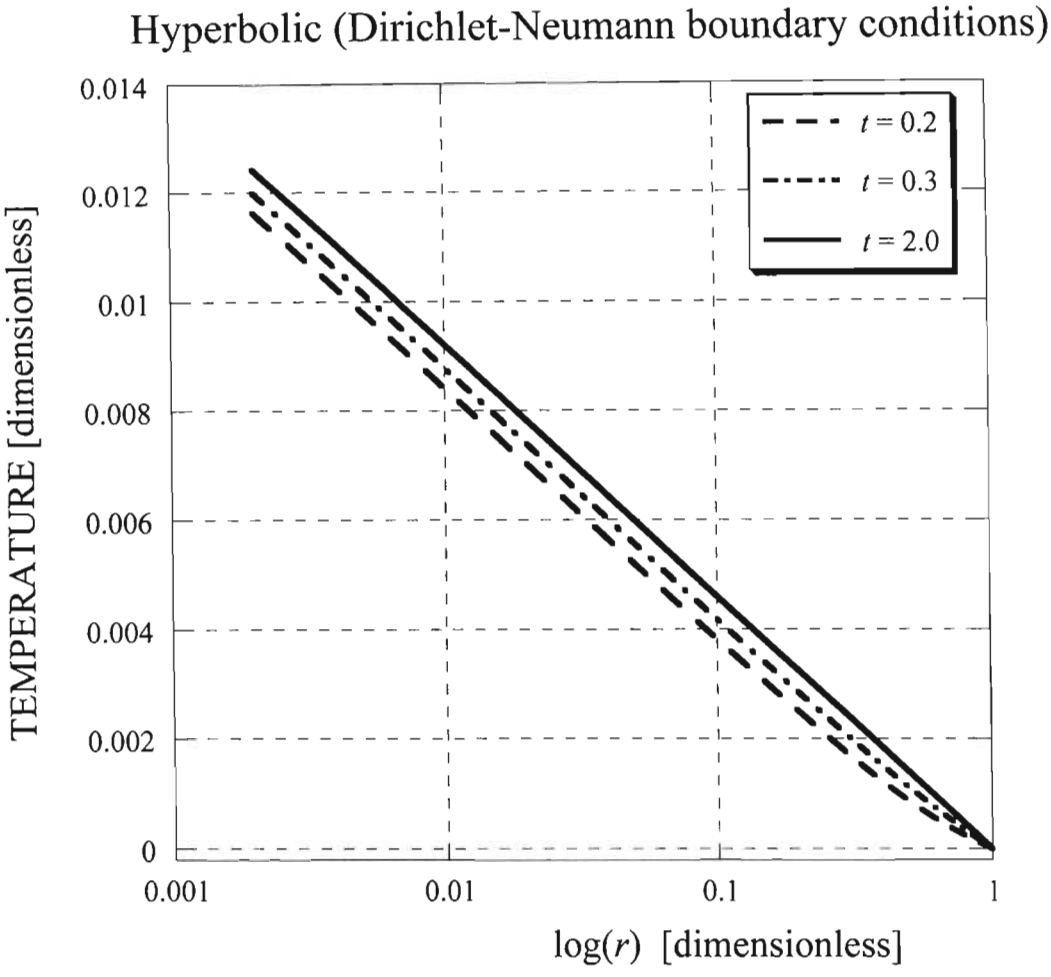

Figure 5-49:Temperature vs. log(r) in dimensionless form using a combination of Dirichlet and Neumann boundary conditions in the Hyperbolic heat conduction problem with Fourier number equal to 0.01.

$Fo = 0.1$

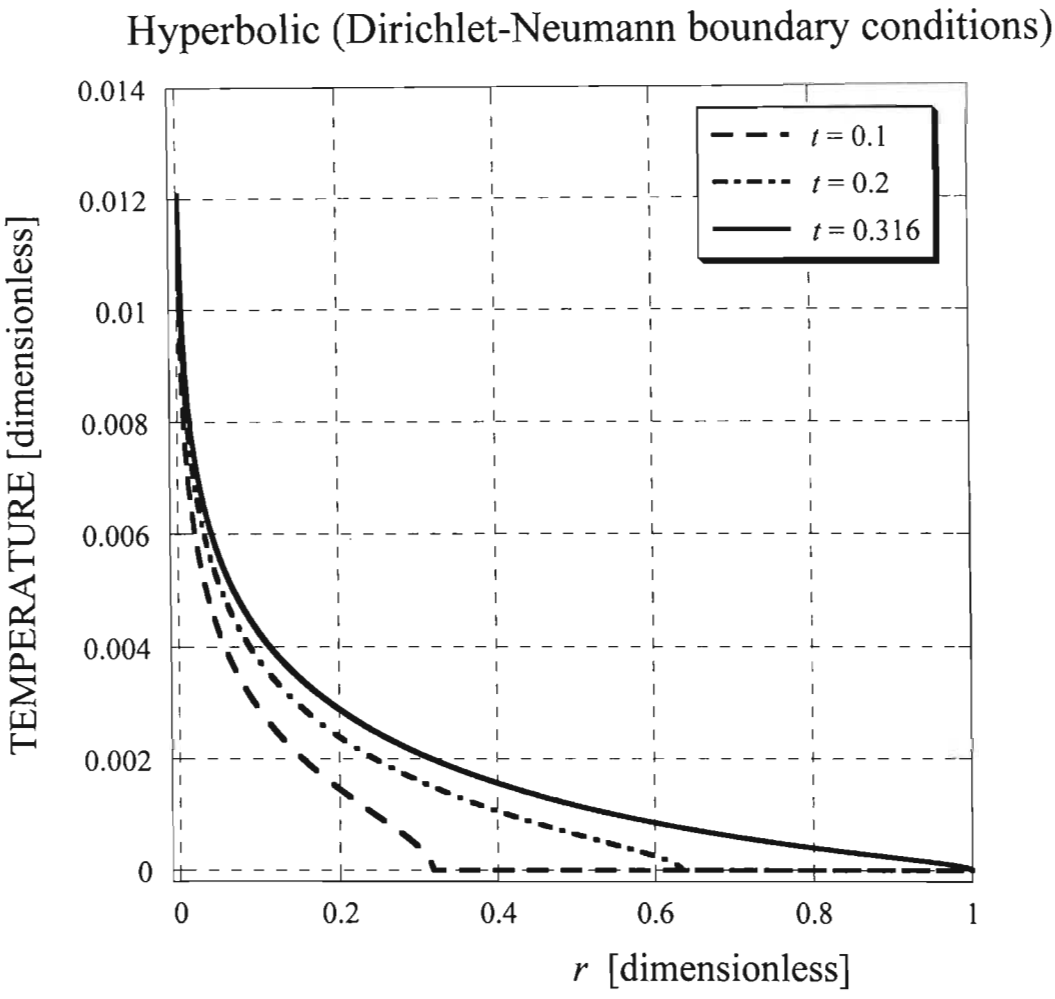

Figure 5-50:Temperature vs. r in dimensionless form using a combination of Dirichlet and Neumann boundary conditions in the Hyperbolic heat conduction problem with Fourier number equal to 0.1.

$Fo = 0.1$

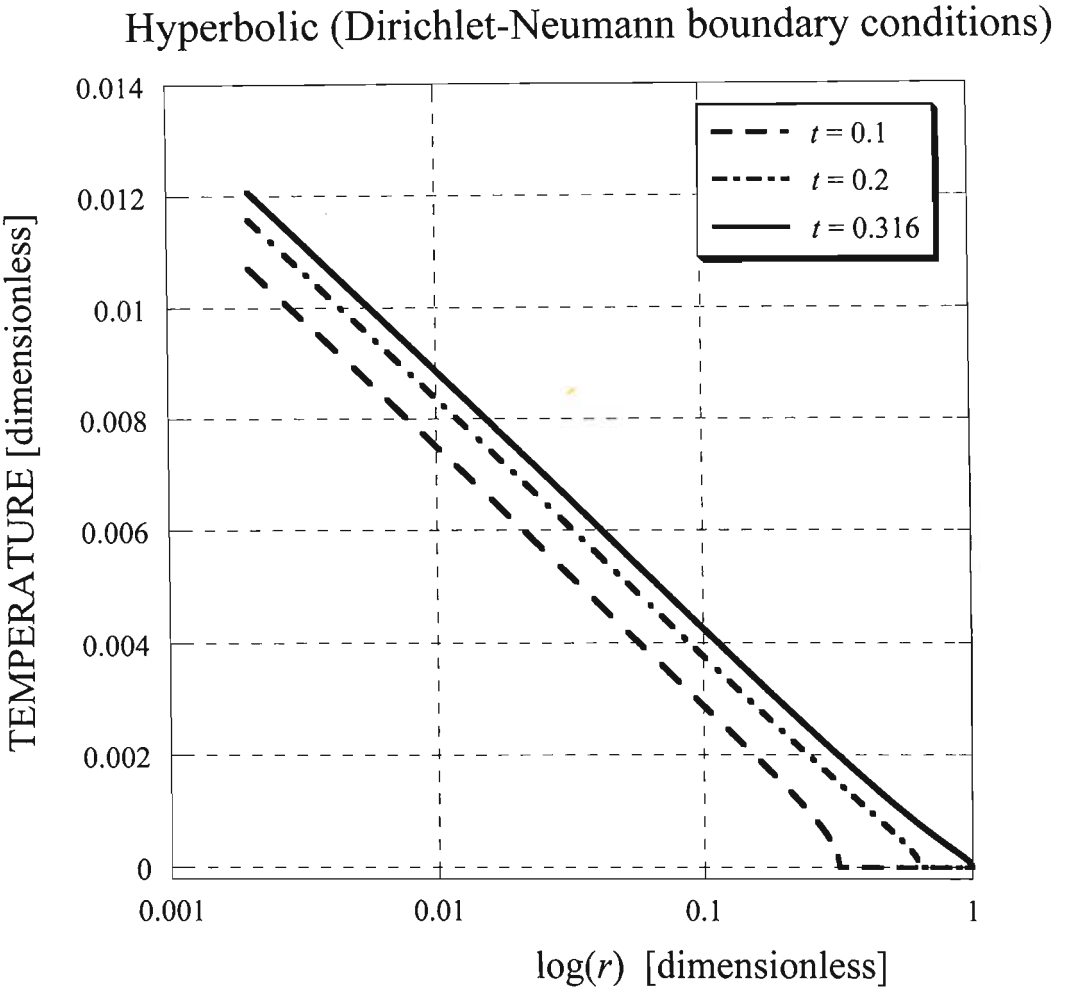

Figure 5-51:Temperature vs. log(r) in dimensionless form using a combination of Dirichlet and Neumann boundary conditions in the Hyperbolic heat conduction problem with Fourier number equal to 0.1.

$Fo = 0.1$

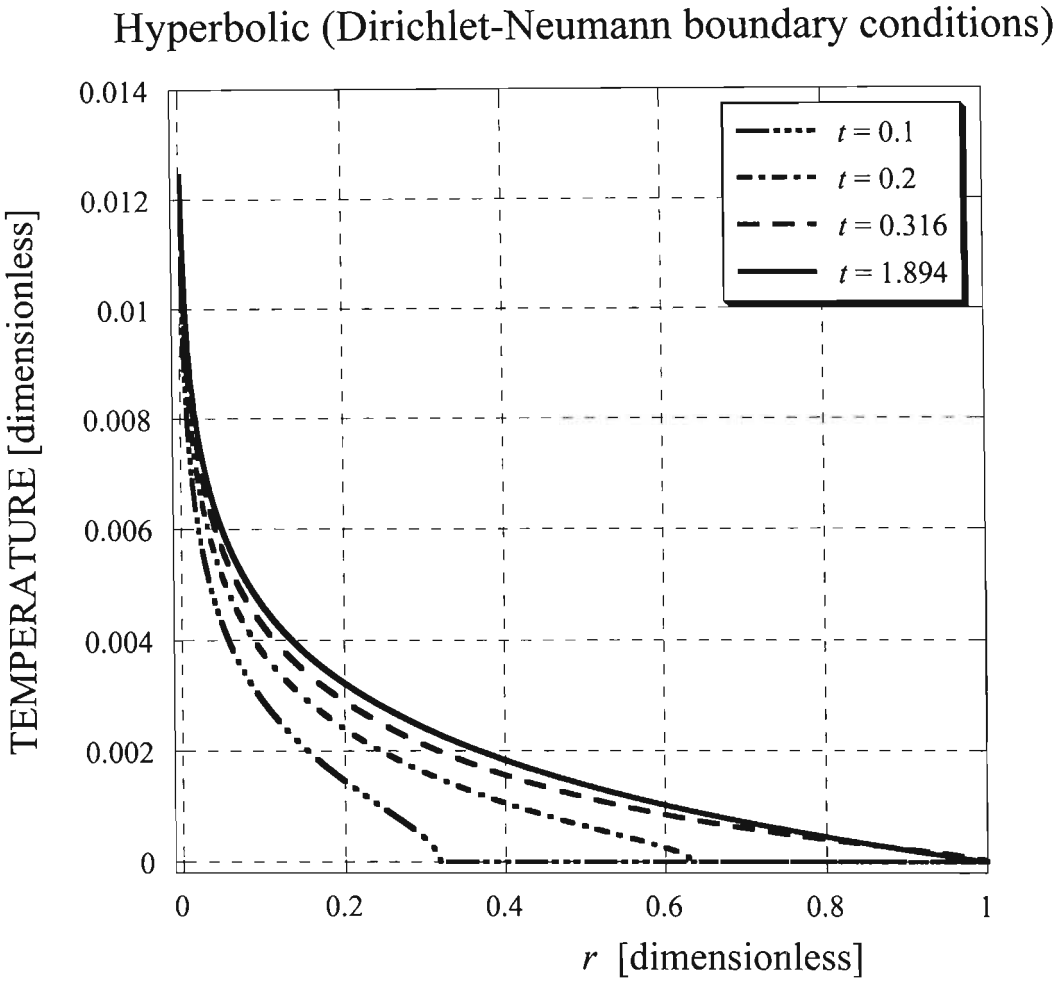

Figure 5-52:Temperature vs. r in dimensionless form using a combination of Dirichlet and Neumann boundary conditions in the Hyperbolic heat conduction problem with Fourier number equal to 0.1.

$Fo = 0.1$

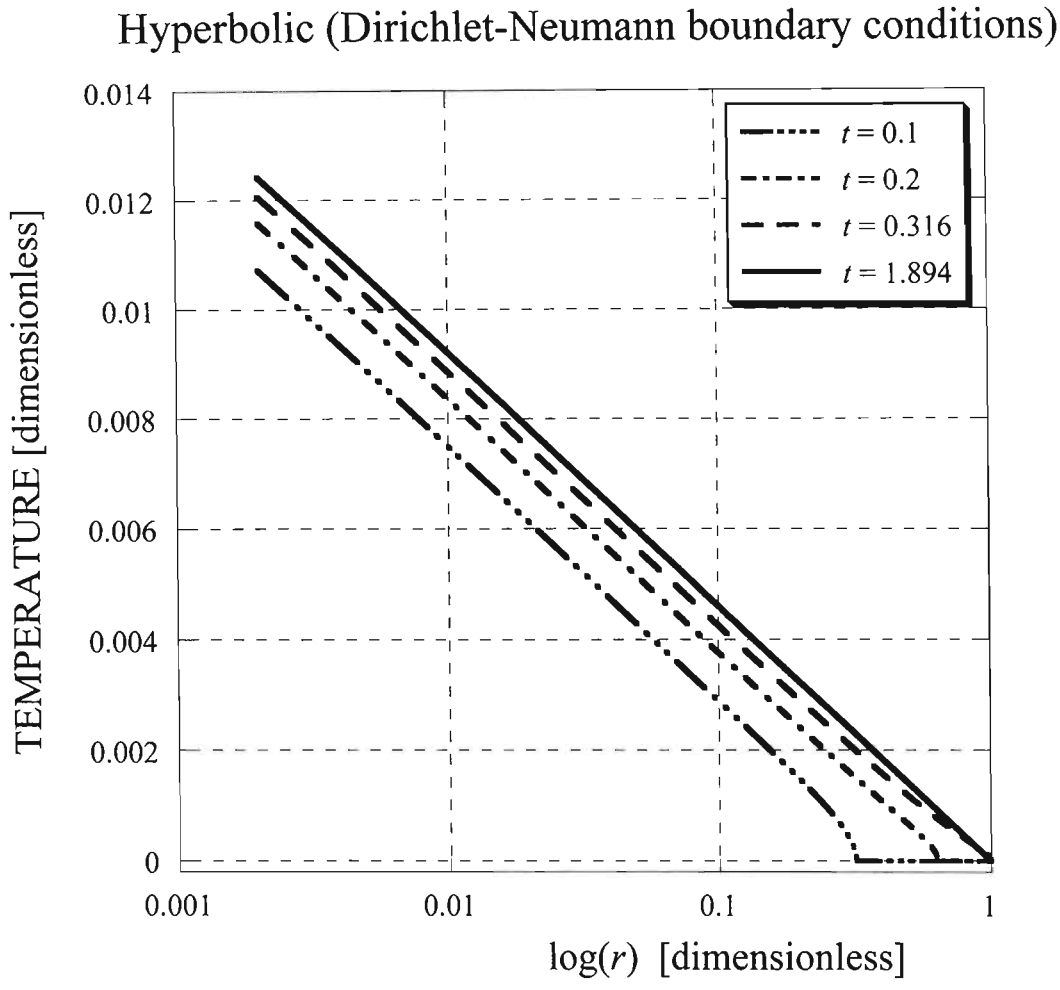

Figure 5-53:Temperature vs. log(r) in dimensionless form using a combination of Dirichlet and Neumann boundary conditions in the Hyperbolic heat conduction problem with Fourier number equal to 0.1.

$Fo = 1$

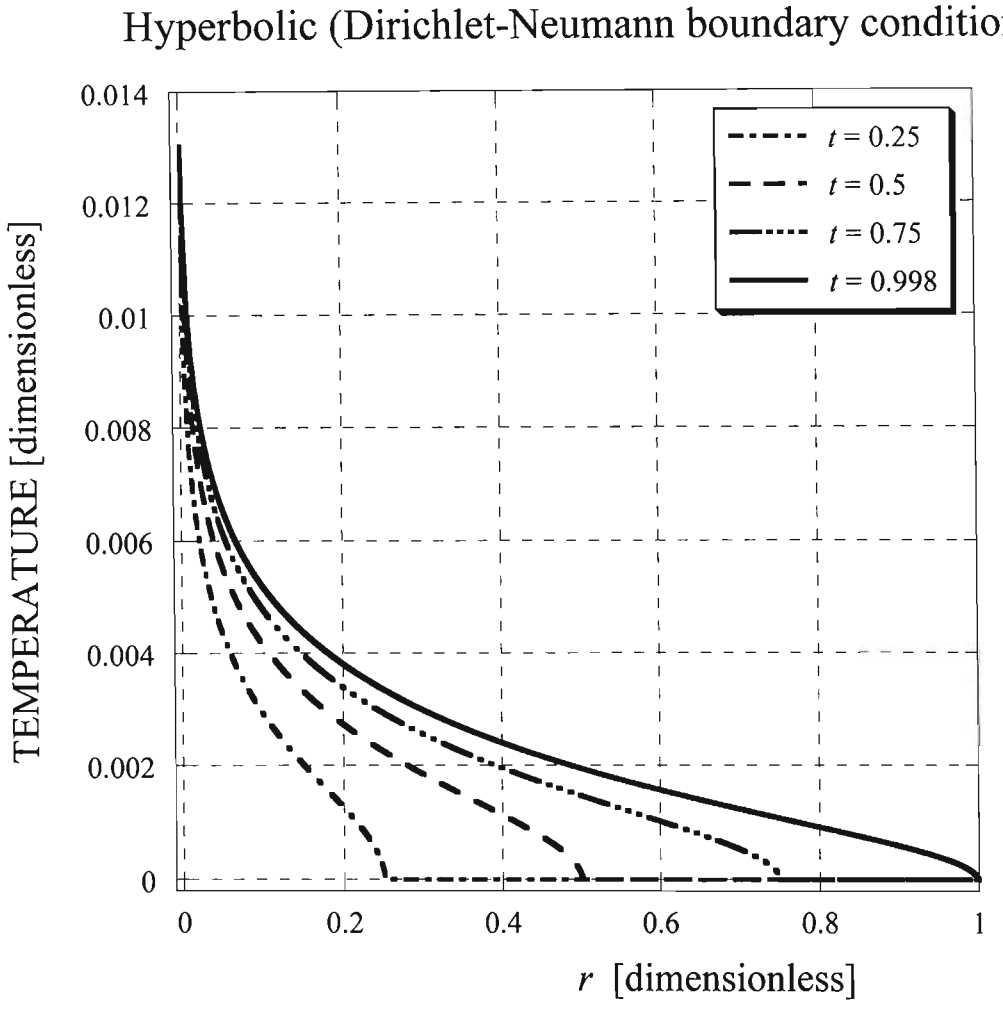

Figure 5-54:Temperature vs. r in dimensionless form using a combination of Dirichlet and Neumann boundary conditions in the Hyperbolic heat conduction problem with Fourier number equal to 1.

$Fo = 1$

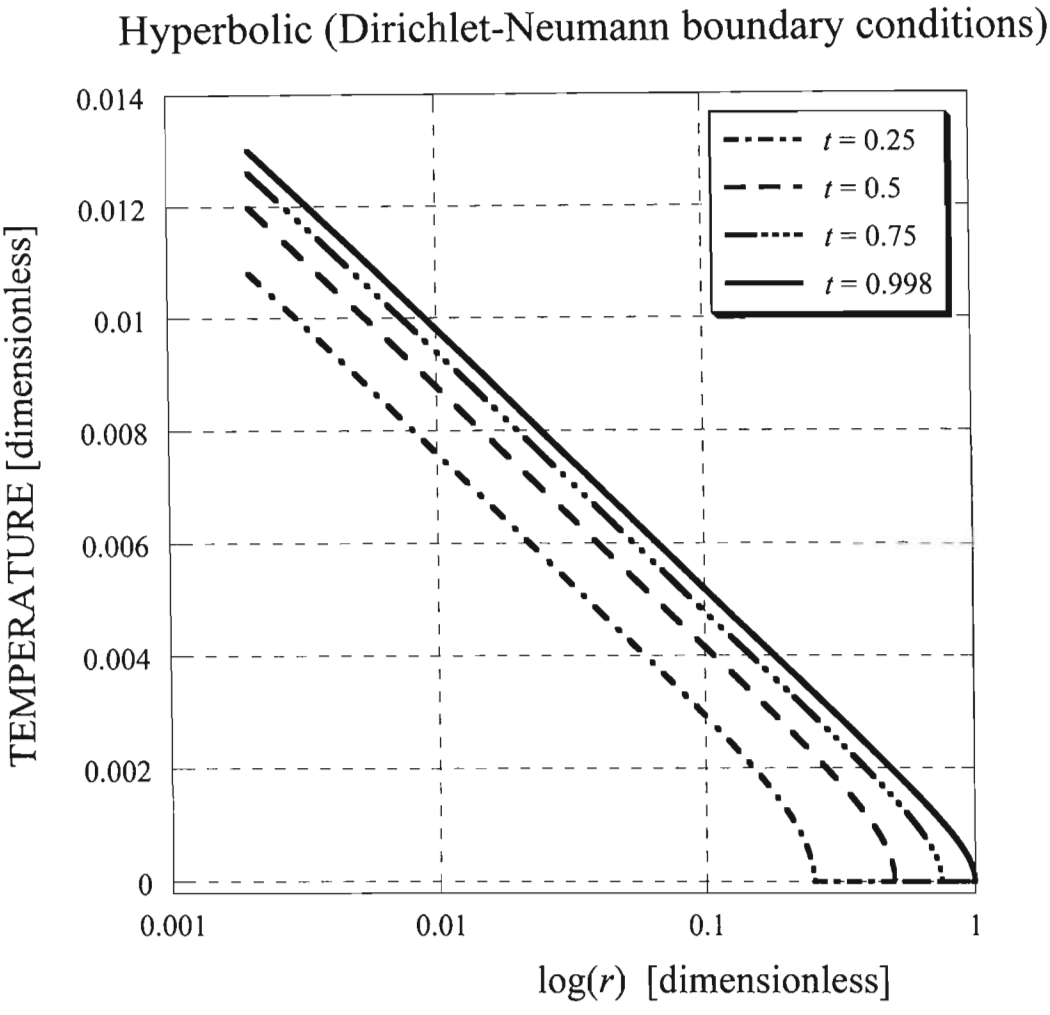

Figure 5-55:Temperature vs. log(r) in dimensionless form using a combination of Dirichlet and Neumann boundary conditions in the Hyperbolic heat conduction problem with Fourier number equal to 1.

$Fo = 1$

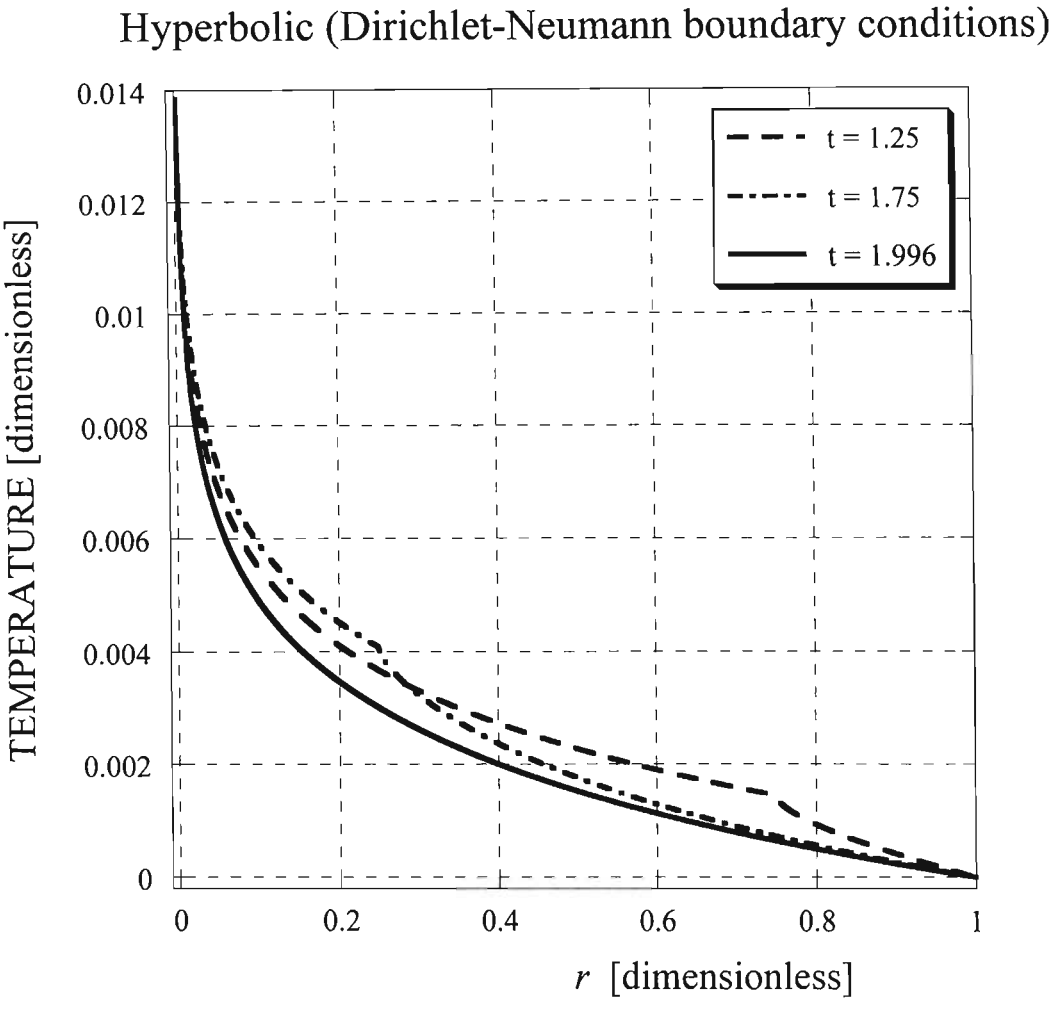

Figure 5-56:Temperature vs. r in dimensionless form using a combination of Dirichlet and Neumann boundary conditions in the Hyperbolic heat conduction problem with Fourier number equal to 1.

$Fo = 1$

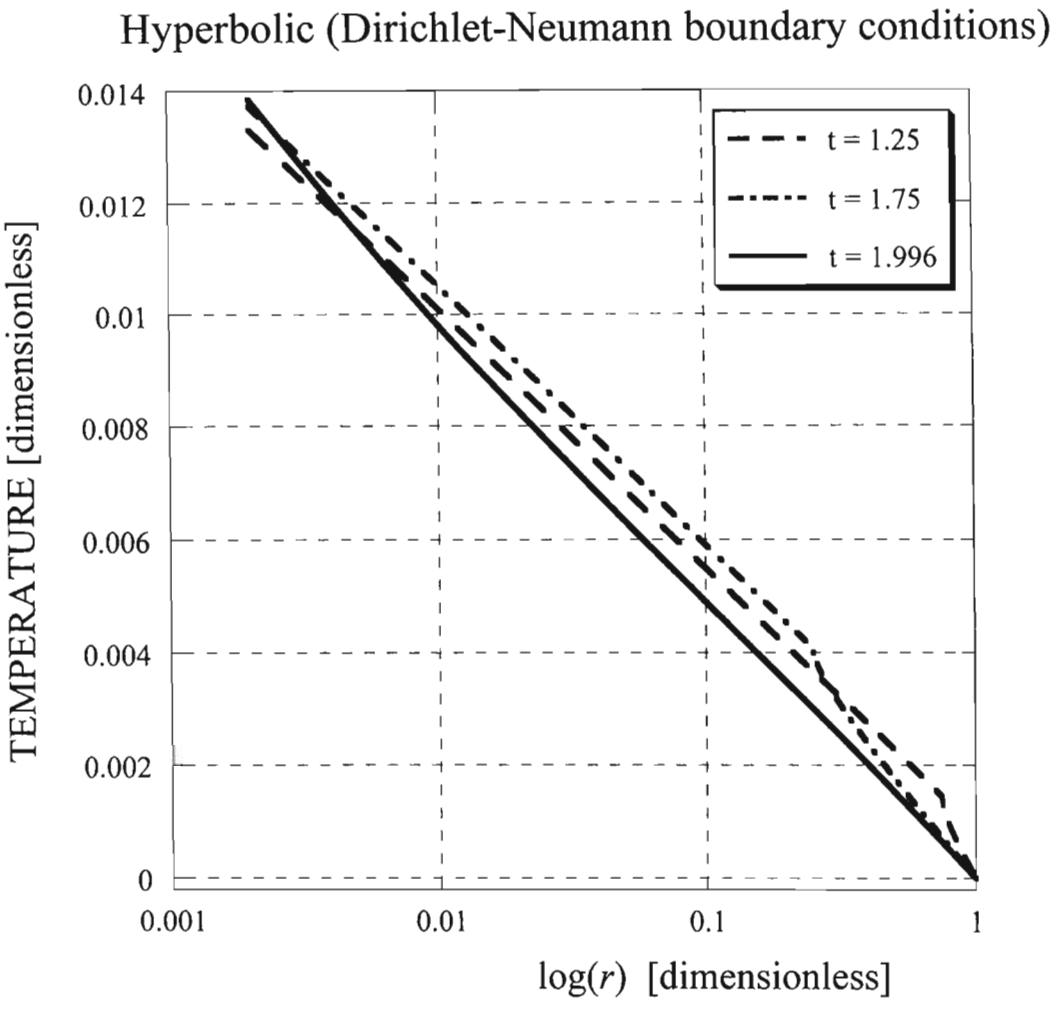

Figure 5-57:Temperature vs. log(r) in dimensionless form using a combination of Dirichlet and Neumann boundary conditions in the Hyperbolic heat conduction problem with Fourier number equal to 1.

Fo = 1

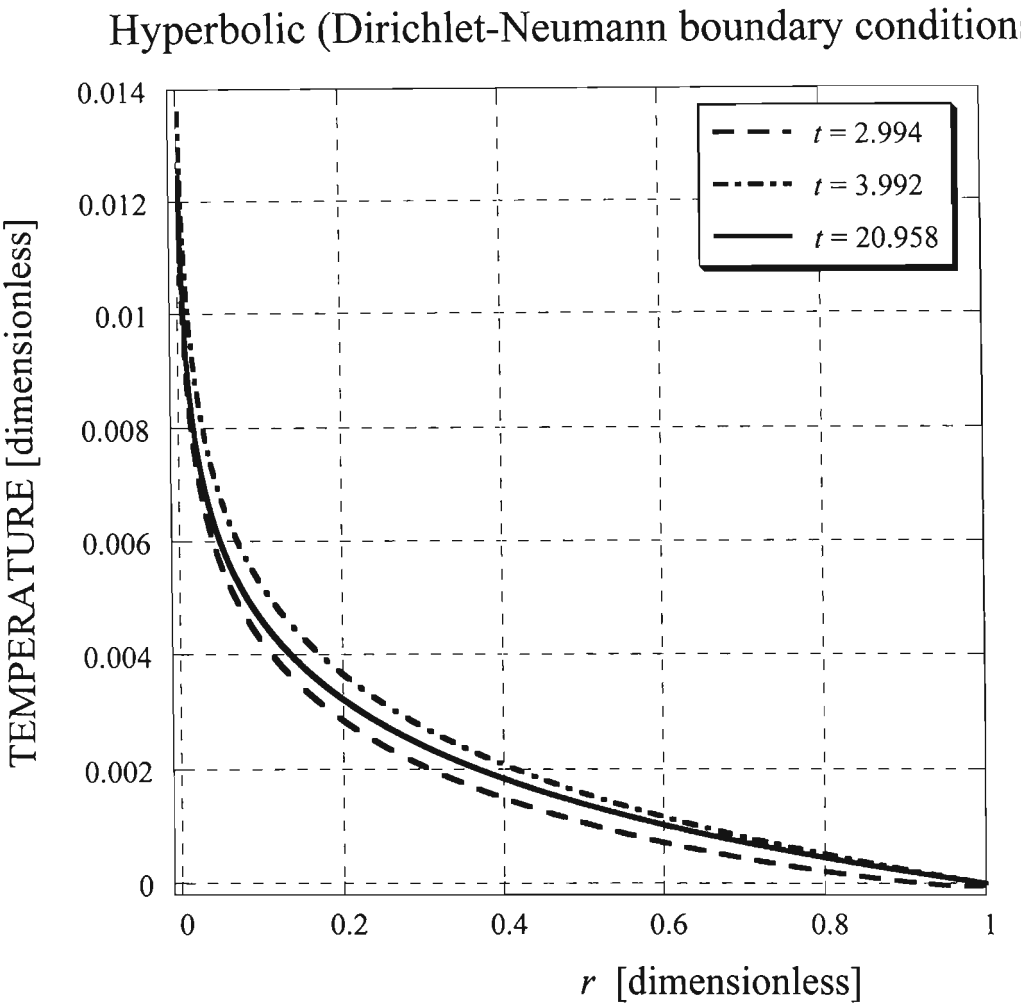

Figure 5-58:Temperature vs. r in dimensionless form using a combination of Dirichlet and Neumann boundary conditions in the Hyperbolic heat conduction problem with Fourier number equal to 1.

Fo = 1

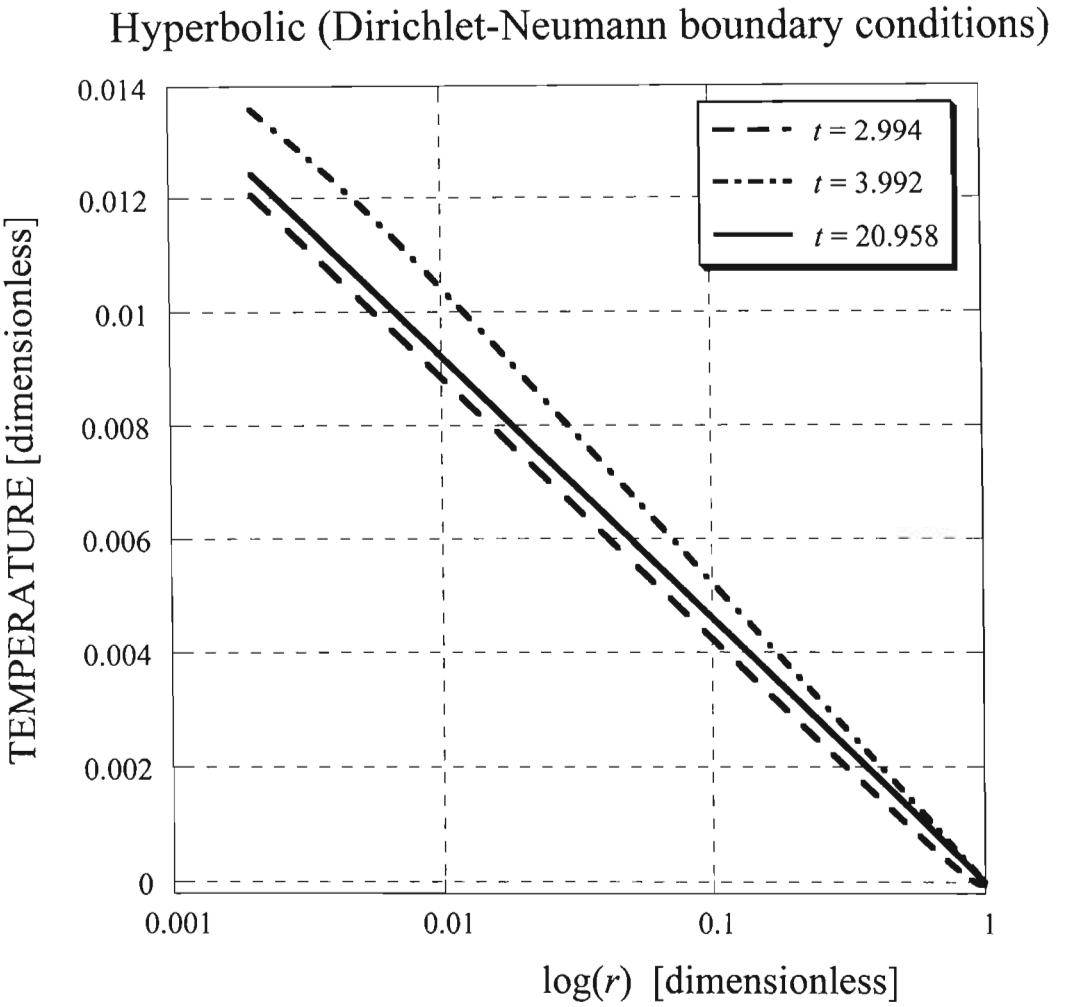

Figure 5-59:Temperature vs. log(r) in dimensionless form using a combination of Dirichlet and Neumann boundary conditions in the Hyperbolic heat conduction problem with Fourier number equal to 1.

$Fo = 10^{-4}$

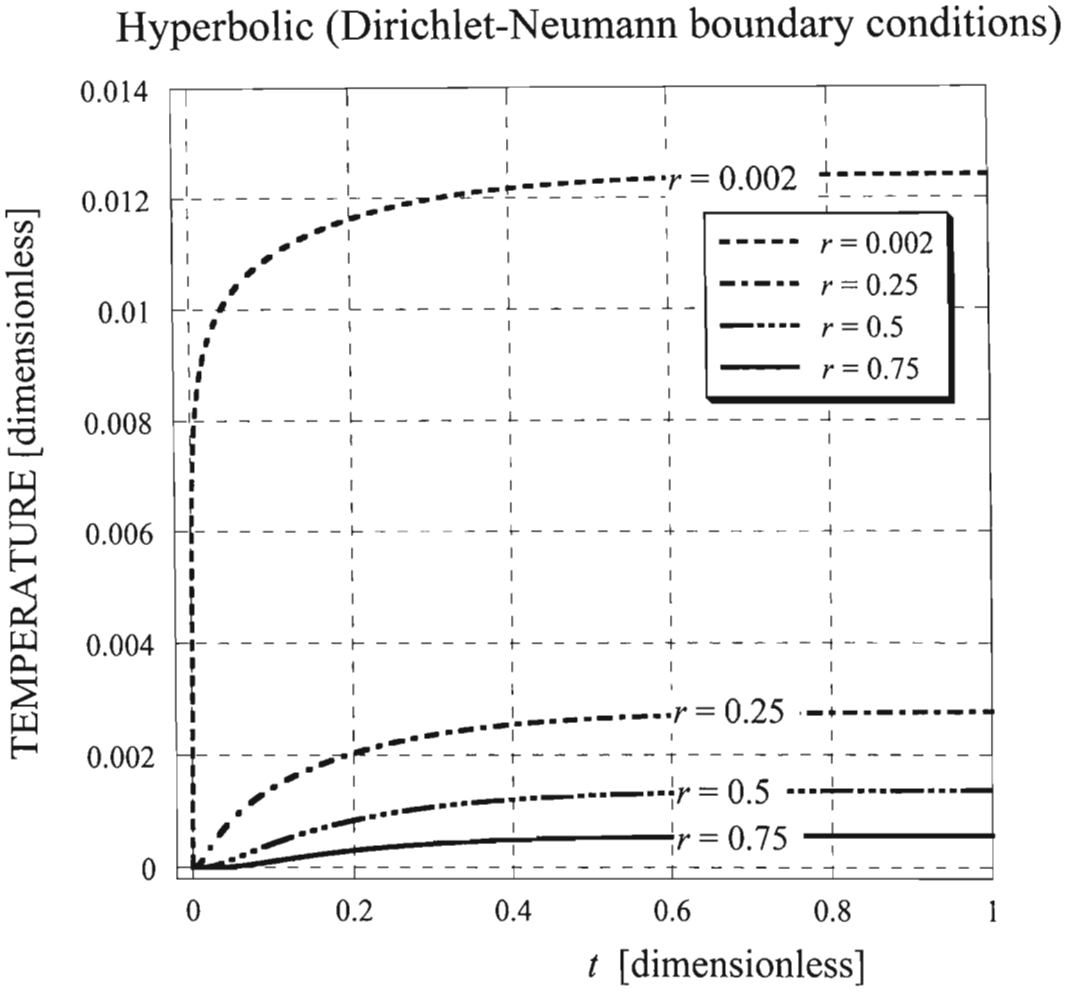

Figure 5-60:Temperature vs. t in dimensionless form using a combination of Dirichlet and Neumann boundary conditions in the Hyperbolic heat conduction problem with Fourier number equal to 10^{-4}.

$Fo = 0.01$

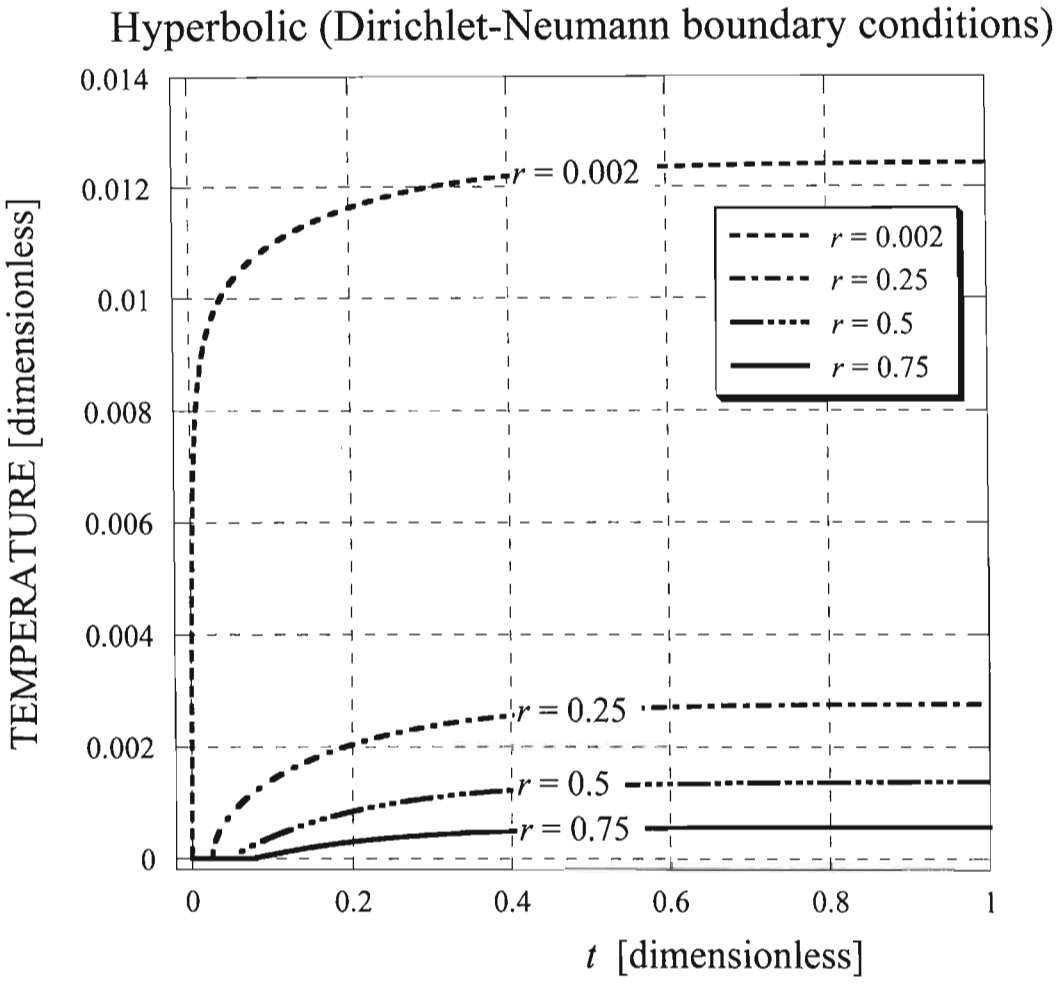

Figure 5-61:Temperature vs. t in dimensionless form using a combination of Dirichlet and Neumann boundary conditions in the Hyperbolic heat conduction problem with Fourier number equal to 0.01.

$Fo = 0.1$

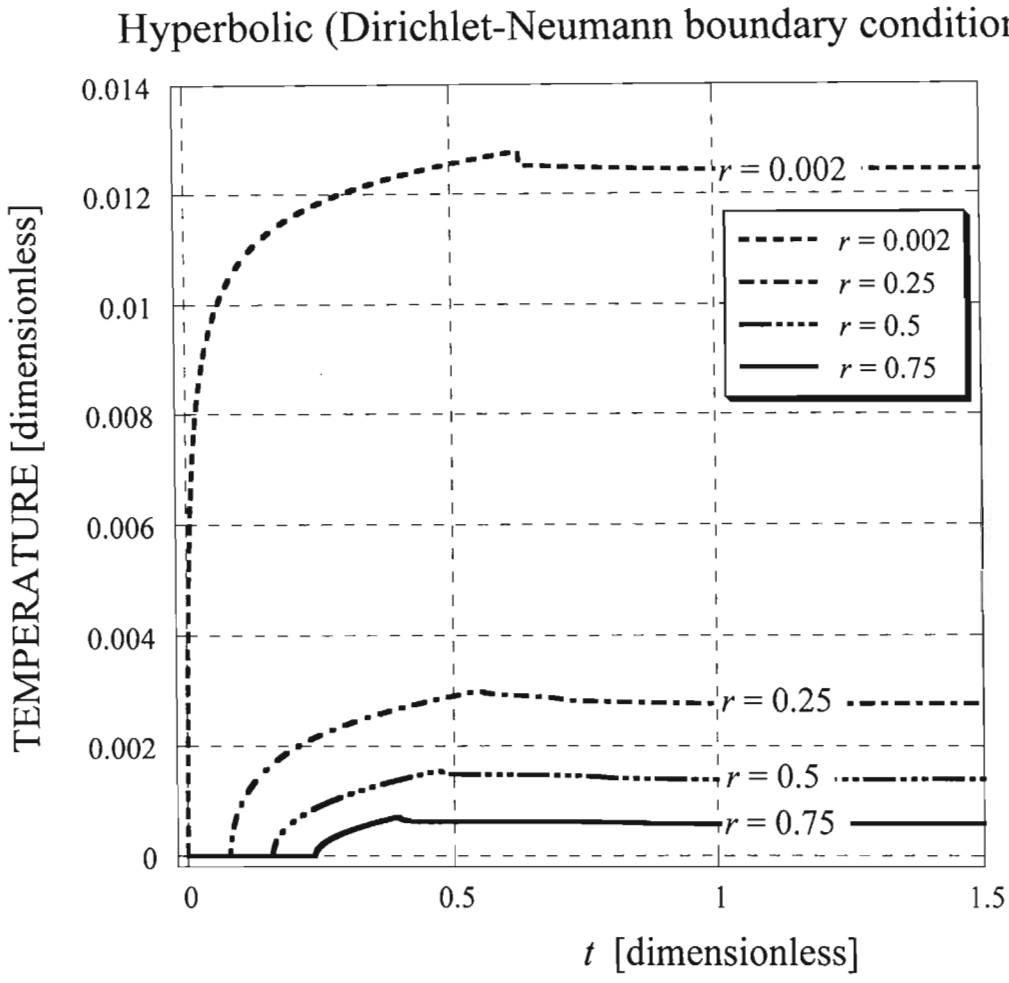

Figure 5-62:Temperature vs. t in dimensionless form using a combination of Dirichlet and Neumann boundary conditions in the Hyperbolic heat conduction problem with Fourier number equal to 0.1.

$Fo = 1$

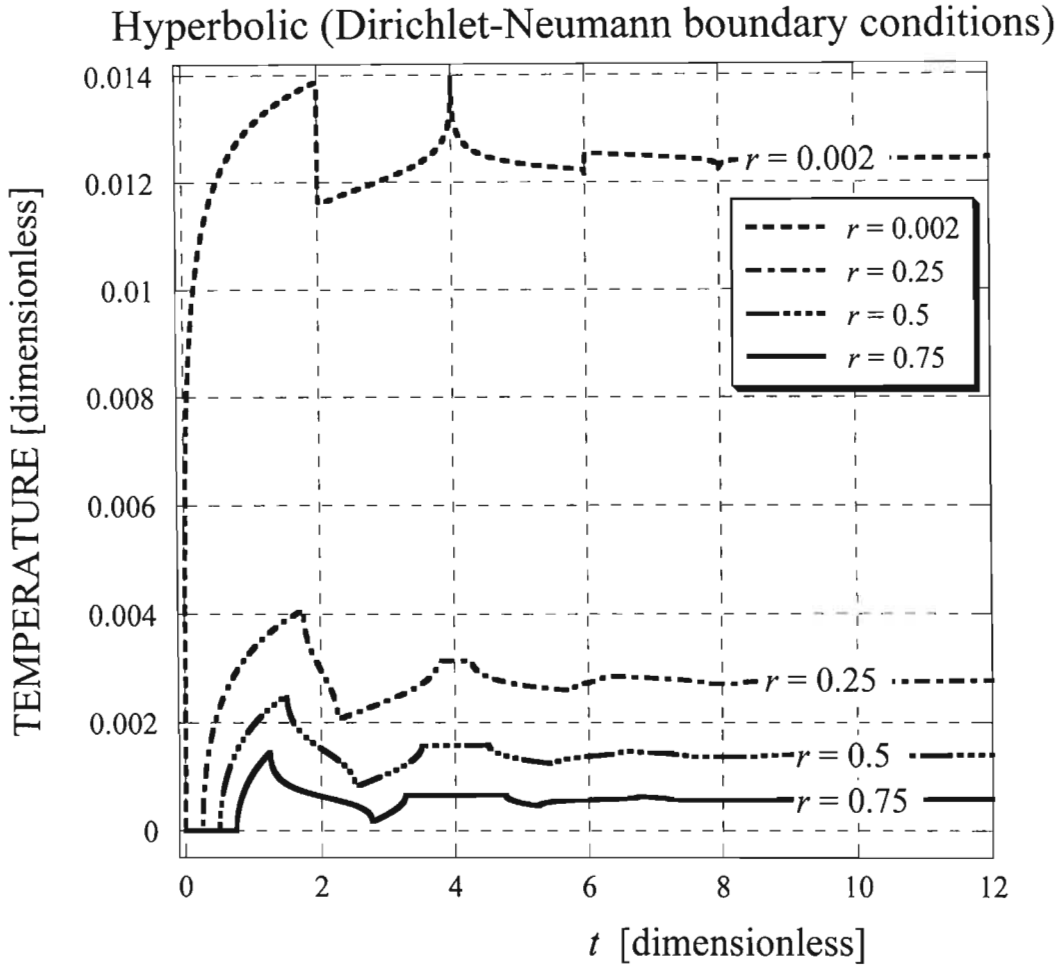

Figure 5-63:Temperature vs. t in dimensionless form using a combination of Dirichlet and Neumann boundary conditions in the Hyperbolic heat conduction problem with Fourier number equal to 1.

5.6 Results of the SEED (Synthetic Experimental Emulation Data) method.

When evaluating the thermal conductivity by applying the Transient Hot Strip method and using the Fourier Law one obtains from equation (4-11) the following solution for the dimensional temperature $T_{L^*}(t)$ at $x = 1$

$$\left[T_{L^*}(t) - T_{C^*}\right] = \frac{|q_{L^*}|\, L_*}{k_{app}}\left[1 + f(t)\right] \tag{5-1}$$

where

$$f(t) = \sum_{n=0}^{\infty} C_n \exp\left[-\frac{(2n+1)^2 \pi^2}{4} t\right] \tag{5-2}$$

and for initial conditions of $T_o = 0$ the values of C_n are evaluated and expressed in the form

$$C_n = -\frac{8}{(2n+1)^2 \pi^2} \tag{5-3}$$

which following substitution into equation (5-2) yields

$$f(t) = \sum_{n=0}^{\infty} -\frac{8}{(2n+1)^2 \pi^2} \exp\left[-\frac{(2n+1)^2 \pi^2}{4} t\right] \tag{5-4}$$

From equation (5-1) the thermal conductivity can be evaluated in the form

$$k_{app} = \frac{|q_{L^*}|\, L_*}{\left[T_{L^*}(t) - T_{C^*}\right]}\left[1 + f(t)\right] \tag{5-5}$$

where the temperature difference $\left[T_{L^*}(t) - T_{C^*}\right]$ is represented by the recorded experimental data and the value of the wall heat flux $|q_L|$ is evaluated from the Joule heating of the hot strip in the form $|q_L| = iV/A_{*strip}$, where $A_{*strip} = d_* l_*$ is the heat transfer area of the hot strip, with l_* being the length of the strip and d_* the depth of the hot strip.

A method of *Synthetic Experimental Emulation Data* (*SEED* is applied now to evaluate the deviation between Fourier and hyperbolic thermal conduction. According to the *SEED* method one assumes that the data expressed by $\left[T_{L^*}(t) - T_{C^*}\right]$ represent a different than Fourier conduction solution, in this case a hyperbolic thermal conduction solution. Then the values of $\left[T_{L^*}(t) - T_{C^*}\right]$ obtained from the hyperbolic solution expressed by equations (4-40) and (4-49) are substituted in equation (5-5) to yield

$$\frac{k_{app}}{k_{act}} = \frac{[1+f(t)]}{[1+h(t)]} \tag{5-6}$$

where k_{app} is the apparent thermal conductivity obtained from the Fourier conduction solution while k_{act} is the actual thermal conductivity that corresponds to data that follow the hyperbolic conduction, and where $f(t)$ can be evaluated from equation (5-4) while $h(t)$ is evaluated from equation (4-39). The ratio between the two will provide the deviation of the apparent thermal conductivity from the actual one.

All the results presented here apply to the dimensional time range that was evaluated in section 2.2 to be consistent with the Transient Hot Wire method.

Figure 5-64 shows the thermal conductivity ratio versus time for $Fo = 10^{-4}$ for copper in Ethylene Glycol for rectangular geometry. It is seen that even with a small $Fo = 10^{-4}$ when the wave effects are small, at short values of time there is an overestimation of the thermal conductivity when using Fourier conduction values. Figure 5-65 shows the thermal conductivity ratio versus time for $Fo = 10^{-4}$ for carbon nanotubes in oil for rectangular geometry. The results are similar to that in Figure 5-64 only slightly higher. This means that the overestimation with carbon nanotubes in oil is higher then that of copper in Ethylene Glycol. Figure 5-66 shows the thermal conductivity ratio versus time for $Fo = 10^{-3}$ for copper in Ethylene Glycol for rectangular geometry. The overestimation of the thermal conductivity at t = 5s is approximately 150%. Figure 5-67 shows the thermal conductivity ratio versus time for $Fo = 10^{-3}$ for carbon nanotubes in oil for rectangular geometry. For carbon nanotubes in oil the overestimation of the thermal conductivity at t = 5s is approximately 160%. Figure 5-68 shows the thermal conductivity ratio versus time for $Fo = 0.01$ for copper in Ethylene Glycol for rectangular geometry. With the increase in the Fourier number the wave effects are more noticeable. For this reason the overestimation of the thermal conductivity is greater. At a time t = 10s in Figure 5-68 the overestimation of the thermal conductivity is approximately 250%. Figure 5-69 shows the thermal conductivity ratio versus time for $Fo = 0.01$ for carbon nanotubes in oil for rectangular geometry. At a time t = 10s in Figure 5-69 the overestimation of the thermal conductivity is approximately 260%. For a cylindrical geometry similar derivations apply. When evaluating the thermal conductivity by applying the Transient Hot Wire method and using the Fourier Law one obtains from

equation (4-47) the following solution for the dimensional temperature $T_{w*}(t)$ at $r = r_w$

$$\left[T_{w*}(t) - T_{C*}\right] = \frac{q_{o*}\, r_{o*}}{k_{app}}\left[-r_w \ln(r_w) + f(t)\right] \tag{5-7}$$

where

$$f(t) = \sum_{n=0}^{\infty} C_n \exp\left[-\beta_n^2\, t\right] \tag{5-8}$$

and for initial conditions of $T_o = 0$ the values of C_n are evaluated by using equations (4-47) and (4-45)

From equation (5-7) the thermal conductivity can be evaluated in the form

$$k_{act} = \frac{q_{o*} L_*}{\left[T_{w*}(t) - T_{C*}\right]}\left[-r_w \ln(r_w) + f(t)\right] \tag{5-9}$$

where the temperature difference $\left[T_{w*}(t) - T_{C*}\right]$ is represented by the recorded experimental data and the value of the wall heat flux q_{o*} is evaluated from the Joule heating of the hot wire in the form $q_{o*} = iV/2\pi r_{w*} l_*$, where $2\pi r_{w*} l_*$ is the heat transfer area of the hot wire, with l_* being the length of the wire i is the electric current flowing through the wire and V is the voltage drop across the wire.

A method of *Synthetic Experimental Emulation Data* (*SEED* is applied now to evaluate the deviation between Fourier and hyperbolic thermal conduction. According to the *SEED* method one assumes that the data expressed by $\left[T_{w*}(t) - T_{C*}\right]$ represent a different than Fourier conduction solution, in this case a hyperbolic thermal conduction solution. Then the values of $\left[T_{w*}(t) - T_{C*}\right]$ were derived by using the hyperbolic solution presented in equations (4-48) evaluated at $r = r_w$ to yield

$$\frac{k_{app}}{k_{act}} = \frac{\left[-r_w \ln(r_w) + f(t)\right]}{\left[-r_w \ln(r_w) + h(t)\right]} \tag{5-10}$$

where k_{app} is the apparent thermal conductivity obtained from the Fourier conduction solution while k_{act} is the actual thermal conductivity that corresponds to data that follow the hyperbolic conduction, and where $f(t)$ can be evaluated from equation (5-8) while $h(t)$ is derived from the hyperbolic solution (4-48) evaluated at $r = r_w$. The ratio between the two will provide the deviation of the apparent thermal

conductivity from the actual one. Figure 5-70 shows the thermal conductivity ratio versus time for $Fo = 10^{-4}$ for copper in Ethylene Glycol for cylindrical geometry. Comparing Figure 5-70 to 5-64 shows that the overestimation in cylindrical geometry is lower then that in the rectangular geometry. Figure 5-71 shows the thermal conductivity ratio versus time for $Fo = 10^{-4}$ for carbon nanotubes in oil for cylindrical geometry. Again the overestimation of the thermal conductivity is less in cylindrical geometry then in rectangular one. Figure 5-72 shows the thermal conductivity ratio versus time for $Fo = 10^{-3}$ for copper in Ethylene Glycol for cylindrical geometry. The overestimation of the thermal conductivity at t = 5s is approximately 105%, which is 45% lower then that in rectangular geometry. Figure 5-73 shows the thermal conductivity ratio versus time for $Fo = 10^{-3}$ for carbon nanotubes in oil for cylindrical geometry. The overestimation of the thermal conductivity at t = 5s is approximately 110%, which is 40% lower then that in rectangular geometry. Figure 5-74 shows the thermal conductivity ratio versus time for $Fo = 0.01$ for copper in Ethylene Glycol for cylindrical geometry. The overestimation of the thermal conductivity at t = 10s is approximately 125%, which is again lower then that in rectangular geometry. Figure 5-75 shows the thermal conductivity ratio versus time for $Fo = 0.01$ for carbon nanotubes in oil for cylindrical geometry. The overestimation of the thermal conductivity at t = 10s is approximately 130%, which is again lower then that in rectangular geometry. In Figures 5-74 and 5-75 the overestimation in thermal conductivity at time t = 5s is approximately 155% and 160% respectively. This shows that even though there is a big difference in the overestimation of thermal conductivity between rectangular and cylindrical geometry it is still significant and of the same magnitude as the experiments predict the enhancement in thermal conductivity.

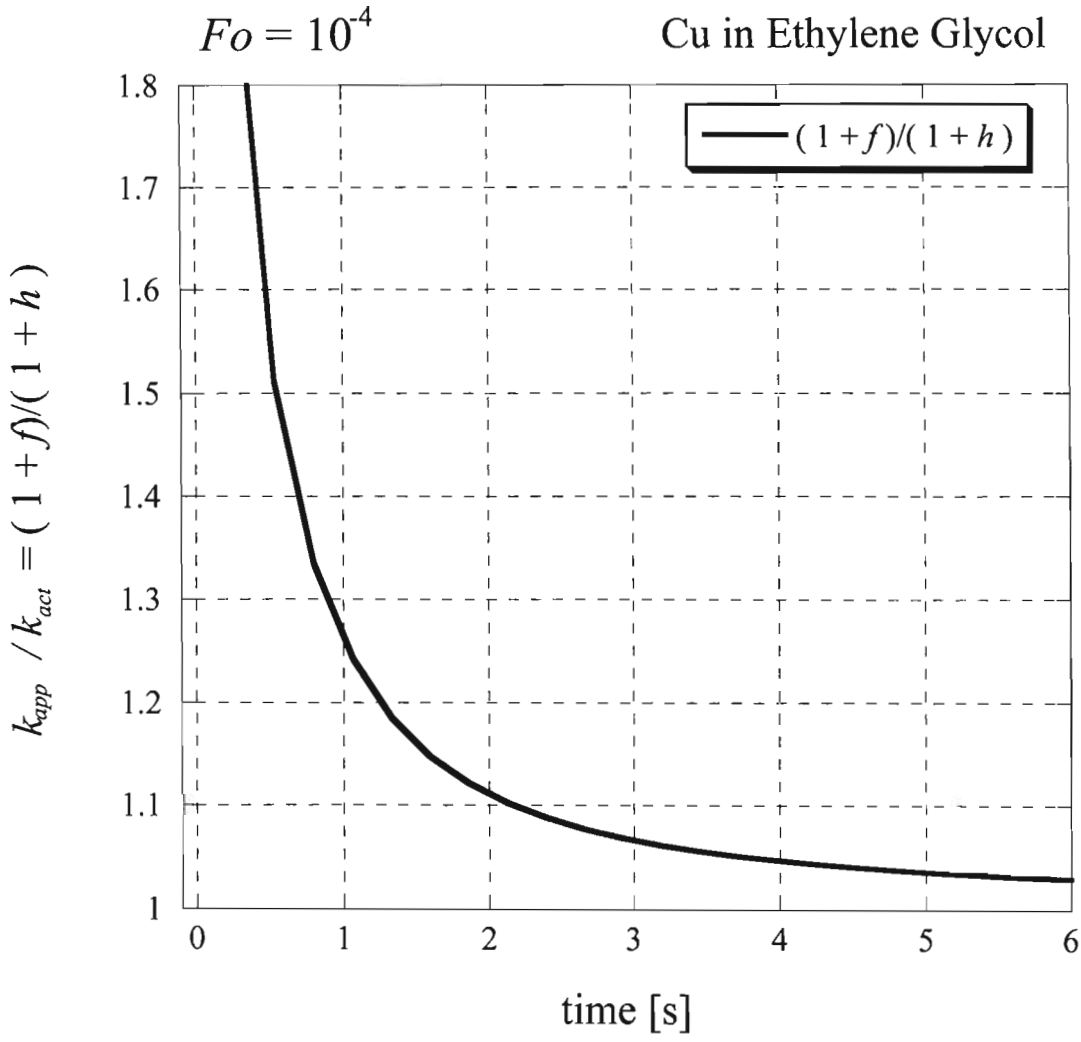

Figure 5-64: Thermal conductivity ratio vs. time in dimensional units for Cu in Ethylene Glycol in rectangular geometry for a Fourier number equal to 10^{-4}.

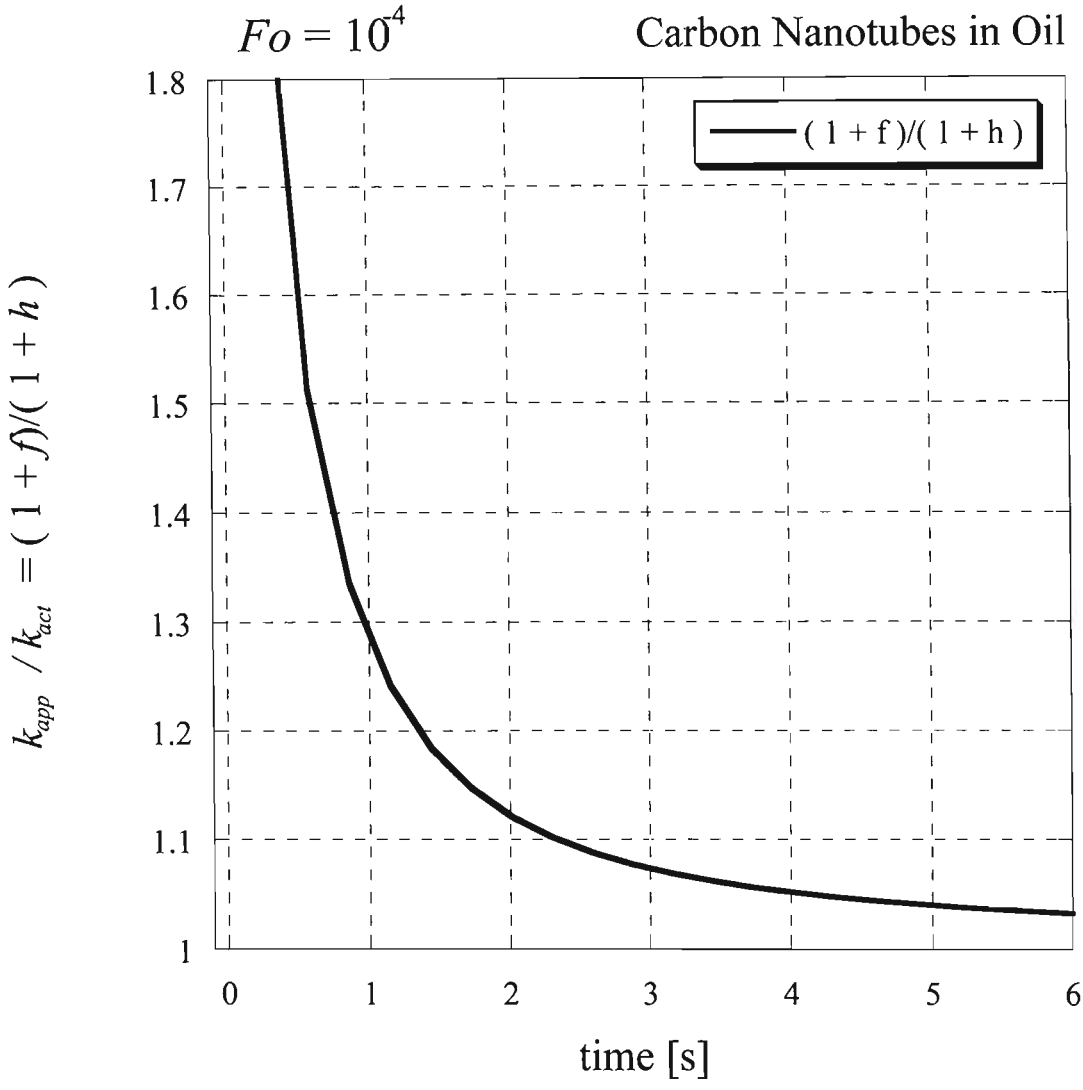

Figure 5-65: Thermal conductivity ratio vs. time in dimensional units for Carbon Nanotubes in Oil in rectangular geometry for a Fourier number equal to 10^{-4}.

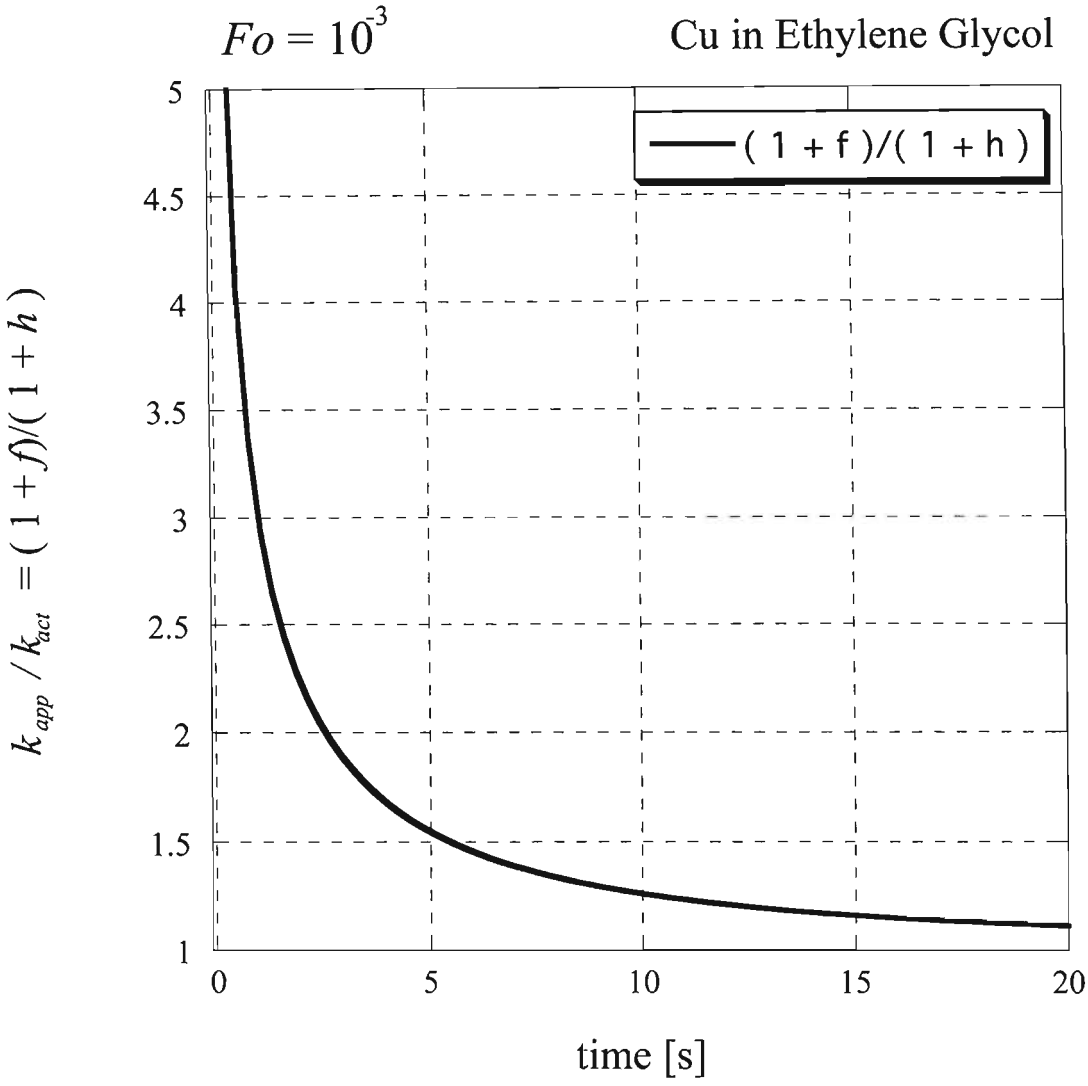

Figure 5-66: Thermal conductivity ratio vs. time in dimensional units for Cu in Ethylene Glycol in rectangular geometry for a Fourier number equal to 10^{-3}.

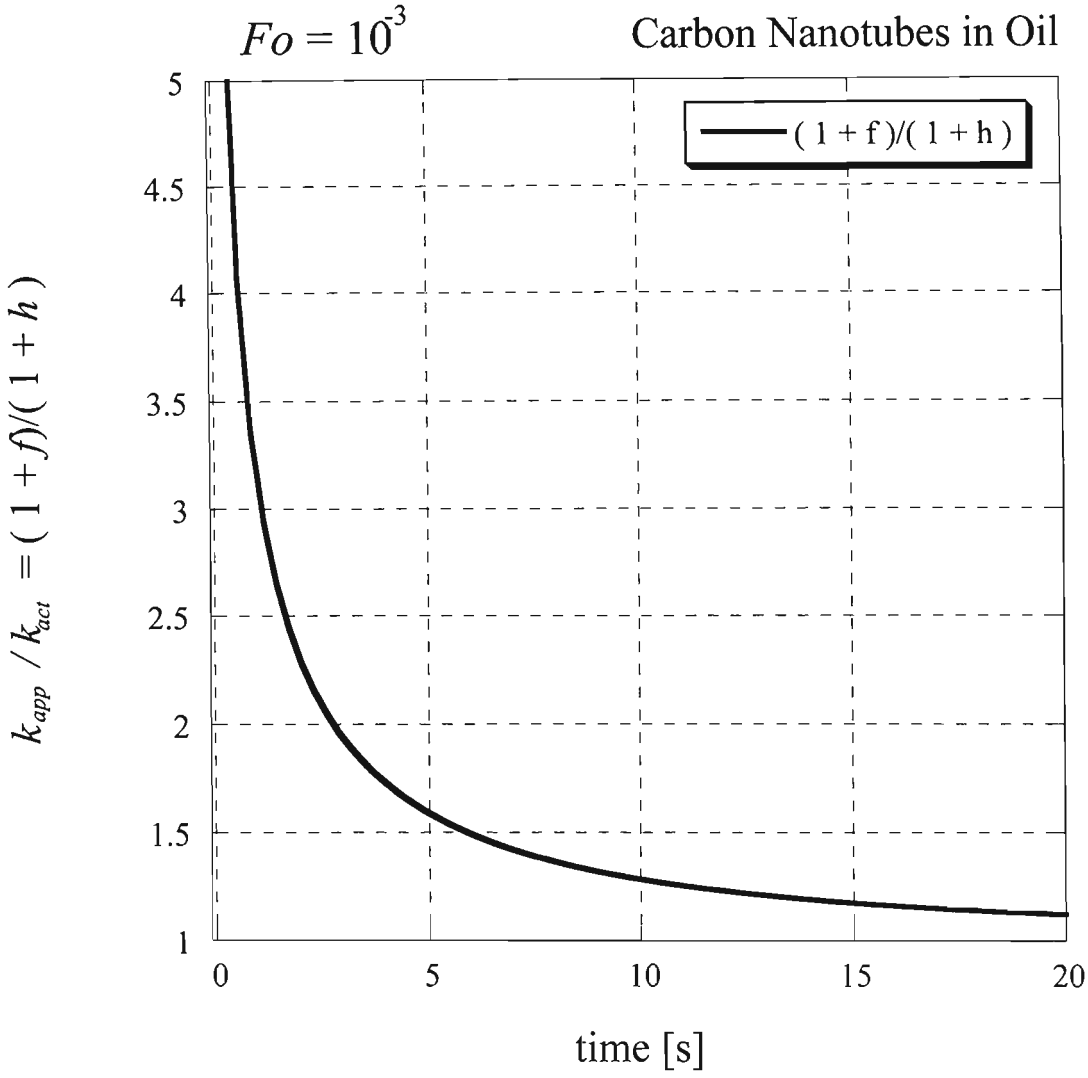

Figure 5-67: Thermal conductivity ratio vs. time in dimensional units for Carbon Nanotubes in Oil in rectangular geometry for a Fourier number equal to 10^{-3}.

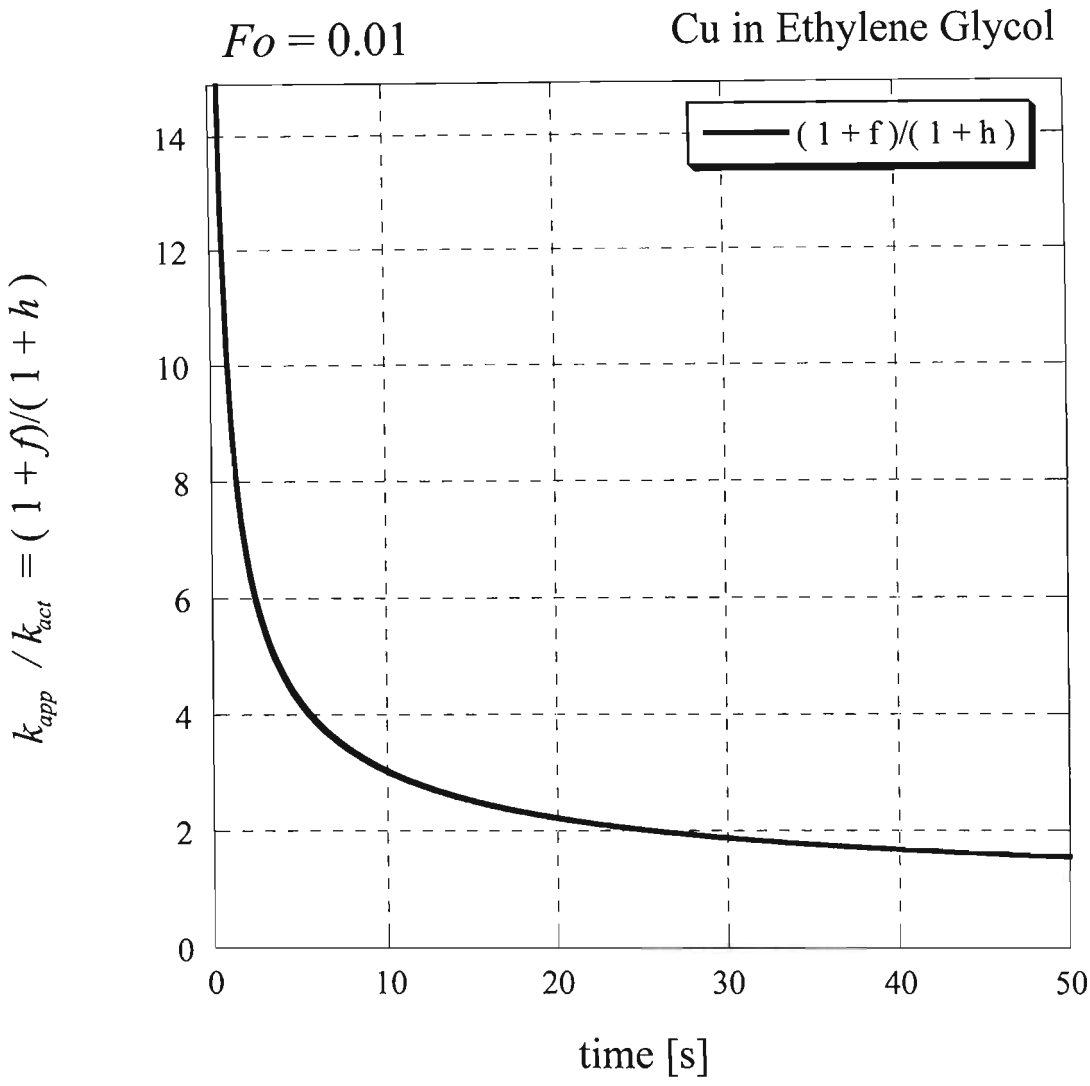

Figure 5-68: Thermal conductivity ratio vs. time in dimensional units for Cu in Ethylene Glycol in rectangular geometry for a Fourier number equal to 0.01.

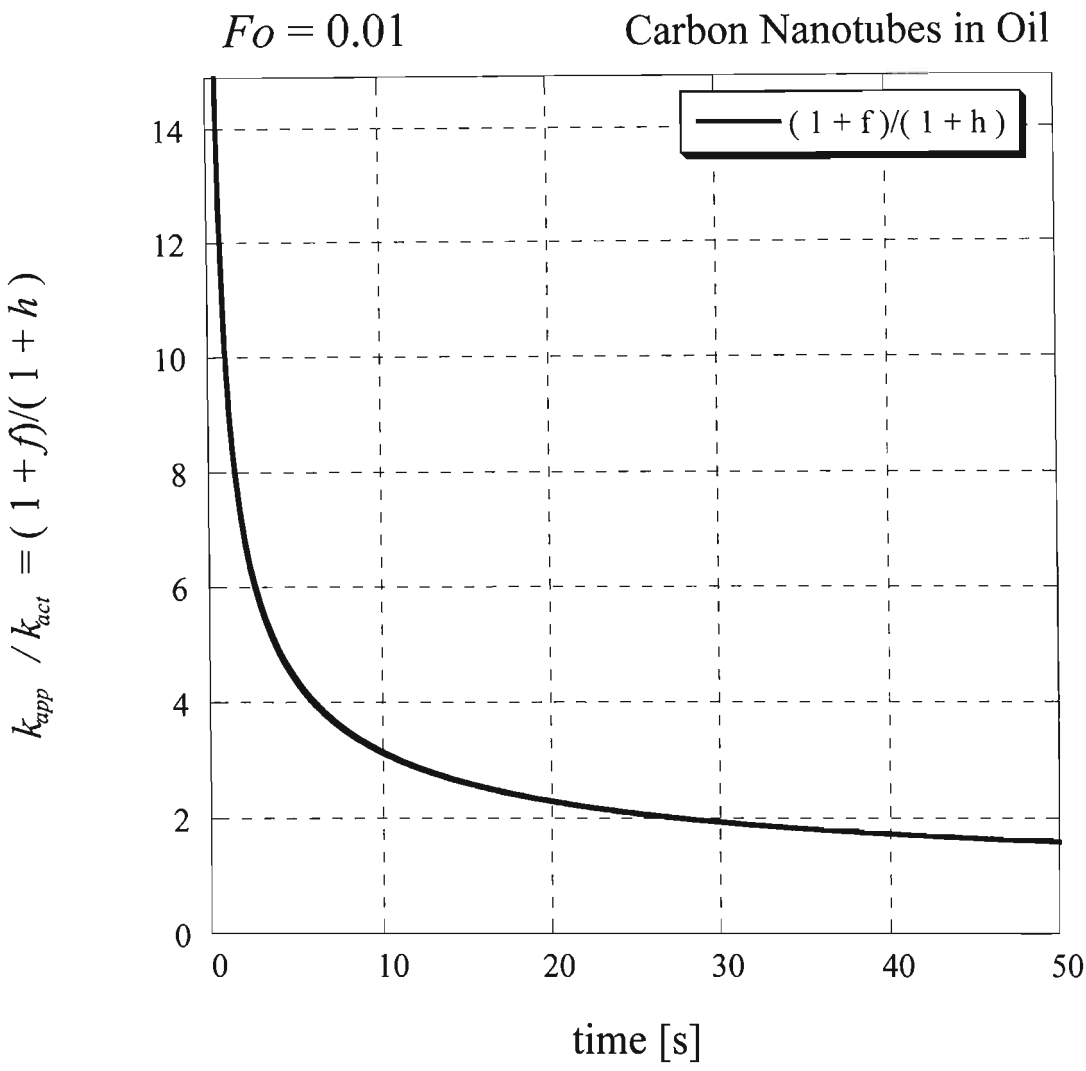

Figure 5-69: Thermal conductivity ratio vs. time in dimensional units for Carbon Nantubes in Oil in rectangular geometry for a Fourier number equal to 0.01.

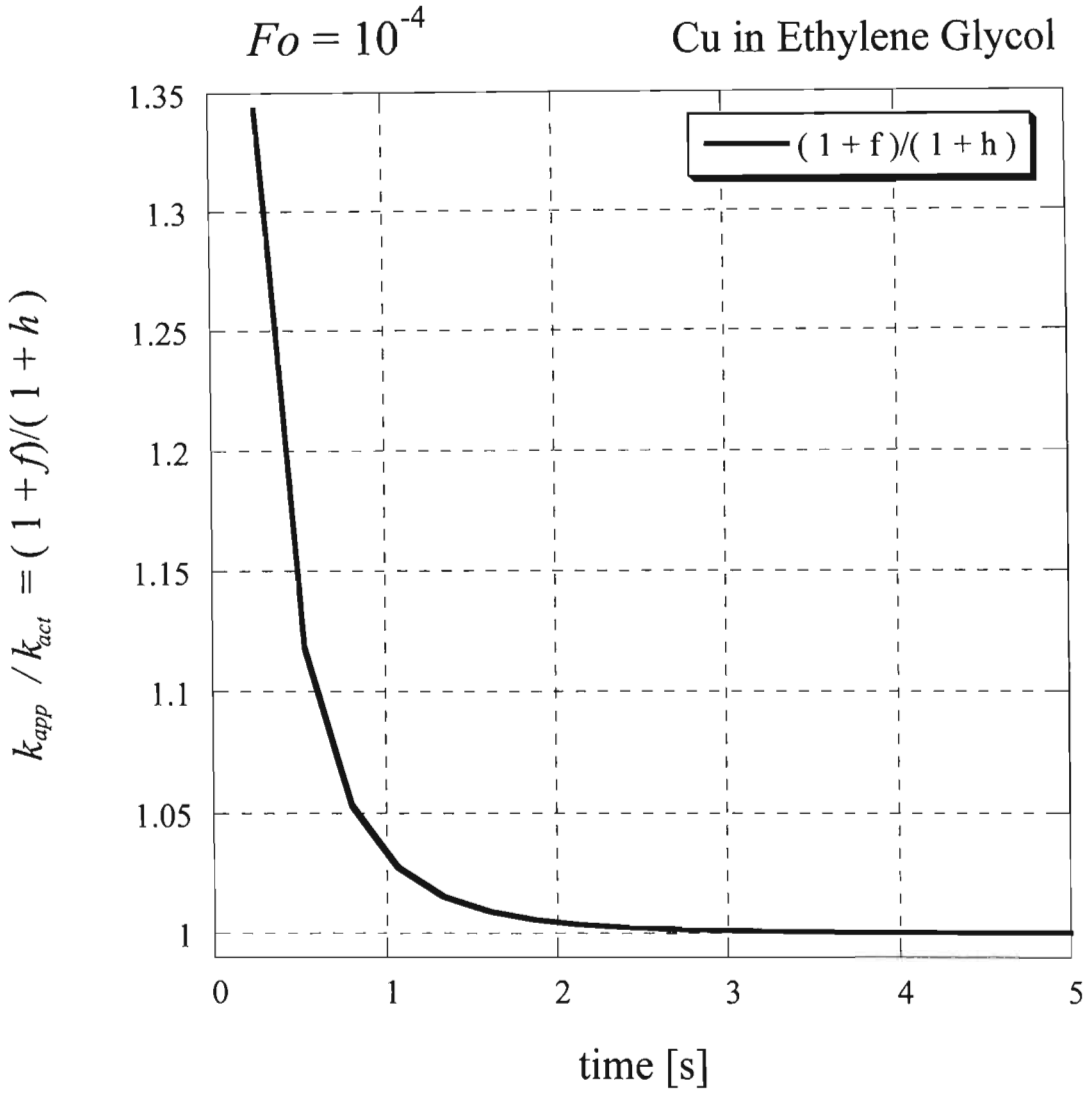

Figure 5-70: Thermal conductivity ratio vs. time in dimensional units for Cu in Ethylene Glycol in cylindrical geometry for a Fourier number equal to 10^{-4}.

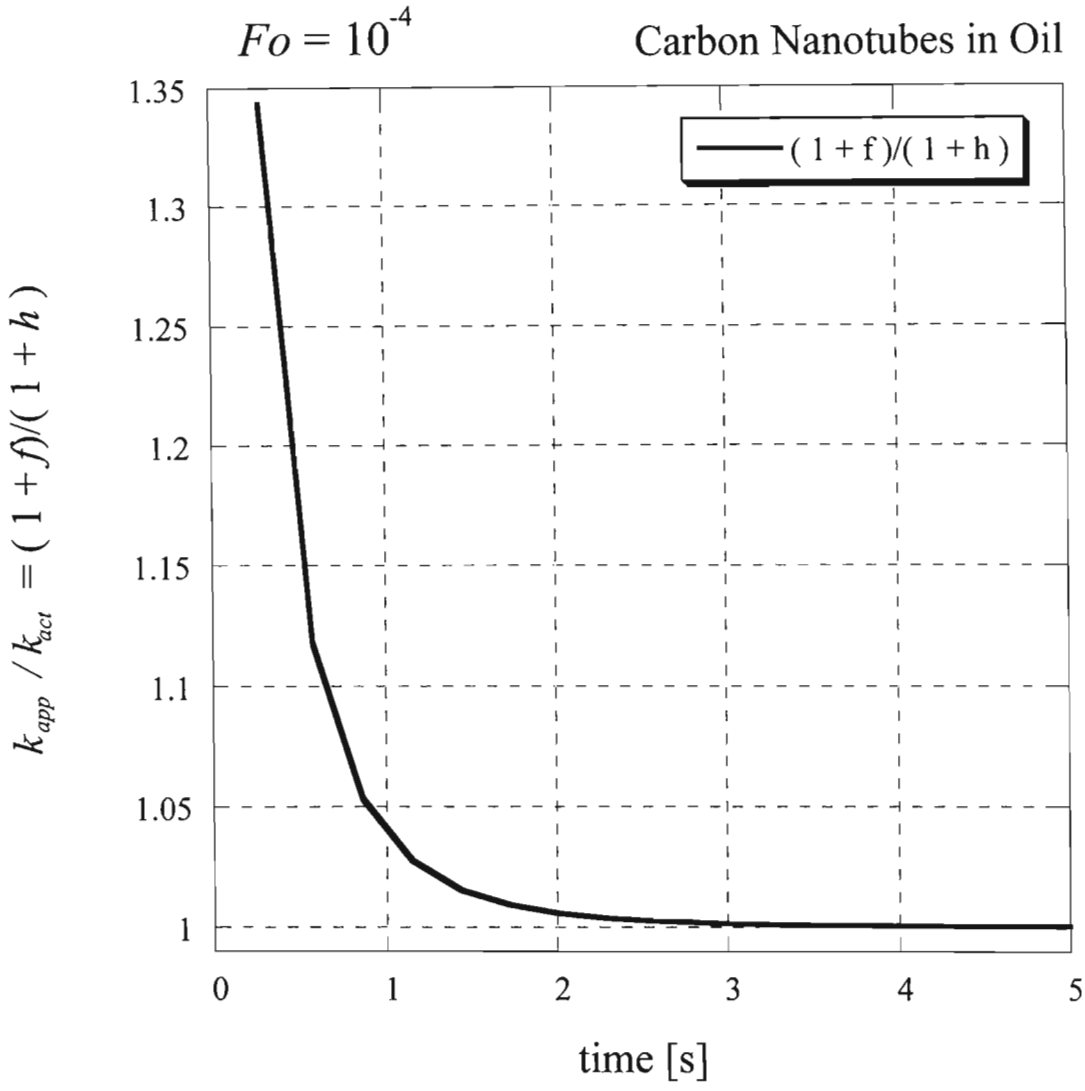

Figure 5-71: Thermal conductivity ratio vs. time in dimensional units for Carbon Nanotubes in Oil in cylindrical geometry for a Fourier number equal to 10^{-4}.

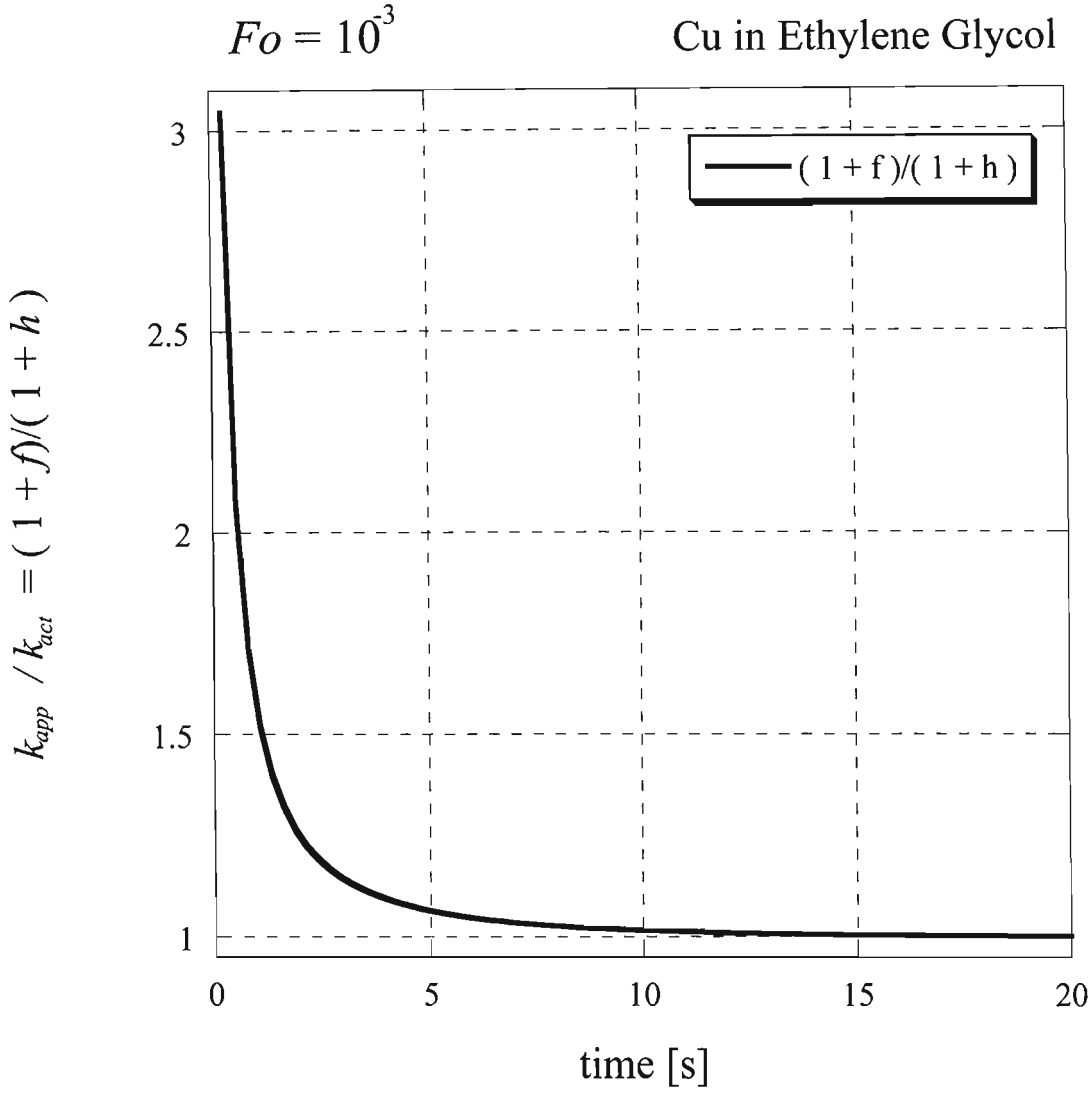

Figure 5-72: Thermal conductivity ratio vs. time in dimensional units for Cu in Ethylene Glycol in cylindrical geometry for a Fourier number equal to 10^{-3}.

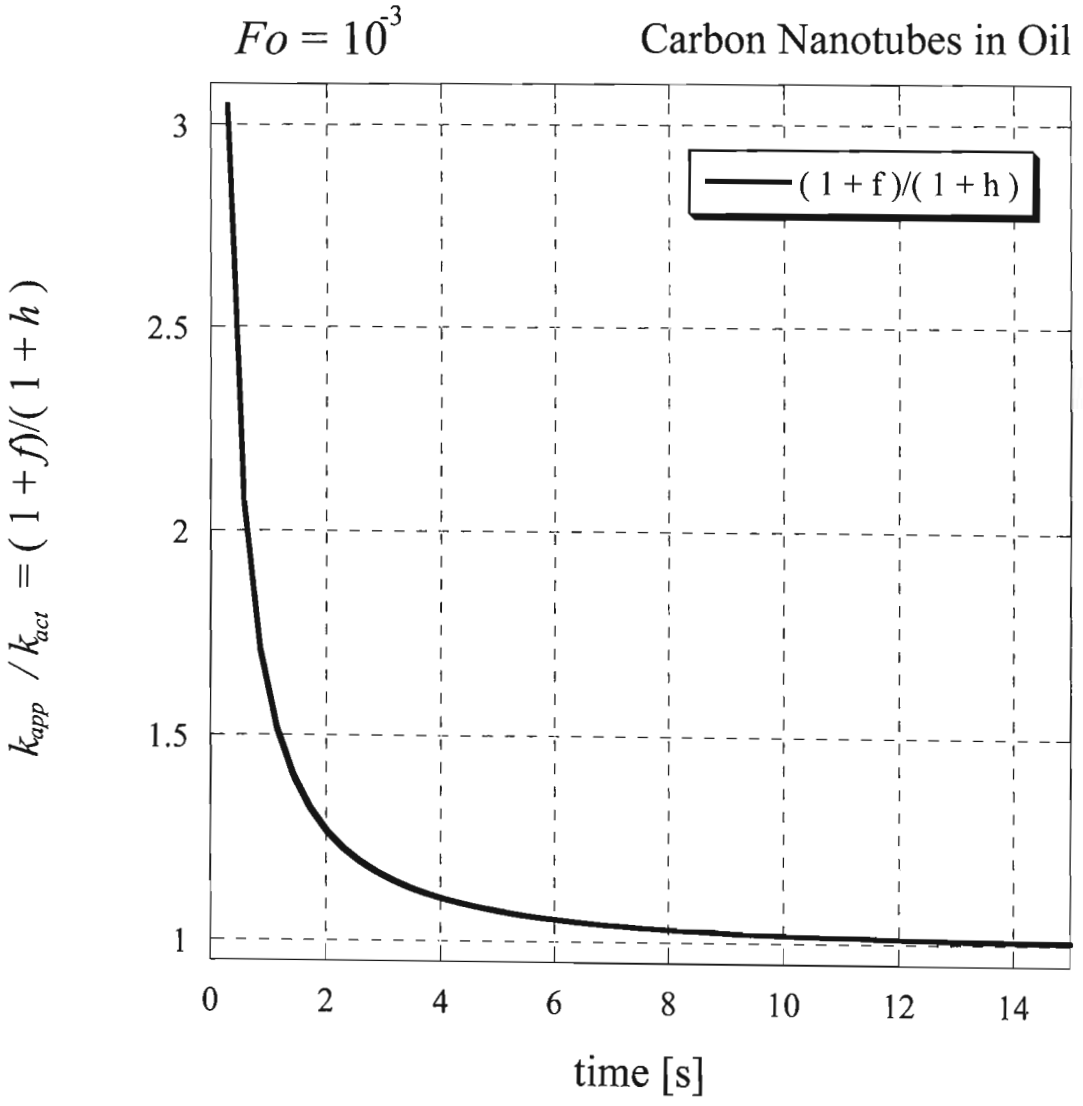

Figure 5-73: Thermal conductivity ratio vs. time in dimensional units for Carbon Nanotubes in Oil in cylindrical geometry for a Fourier number equal to 10^{-3}.

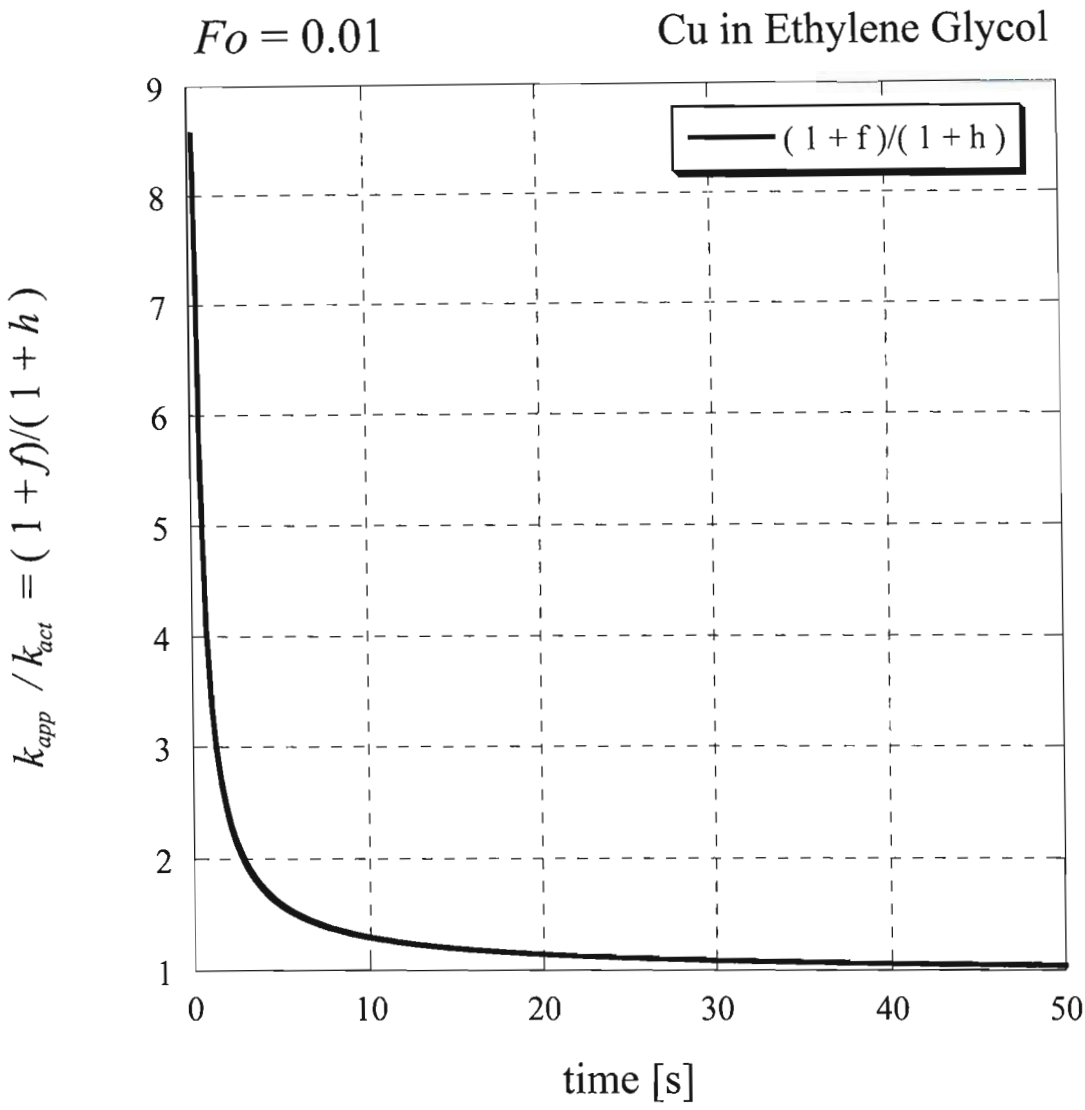

Figure 5-74: Thermal conductivity ratio vs. time in dimensional units for Cu in Ethylene Glycol in cylindrical geometry for a Fourier number equal to 0.01.

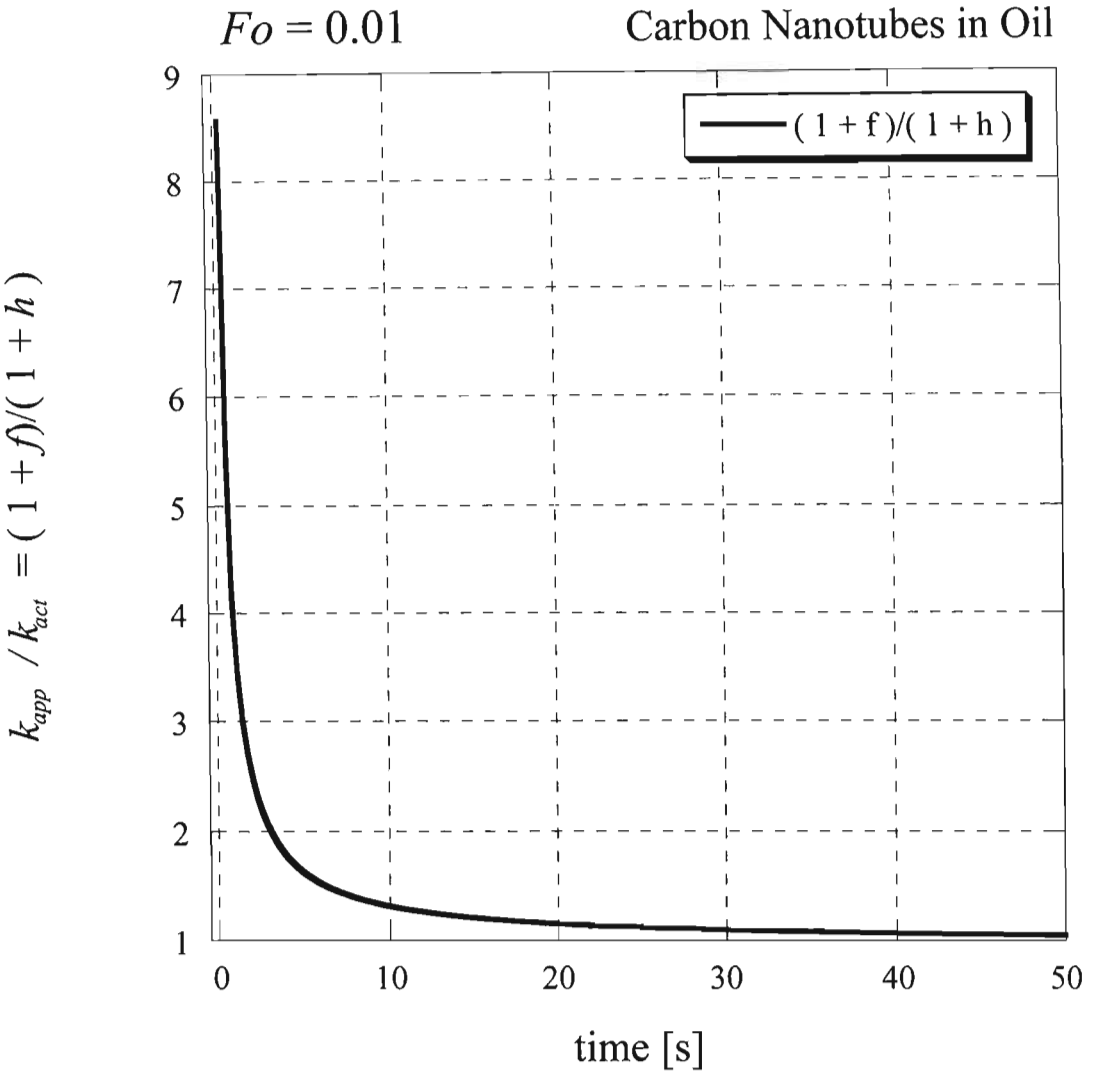

Figure 5-75: Thermal conductivity ratio vs. time in dimensional units for Carbon Nanotubes in Oil in cylindrical geometry for a Fourier number equal to 0.01.

A comparison between the wire temperatures evaluated via Fourier and Hyperbolic solutions is presented in what follows. Figure 5-76 shows the dimensionless Wire Temperature vs. t in dimensional units for Ethylene Glycol using a combination of Dirichlet and Neumann boundary conditions for Fourier and Hyperbolic heat conduction problems with a Fourier number equal to 10^{-3} for copper in Ethylene glycol. Figure 5-76 shows that for the time window of 10 seconds the Fourier heat conduction displays a linear result, and for the hyperbolic heat conduction the result looks almost linear. Only at times past 10 seconds the hyperbolic solution turns toward the Fourier solution and shows a non-linear curve. Therefore, when using the transient hot wire method for a time window of up to 10 seconds to prevent convection a hyperbolic solution may seem linear and may be confused with the Fourier solution. Figure 5-77 shows the dimensionless Wire Temperature vs. t in dimensional units for Ethylene Glycol using a combination of Dirichlet and Neumann boundary conditions for Fourier and Hyperbolic heat conduction problems with Fourier number equal to 10^{-3} for carbon nanotubes in oil. This graph in Figure 5-77 shows a similar result to the one in Figure 5-76. Again for the time window of 10 seconds the hyperbolic heat conduction solution looks linear and can be mistaken for the Fourier solution when using the transient hot wire method. Figure 5-78 shows the dimensionless Wire Temperature vs. t in dimensional units for Ethylene Glycol using a combination of Dirichlet and Neumann boundary conditions for Fourier and Hyperbolic heat conduction problems with Fourier number equal to 0.01 for copper in Ethylene glycol. As the Fourier number is increased the wave effect becomes more apparent, however with $Fo = 0.01$ the hyperbolic solution for the time window of 10 seconds still may pass for linear. For this reason it may be mistaken for the Fourier solution when using the transient hot wire method. Figure 5-79 shows the dimensionless Wire Temperature vs. t in dimensional units for Ethylene Glycol using a combination of Dirichlet and Neumann boundary conditions for Fourier and Hyperbolic heat conduction problems with Fourier number equal to 0.01 for carbon nanotubes in oil. The same effect is seen here as in Figure 5-78. From Figure 5-79 one can draw the same conclusions as from Figure 5-78. Figure 5-80 shows the dimensionless Wire Temperature vs. t in dimensional units for Ethylene Glycol using a combination of Dirichlet and Neumann boundary conditions for Fourier and Hyperbolic heat conduction problems with Fourier number equal to 1 for copper in Ethylene glycol. Figure 5-81 shows the dimensionless Wire Temperature vs. t in

dimensional units for Ethylene Glycol using a combination of Dirichlet and Neumann boundary conditions for Fourier and Hyperbolic heat conduction problems with Fourier number equal to 1 for carbon nanotubes in oil. Figures 5-80 and 5-81 show that even when the Fo = 1, at a time window of 10 seconds the hyperbolic solution still may seem linear. This may be mistaken when using the transient hot wire method for a Fourier solution. The significance of the conclusions discussed above about Figures 5-76 to 5-81 is that when looking at the results from the transient hot wire method a Fourier solution is used, even though a hyperbolic solution might be the one revealed. This may cause an overestimation of the thermal conductivity ratio presented in the graphs shown in Figures 5-64 to 5-75.

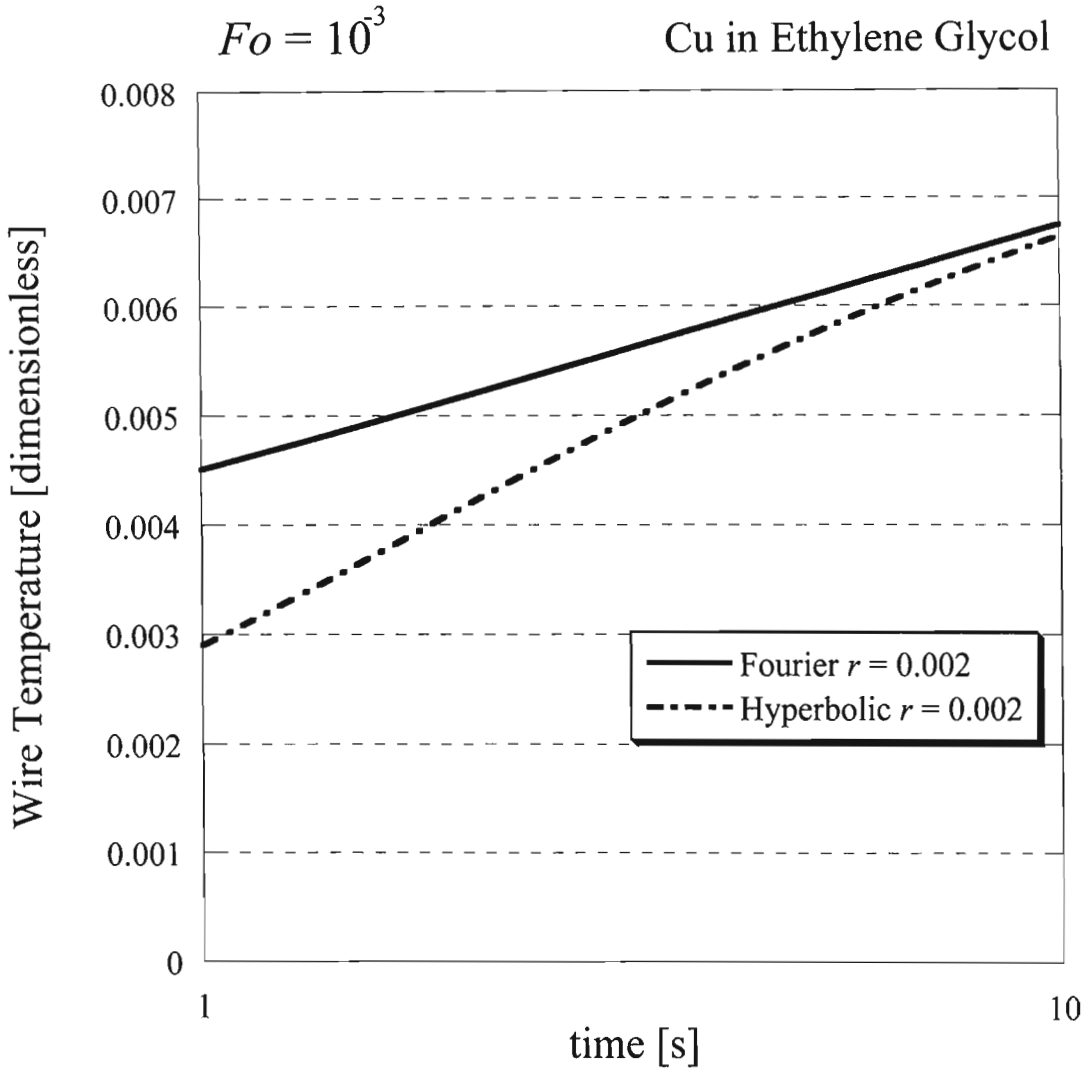

Figure 5-76: Temperature [dimensionless] vs. t in dimensional units for Ethylene Glycol using a combination of Dirichlet and Neumann boundary conditions for Fourier and Hyperbolic heat conduction problems with Fourier number equal to 10^{-3}.

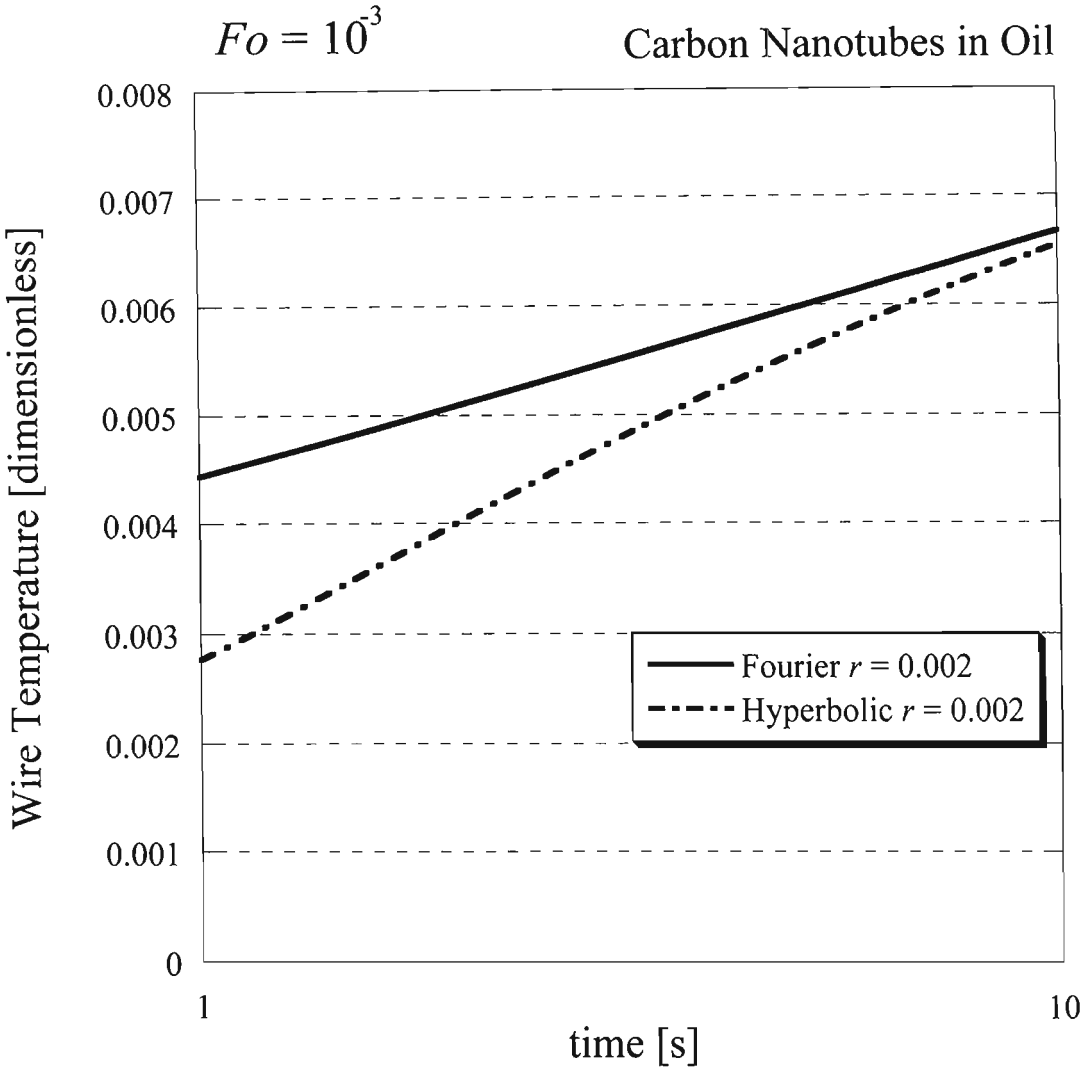

Figure 5-77: Temperature [dimensionless] vs. t in dimensional units for Carbon Nanotubes in oil using a combination of Dirichlet and Neumann boundary conditions for Fourier and Hyperbolic heat conduction problems with Fourier number equal to 10^{-3}.

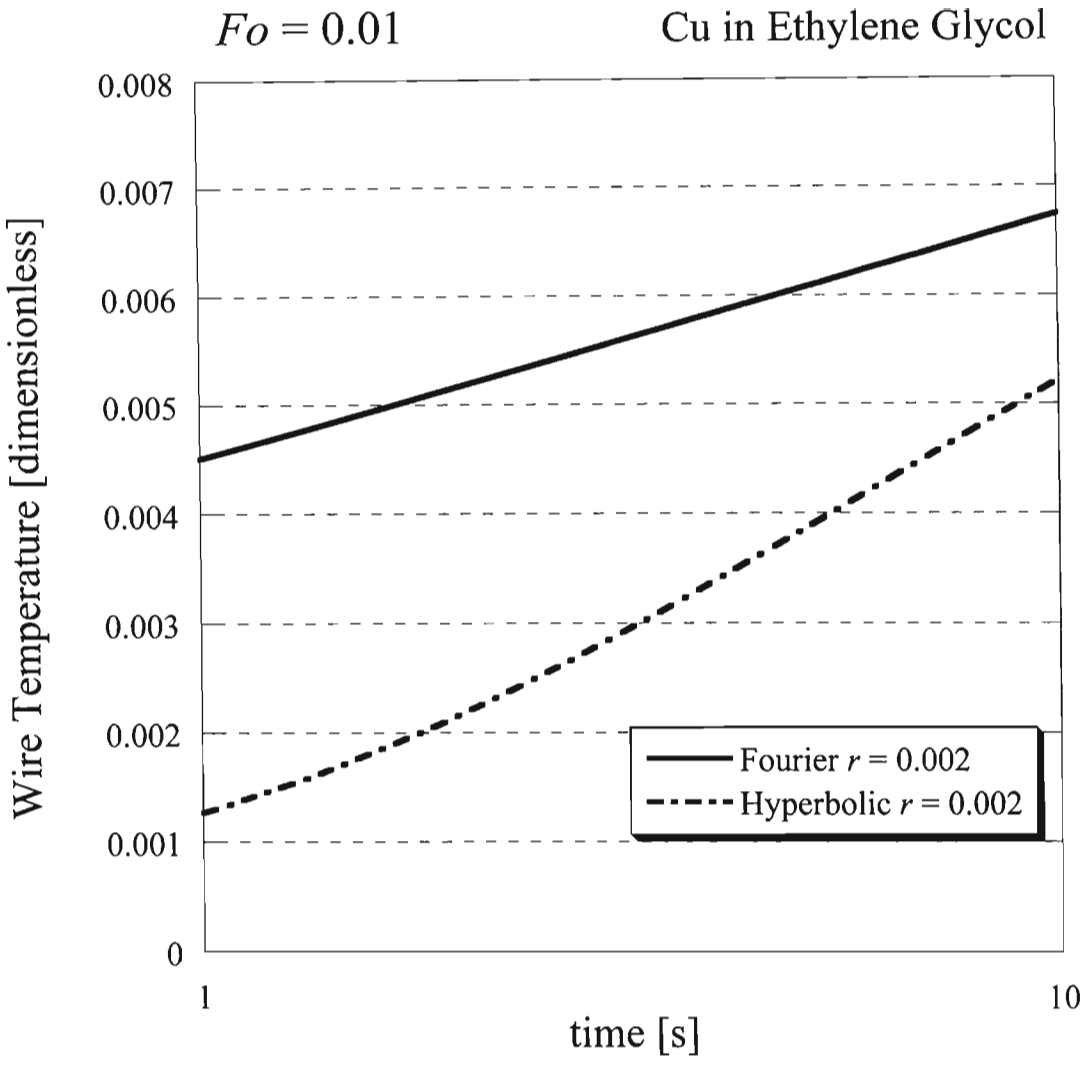

Figure 5-78: Temperature [dimensionless] vs. t in dimensional units for Ethylene Glycol using a combination of Dirichlet and Neumann boundary conditions for Fourier and Hyperbolic heat conduction problems with Fourier number equal to 0.01.

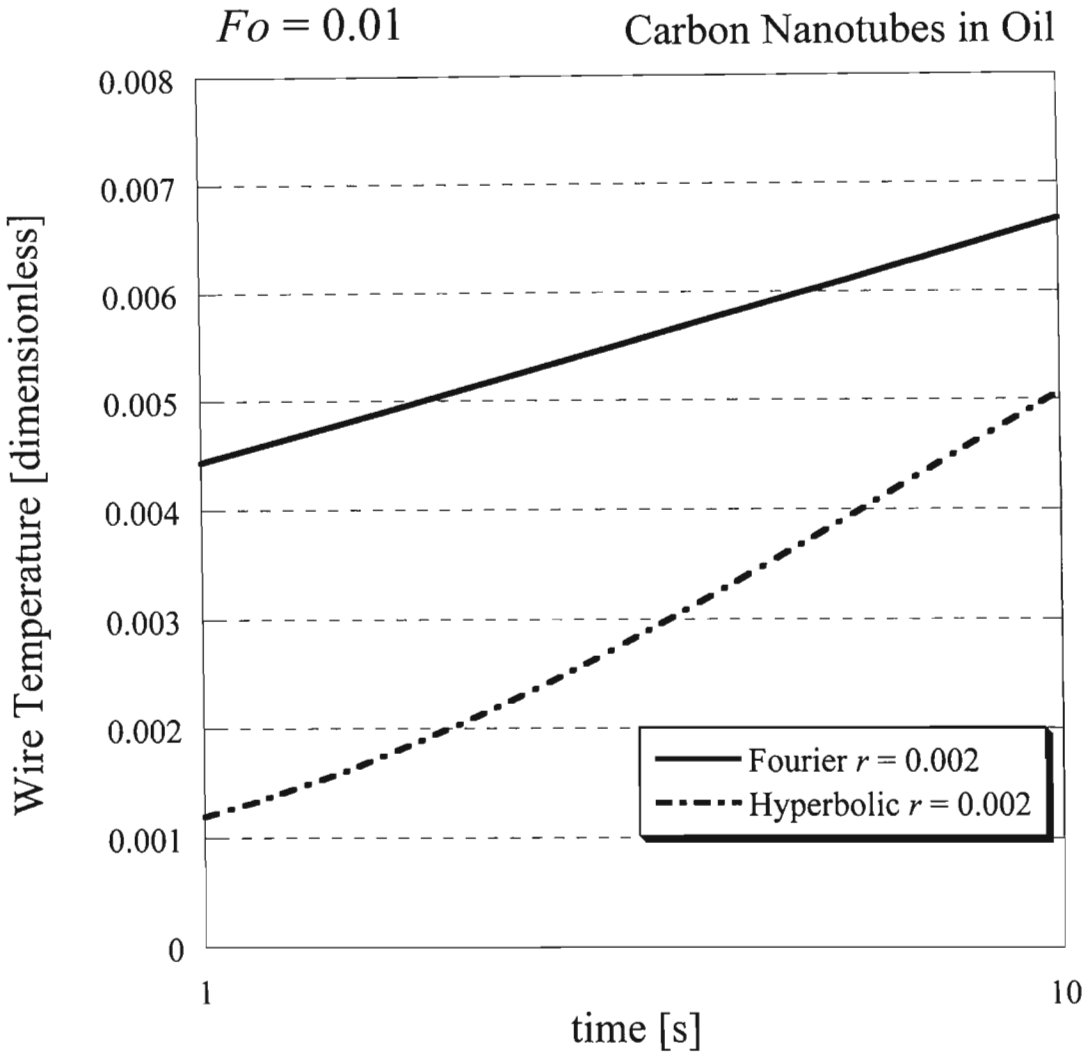

Figure 5-79: Temperature [dimensionless] vs. t in dimensional units for Carbon Nanotubes in oil using a combination of Dirichlet and Neumann boundary conditions for Fourier and Hyperbolic heat conduction problems with Fourier number equal to 0.01.

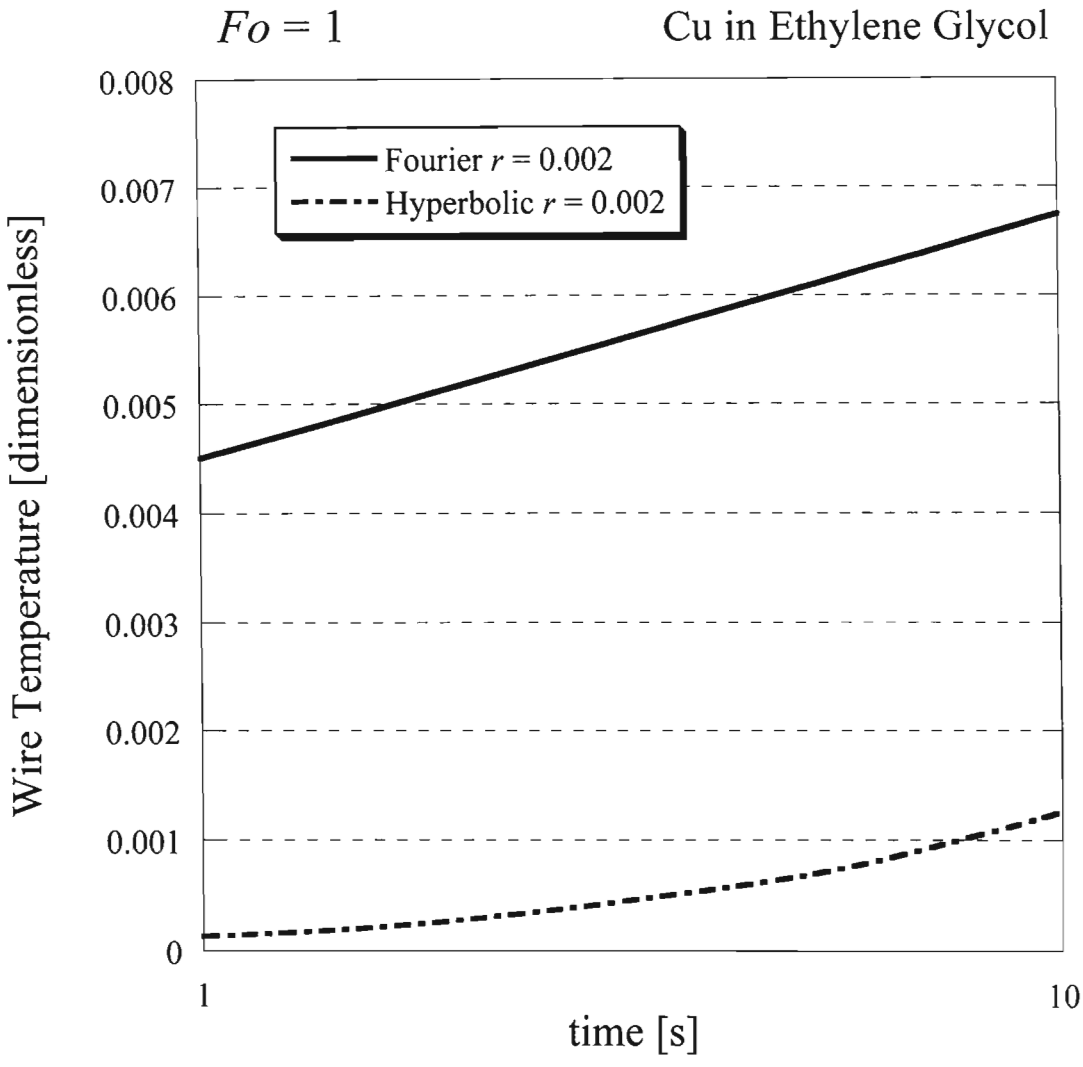

Figure 5-80: Temperature [dimensionless] vs. t in dimensional units for Ethylene Glycol using a combination of Dirichlet and Neumann boundary conditions for Fourier and Hyperbolic heat conduction problems with Fourier number equal to 1.

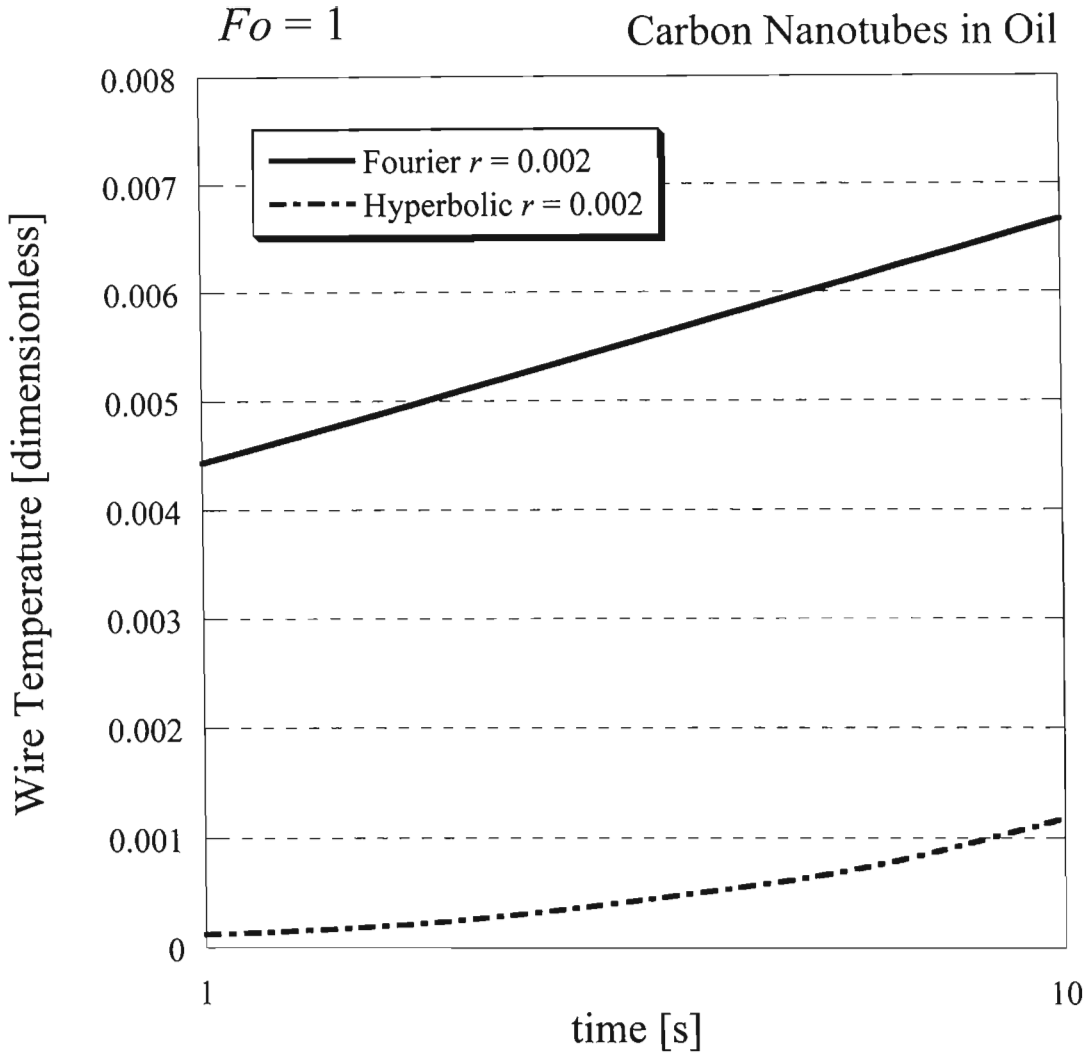

Figure 5-81: Temperature [dimensionless] vs. t in dimensional units for Carbon Nanotubes in oil using a combination of Dirichlet and Neumann boundary conditions for Fourier and Hyperbolic heat conduction problems with Fourier number equal to 1.

The last set of results to be presented are related to the frequencies of oscillations that are obtained from the hyperbolic solution (4-12). Converting the dimensionless frequency λ_{in} (4-14c) to its corresponding dimensional form and considering a very small relaxation time of $\tau = 10^{-10}$s leads to the results presented in Figure 5-82. Any external forcing at frequencies close to the ones presented in Figure 5-82 may produce resonant effects.

The graph presented in Figure 5-82 shows that for length scales larger than 10 nm the relationship between the dimensional critical frequency and the length scale is approximately a linear function on a log-log scale. It also demonstrates that large critical frequencies are associated with very small length scales. Figure 5-83 shows the graph for the critical value of n, n_{cr} versus Fo, on a log-log scale evaluated by using equation (4-15). It shows that for values of Fourier number below 10^{-4}, the critical value of n, n_{cr}, is below 10. This means that the wave effects in the hyperbolic solution should be observed as they appear in the first ten terms of the series solution (4-12). The critical value of n, n_{cr} is accurately related to the length scale by a linear relationship on a log-log scale as presented in Figure 5-84. For the experiments related to fluid nano-suspensions that are considered, there are two points of interest that are the focus of the following observations. The first is the nano-fluid suspension, for which it is still difficult at this stage to draw conclusions. The second is the transient hot wire, typically a micron-scale platinum wire, for which the hyperbolic effects appear at about the 150th term in the series shown in Figure 5-84 and the corresponding natural frequencies are about 1000 Mhz or higher as shown in Figure 5-82. The latter suggests the possibility of resonance due to an oscillatory thermal forcing which may occur from various sources including induced high frequency radio waves.

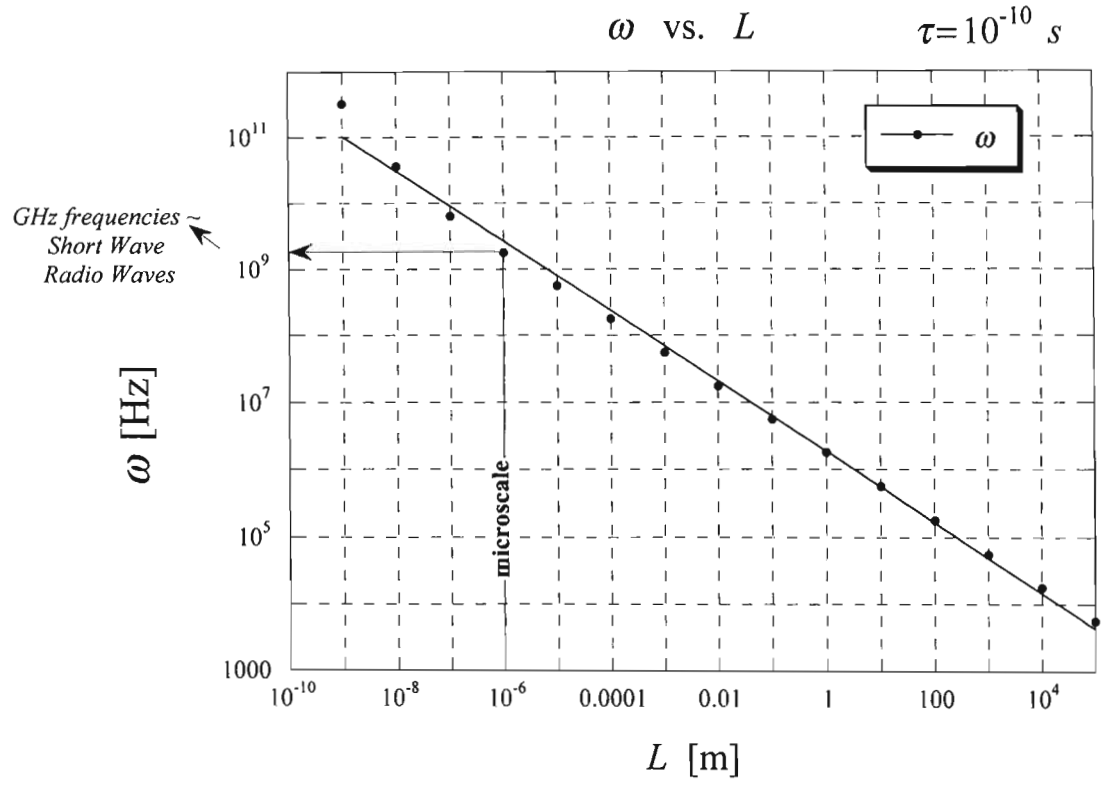

Figure 5-82: Frequency vs. length scale with $\tau = 10^{-10}$ s showing possible resonance effects at micro-scale level.

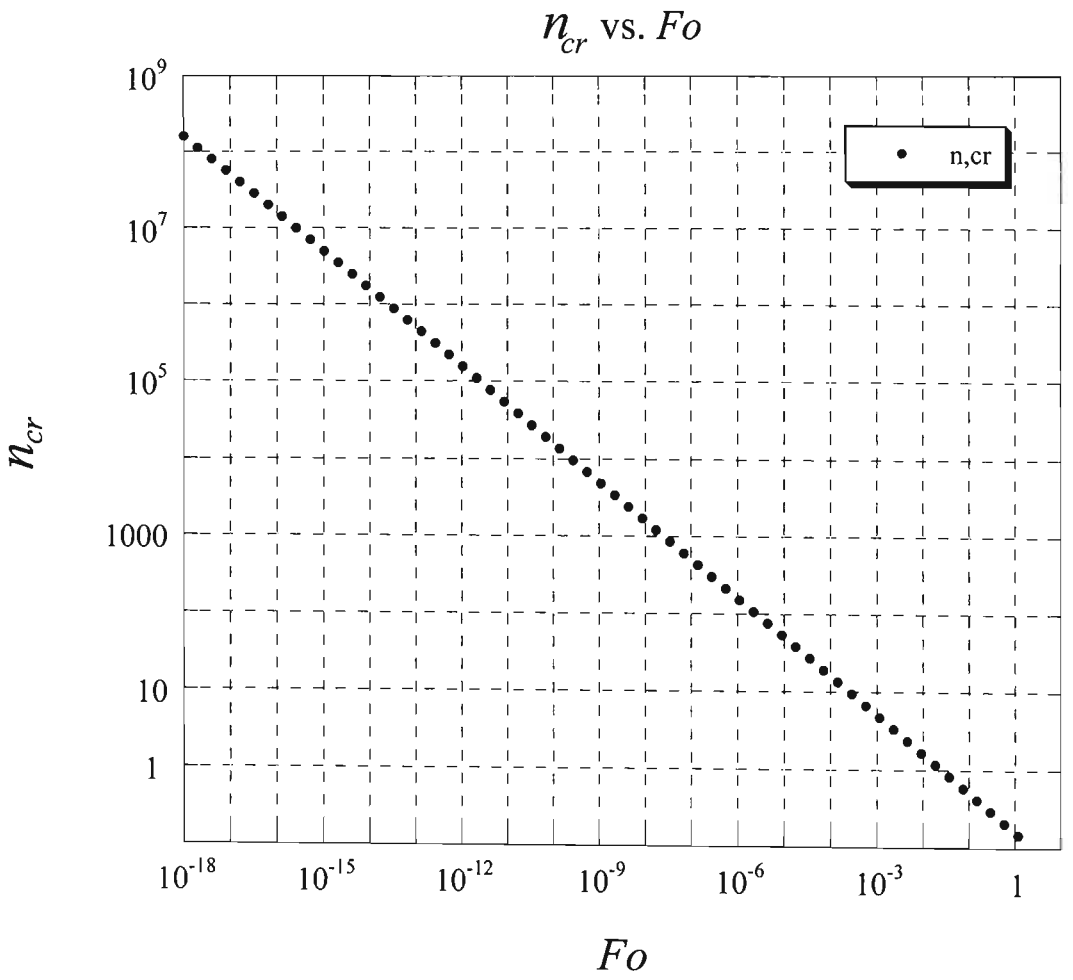

Figure 5-83: The relationship between the critical value of n, i.e. $n_{cr,}$ and the Fourier number Fo.

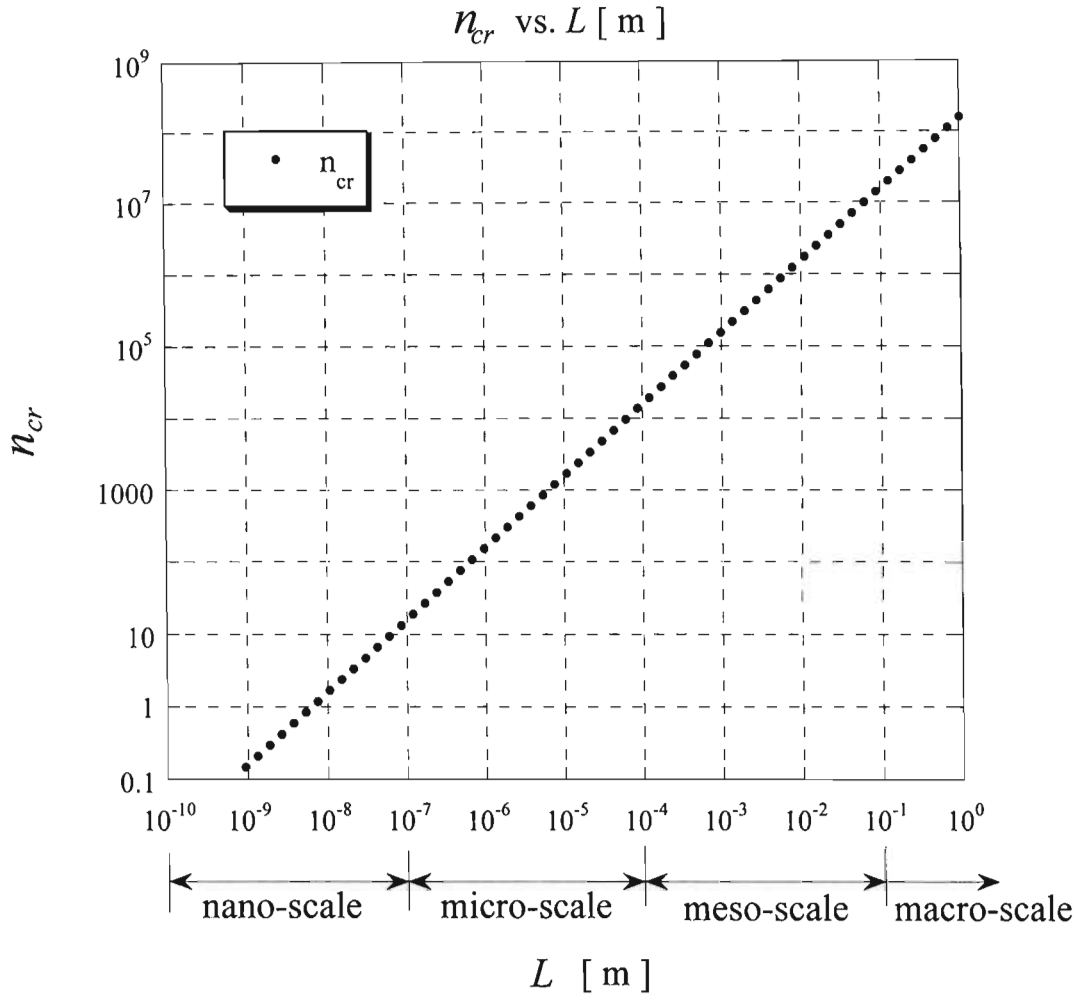

Figure 5-84: The relationship between the critical value of n, i.e. $n_{cr,}$ and the length scale.

CHAPTER 6
CONCLUSIONS

The results presented show that thermal wave effects via hyperbolic heat conduction may lead to an overestimation of the effective thermal conductivity when evaluated by using the Transient Hot Wire method. The apparent linearity of the hyperbolic wire temperature profile over an experimental time window of below 10s may be confused with the linear Fourier temperature profile over the same time window. While reported experimental values of the relaxation time in heterogeneous materials (e.g. particles suspended in fluids) exceed the value of 10s leading to Fourier numbers of about $Fo = 10^{-2}$ to $Fo = 1$, the latter are not yet well established results. Therefore, more work is needed in this direction before a final conclusion may be drawn.

APPENDICES

Appendix A: The solution of a line heat source.

All variables in this appendix apart from η and η_1 are dimensional.

Consider a radial heat flux q_r from a cylindrical rod of radius a and length L. Then, the heat rate per unit length of the rod, at $r = a$, is:

$$\dot{q}_L = \frac{\dot{Q}_g}{L} = \left(q_r\right)_{r=a} \cdot \frac{2\pi aL}{L} = 2\pi a\left(q_r\right)_{r=a} = -2\pi ak\left(\frac{\partial T}{\partial r}\right)_{r=a} = -2\pi k\left(r\frac{\partial T}{\partial r}\right)_{r=a} \qquad \text{(A-1)}$$

The limit of this heat rate as $a \to 0$ while $\dot{q}_L$ remains unchanged is

$$\dot{q}_L = -2\pi k \lim_{a\to 0}\left[\left(r\frac{\partial T}{\partial r}\right)_{r=a}\right] \qquad \text{(A-2)}$$

or:

$$\lim_{a\to 0}\left[\left(r\frac{\partial T}{\partial r}\right)_{r=a}\right] = -\frac{\dot{q}_L}{2\pi k} \qquad \text{(A-3)}$$

The governing equation is:

$$\frac{\partial T}{\partial t} = \frac{\alpha}{r}\frac{\partial}{\partial r}\left(r\frac{\partial T}{\partial r}\right) \qquad \text{(A-4)}$$

subject to the following initial and boundary conditions,

$$\left.\begin{array}{l} t = 0 \quad : T = 0 \\ r \to \infty \; : T = 0 \end{array}\right\} \text{ reference temperature: } T = T_* - T_{0_*} \text{ uniform initially.}$$

$$r = 0 \; : \lim_{a\to 0}\left(r\frac{\partial T}{\partial r}\right)_{r=a} = -\frac{\dot{q}_L}{2\pi k}$$

Introducing the similitude variable η

$$\eta = \frac{r^2}{\alpha t} \qquad \text{(A-5)}$$

and using:

$$\frac{\partial}{\partial t} = \frac{\partial \eta}{\partial t}\frac{d}{d\eta} \;\; ; \;\; \frac{\partial}{\partial r} = \frac{\partial \eta}{\partial r}\frac{d}{d\eta} \qquad \text{(A-6)}$$

substituting into equation (A-4):

$$\frac{d}{d\eta}\left(\eta\frac{dT}{d\eta}\right) + \frac{\eta}{4}\frac{dT}{d\eta} = 0 \qquad \text{(A-7)}$$

Using the following notation

$$\theta = \eta \frac{dT}{d\eta} \tag{A-8}$$

equation (A-7) becomes

$$\frac{d\theta}{d\eta} + \frac{1}{4}\theta = 0 \tag{A-9}$$

which leads to

$$\frac{d\theta}{d\eta} = -\frac{1}{4}\theta \rightarrow \frac{d\theta}{\theta} = -\frac{1}{4}d\eta \tag{A-10}$$

which leads to the following

$$T = A_0 \int_{\frac{\eta}{4}}^{\infty} \frac{e^{-\frac{\eta}{4}}}{\left(\frac{\eta}{4}\right)} d\left(\frac{\eta}{4}\right) = A_0 \int_{\frac{\eta}{4}}^{\infty} \frac{e^{-u}}{u} du \tag{A-11}$$

$$T = A_0 Ei\left(\frac{\eta}{4}\right) = A_0 Ei\left(\frac{r^2}{4\alpha t}\right) \tag{A-12}$$

where $Ei(\cdot)$ is the exponential integral function defined by

$$Ei(x) = \int_{x}^{\infty} \frac{e^{-u}}{u} du \tag{A-13}$$

$$\frac{dEi(x)}{dx} = \frac{-e^{-x}}{x} \rightarrow x\frac{dEi(x)}{dx} = -e^{-x} \tag{A-14}$$

let $\eta_1 = \frac{\eta}{4}$ which leads to,

$$T = A_0 Ei(\eta_1) \tag{A-15}$$

where $A_0 = \frac{\dot{q}_L}{4\pi k}$

Now, since

$$\dot{q}_L = \frac{\dot{Q}_g}{L} = \frac{i^2 \rho_e L}{AL} = \frac{i^2 \rho_e}{A} = \frac{i^2 R}{L} \quad \left[\frac{W}{m}\right] \tag{A-16}$$

$$T_* - T_{0_*} = T = \frac{i^2 R}{4\pi k L} Ei\left(\frac{r^2}{4\alpha t}\right) \tag{A-17}$$

Equation (A-17) was used in the derivations starting from equation (2-1).

REFERENCES

Antaki, P.J., 1998, "Solution to non-Fourier dual phase lag heat conduction in a semi-infinite slab with surface heat flux", *International Journal of Heat and Mass Transfer*, **41** (14), pp. 2253-2258.

Assael, M.J., Dix, M., Gialou, K., Vozar, L. & Wakeham, W.A., 2002, "Application of the Transient Hot-Wire technique to the measurement of the thermal conductivity of solids", *International Journal of Thermophysics,* **23**, 615-633.

Barletta, A., Zanchini, E., 1996, "Hyperbolic heat conduction and thermal resonances in a cylindrical solid carrying a steady-periodic electric field", *International Journal of Heat and Mass Transfer*, **39** (6), pp. 1307-1315.

Bonnecaze, R.T., Brady, J.F., 1990, "A method for determining the effective conductivity of dispersions of particles", *Proc. Royal Society of London A,* **430**, pp. 285-313.

Bonnecaze, R.T., Brady, J.F., 1991, "The effective conductivity of random suspensions of spherical particles", *Proc. Royal Society of London A*, **432**, pp. 445-465.

Cattaneo, M.C., 1958, "Sur une forme de l'equation de la chaleur eliminant le paradoxe d'une propagation instantanee", *Comptes Rendus Hebd. Seances Acad. Sci.* **247** (4), pp. 431-433.

Chen, G., 2001, "Ballistic-Diffusive Heat Conduction Equations", *Physical Review Letters,* **86**, pp. 2297-2300.

Chen, G., 1996, "Nanolocal and nonequilibrium heat conduction in the vicinity of nanoparticles", *Journal Heat Transfer* **118**, pp. 539-545.

Chen, G., 2000, "Particularities of heat conduction in nanostructures", *Journal of Nanoparticle Research* **2**, pp. 199-204.

Choi, S.U.S., Zhang, Z.G., Yu, W., Lockwood, F.E., and Grulke, E.A., 2001, "Anomalous thermal conductivity enhancement in nanotube suspensions", *Applied Physics Letters*, **79** (14), pp. 2252-2254.

Davis, R.H., 1986, "The effective thermal conductivity of a composite material with spherical inclusions", *International Journal of Thermophysics* , **7**, pp. 609-620.

De Groot, J.J., Kestin, J. & Sookiazian, H., 1974, "Instrument to measure the thermal conductivity of gases", *Physica,* , **75**, pp. 454-482.

Eastman, J.A., Choi, S.U.S., Li, S., Yu, W., and Thompson, L.J., 2001, "Anomalously increased effective thermal conductivities of ethylene glycol-based nanofluids containing copper nanoparticles", *Applied Physics Letters* , **78** (6), pp. 718-720.

Frankel, J.I., Vick, B., Özisik, M.N., 1985, "Flux formulation of hyperbolic heat conduction", *J. Applied Physics* , **58**, pp. 3340-3345.

Gustafsson, S.E., 1987, "Transient Hot Strip techniques for measuring thermal conductivity and thermal diffusivity", *The Rigaku Journal* , **4**, pp. 16-28.

Haji-Sheikh, A., Minkowycz, W.J., Sparrow, E.M., 2002, "Certain anomalies in the analysis of hyperbolic heat conduction", *Journal of Heat Transfer* , **124** , pp. 307-319.

Hamilton, R.L., Crosser, O.K., 1962, "Thermal Conductivity of Heterogeneous Two-Component Systems", *I&EC Fundamentals* **1**, pp. 187-191.

Hammerschmidt, U. & Sabuga, W., 2000, "Transient Hot Wire (THW) method: Uncertainty assessment", *International Journal of Thermophysics,* **21**, pp. 1255-1278.

Healy, J.J., de Groot, J.J. & Kestin, J., 1976, "The theory of the Transient Hot-Wire method for measuring thermal conductivity", *Physica,* **82C**, pp. 392-408.

Jeffrey, D.J., 1973, "Conduction through a random suspension of spheres", *Proc. Royal Society of London A* **335**, pp. 355-367.

Kaminski, W., 1990, "Hyperbolic Heat Conduction equation for materials with a nonhomogeneous inner structure", *Journal of Heat Transfer*, **112**, pp. 555-560.

Keblinski, P., Phillpot, S.R., Choi, S.U.S., Eastman, J.A., 2002, "Mechanisms of heat flow in suspensions of nano-sized particles (nanofluids)", *International Journal of Heat and Mass Transfer* **45**, pp. 855-863.

Kestin, J., & Wakeham, W.A., 1978, "A contribution to the theory of the transient hot-wire technique for thermal conductivity measurements", *Physica,* **92A**, pp. 102-116.

Lee, S., Choi, S.U.-S., Li, S., Eastman, J.A., 1999, "Measuring thermal conductivity of fluids containing oxide nanoparticles", *ASME Journal of Heat Transfer*, **121**, pp. 280-289.

Lu, S., Lin, H., 1996, "Effective conductivity of composites containing aligned spheroidal inclusions of finite conductivity", *J. Applied Physics*, **79**, pp. 6761-6769.

Maxwell, J.C., 1904, *A Treatise on Electricity and Magnetism*, 2nd edition, Oxford University Press, Cambridge, U.K., pp. 435-441.

Mitra, K., Kumar, S., Vedavarz, A., Moallemi, M.K., 1995, "Experimental evidence of hyperbolic heat conduction in processed meat", *Journal of Heat Transfer*, **117**, pp. 568-573.

Nagasaka, Y. & Nagashima, A., 1981, "Absolute measurement of the thermal conductivity of electrically conducting liquids by the transient hot-wire method", *J. Phys. E: Sci. Instrum.*, **14**, pp. 1435-1440.

Özisik, M.N., Tzou, D.Y., 1994, "On the wave theory in Heat Conduction", *Journal of Heat Transfer*, **116**, pp. 526-535.

Perkins, R.A., Ramires, M.L.V. and Nieto de Castro, C.A., 2000, "Thermal Conductivity of Saturated Liquid Toluene by Use of Anodized Tantalum Hot Wires at High Temperatures", *J. Research National Institute of Standards and Technology*, **105**, pp. 255-265.

Tzou, D.Y., 1995, "Experimental support for the lagging behavior in heat propagation", *Journal of Thermophysics and Heat Transfer*, **9** (4), pp. 686-693.

Tzou, D.Y., *Macro-to-Microscale Heat Transfer; The Lagging Behavior*, Taylor&Francis, Washington DC, 1997.

Tzou, D.Y., 2001, "Temperature-dependent thermal lagging in ultrafast laser heating", *International Journal of Heat and Mass Transfer*, **44**, pp. 1725-1734.

Vadasz, J.J., Govender, S. & Vadasz, P., 2005, "Heat transfer enhancement in nanofluids suspensions: possible mechanisms and explanations", *International Journal of Heat Mass Transfer*, **48**, pp. 2673-2683.

Vadasz, P., 2005, "Explicit conditions for local thermal equilibrium in porous media heat conduction", *Transport in Porous Media*, **59**, pp. 341-355.

Vadasz, P., 2005, "Absence of oscillations and resonance in porous media dual-phase-lagging Fourier heat conduction", *ASME Journal of Heat Transfer*, **127**, pp. 307-314.

Vadasz, P., Vadasz, J. J., Govender, S., 2004, "Heat transfer enhancement in nanofluid suspensions, *Proceedings of IMECE2004*, Paper No. IMECE2004-59840.

Vernotte, P., 1958, "Les paradoxes de la theorie continue de l'equation de la chaleur", *Comptes Rendus Hebd. Seances Acad. Sci.* **246** (22), pp. 3154-3155.

Vernotte, P., 1958, "La veritable equation de la chaleur", *Comptes Rendus Hebd. Seances Acad. Sci.* **247** (23), pp. 2103-2105.

Vernotte, P., 1961, "Some possible complications in the phenomena of thermal conduction", *Comptes Rendus Hebd. Seances Acad. Sci.* **252**, pp. 2190-2191.

Vick, B., Özisik, M.N., 1983, "Growth and decay of a thermal pulse predicted by the hyperbolic heat conduction equation", *Journal of Heat Transfer* **105**, pp. 902-907.

Wang, L., 2000, "Solution structure of hyperbolic heat-conduction equation", *International Journal of Heat and Mass Transfer*, **43**, pp. 365-373.

Wang, B.X., Zhou, L.P. and Peng, X.F., 2003, "A fractal model for predicting the effective thermal conductivity of liquid with suspension of nanoparticles", *International Journal of Heat and Mass Transfer*, **46**, pp. 2655-2672.

Xuan, Y. and Li, Q., 2003, "Investigation on Convective Heat Transfer and flow Features of Nanofluids, *ASME Journal of Heat Transfer*, **125**, pp. 151-155.

Xuan, Y. and Li, Q., 2000, "Heat transfer enhancement of nanofluids", *International Journal of Heat and Mass Transfer*, **21**, pp. 58-64.

Xue, L., Keblinski, P., Phillpot, S.R., Choi, S.U.-S., Eastman, J.A., 2004, "Effect of fluid layering at the liquid-solid interface on thermal transport", *International Journal of Heat and Mass Transfer*, **47**, pp. 4277-4284.